# NONLINEAR EVOLUTION OF VLASOV EQUILIBRIA

by

Lucio Demeio

Dissertation submitted to the Faculty of the

Virginia Polytechnic Institute and State University

in partial fulfillment of the requirements for the degree of

DOCTOR OF PHILOSOPHY

in

Physics

APPROVED:

P. F. Zweifel, Chairman

R. L. Bowden

B. Dennison

W. Greenberg

M. Klaus

April, 1989

Blacksburg, Virginia

NONLINEAR EVOLUTION OF VLASOV EQUILIBRIA

by

Lucio Demeio

Committee Chairman: P. F. Zweifel

Physics

(ABSTRACT)

In this work, we investigate numerically the evolution of perturbed Vlasov equilibria, according to the full nonlinear system, with particular emphasis on analysing the asymptotic states towards which the system evolves. The simulations are carried out with the numerical code that we have implemented on the Cray X-MP of the Pittsburgh Supercomputing Center and which is based on the splitting scheme algorithm. Maxwellian, symmetric and one sided bump-on-tail and two-stream type of equilibrium distributions are considered: the only distribution which seems to evolve towards a BGK equilibrium is the two-stream while the asymptotic states for the other distributions are better described by superpositions of possible BGK modes. Perturbations with wave-like dependence in space and both symmetric and non-symmetric dependence on velocity are considered.

For weakly unstable modes, the problem of the discrepancy between different theoretical models about the scaling of the saturation amplitude with the growth rate is addressed, for the first time with the splitting scheme algorithm. The results are in agreement with the ones obtained in the past with less accurate algorithms and do not exhibit spurious numerical effects present in those.

Finally, collisions are included in the splitting scheme, in the form of the Krook model, and some simulations are performed, whose results are in agreement with

existing theoretical models.

## Acknowledgements

In first place, I would like to thank my adviser, Prof. Paul F. Zweifel, for suggesting the main ideas behind this work, for his competent help, his continuous interest and assistance and his illuminated guidance.

I would also like to express my gratitude to Dr. A. Klimas, for his constant availability to many fruitful discussions and for the many most valuable advices both on numerical and on analytical aspects of the topic.

Useful discussions with Prof. J. Batt, Prof. G. Hagedorn, Prof. S. Paveri Fontana, Prof. R. L. Bowden, Dr. J. Holloway and Dr. P. Hislop are gratefully acknowledged.

Physics and Mathematics have, quite often, to come down to earth and deal and fight with computer budgets, administrative difficulties and daily organization. It is the patience, dedication, sense of self-denial and exquisite friendliness of

that alleviate us from these burdens.

The people of the administrative and technical staff of the Pittsburgh Supercomputing Center are gratefully acknowledged for their helpful and competent assistance.

Finally, I would like to thank the closest friends I had during these three years here in Blacksburg for patiently bearing my moments of depression as well as sharing my moments of euphoria.

This work was supported by the Center for Transport Theory and Mathematical Physics through DOE grant DE-FG05-87ER25033 and NSF grant DMS8701050.

## Contents

# Chapter 1: Introduction.

It is the purpose of the present work to investigate numerically several aspects of the nonlinear behaviour of spatially homogeneous Vlasov equilibria of a one-dimensional unmagnetized plasma. Vlasov's equation governs the time evolution of the distribution function of the plasma species (ions and electrons) in those situations where the importance of binary collisions is negligible and collective effects dominate the dynamics of the particles' motion [1]. Under these circumstances, the force felt by each particle, due to the collective action of all the other particles, is represented by an average electromagnetic field (called self-consistent electromagnetic field) which has to obey Maxwell's equations; therefore, the whole set of the four Maxwell's equations has to be added to Vlasov's equation, yielding a set of simultaneous equations for the unknown distributions and fields. The nonlinearity of the problem arises from the fact that the source terms in Maxwell's equations, giving charge and current densities, contain velocity moments of the distribution function.

Since we shall consider only longitudinal electron waves, with fixed ions, only the electron distribution function will be of our concern and no magnetic field terms are present in our equations; this is also called electrostatic approximation. In particular, we shall be concerned with those cases in which Poisson's equation only is needed for the determination of the self-consistent electric field; we will comment on the Maxwell-Poisson reduction in the next chapter.

The integro-differential syatem of the coupled Vlasov and Poisson equations is known in the literature as the Vlasov-Poisson (VP) system and it is the simplest possible plasma kinetic model. While its linearized version has been extensively studied and its solution has been known for many years [2-3-4-5-6], no rigorous analyti-

cal result has ever been obtained for the full nonlinear system: only some heuristic models, that in some cases conflict with each other, have been formulated. Linear theory is supposed to give good account of the stability properties of the equilibrium solutions of (VP), although results have been recently reported [7] that question this point. The linearized equations have been solved in several ways, by means of Laplace transforms techniques [3], normal modes or eigenfunction expansions [4-5] and resolvent integration techniques [6]. The answer of all these models about the stability of spatially homogeneous equilibria are in full agreement, although different assumptions on the initial data are made in the different mathematical approaches. One of the motivations behind this work is to understand, on the basis of the numerical results, what the concepts of linear theory can tell about the behaviour of the system in the nonlinear regime. It turns out, as we shall point out, that the ideas underlying linear theory can still be used in the description of the asymptotic states. We shall also try to understand the relationship between the linear stability properties of spatially homogeneous equilibria and their stability as it results from the solution of the full nonlinear system, about which a rigorous result has recently been obtained [8].

A class of exact equilibrium solutions of (VP) was found by Bernstein, Green and Kruskal [9]. These solutions, which are called BGK equilibria and which we shall describe in some more detail in the next chapter, are often believed to represent the asymptotic states towards which the system evolves; however, as we shall see in Chapter 5, the numerical evidence goes against this belief in most cases. Indeed, the problem of whether BGK equilibria can be reached by the time evolution of the system from given initial data is still open.

Models that describe the nonlinear evolution of the system have been formulated in the past, either by using heuristic approaches [10-11] or small parameter expan-

sions [12-13-14]. Some of these models show serious discrepancies that we shall address numerically.

While analytical results for the full nonlinear Vlasov-Poisson system are lacking, numerical results have been made available in recent years by the appearance of more sophisticated algorithms and more powerful computational resources. The old techniques based on polynomial expansions [15-16-17] or particle simulation models [18] have been replaced by the more accurate splitting scheme algorithm [19] which allows long simulations to be carried out with much less computational effort than was required before. With the splitting scheme, some of the equilibria that we shall investigate have been followed for very long times and indications about the asymptotic states have been obtained [19-20-21]. In reproducing those results, we came to different conclusions (on the basis of the same numerical data) than the ones drawn by other authors.

The problems present in the numerical approach to Vlasov's equation are not entirely solved by the splitting scheme, and much work is still to be done in order to devise an algorithm that allows arbitrarily long simulations at a relatively small cost. A common practice is that of introducing filtered distributions [19-22], but no satisfactory result in this direction has been obtained so far with the splitting scheme: other algorithms, that unfortunately suffer from other more serious problems, seem to be better suited for this purpose [22].

This work is organized as follows. In Chapter 2 we describe the model and introduce the equations, outlining some important symmetry properties of the solutions, and the conservation laws for (VP). Also, the conditions under which the Maxwell-Poisson reduction is valid are specified. In the last section of the chapter, BGK

equilibria are discussed. In Chapter 3, the linearized Vlasov-Poisson system is presented and the two classical ways of obtaining the linear dispersion relation (á la Landau and á la Case-Van Kampen) are shown. Finally, the numerical solution of the dispersion relation is outlined, with a proposed method for the case when the equilibrium distribution is not analytically known, but only given on a set of points. In Chapter 4, the splitting scheme algorithm is discussed and the main problems arising in the numerical approach are indicated. In Chapter 5 we present the numerical results. The analogies between linearly stable and linearly unstable distributions in the nonlinear evolution of the system and, especially, in the asymptotic states, are stressed and a better understanding of these asymptotic states is achieved, sometimes in disagreement with the conclusions drawn by other authors. Only in one case (when perturbing the Two-Stream equilibrium distribution) the system is seen to approach asymptotically a BGK equilibrium. Perturbations of a different type than the ones that are usually considered are also analysed, and the specific differences in the linear and nonlinear behaviour are explained. In all the cases that we followed long enough for the system to be close to its asymptotic state, it is seen that this asymptotic state can be at least partially understood with a judicious use of linear theory concepts. In particular, the frequency of the oscillations never changes from the value given by the linear dispersion relation; also, the shape of the asymptotic space averaged distribution and the time behaviour of the electric field are consistent with linear theory. Then, the discrepancy between different models about the saturation of weakly unstable modes is addressed, for the first time with the splitting scheme algorithm. Some of the results previously obtained with less accurate algorithms [23-24] are confirmed, and two moderately long simulations are presented, which show some new feature with respect to earlier simulations. The relationship between the frequency of the amplitude oscillations and the strength of the initial perturbation in the linearly

stable cases and the saturation amplitude in the linearly unstable ones is also investigated. Finally, in Appendix A we show how a collisional term can be included in the splitting scheme and present a few simulations which show good agreement with existing theoretical models.

# Chapter 2: The Model

## 2.1 The Vlasov-Maxwell and the Vlasov-Poisson systems.

We shall consider a one-dimensional, unmagnetized and collisionless plasma, spatially confined in a box of length $L$ upon which periodic boundary conditions are imposed. The ions are assumed infinitely massive and form a neutralizing background. Moreover, charge neutrality is assumed throughout, i. e. the number of ions equals the number of electrons in the box.

The electron distribution function $f(x, v, t)$ and the self-consistent electric field $E(x, t)$ are the relevant physical quantities that describe this system. Here, $x \in [0, L]$ indicates the space variable, $v \in \mathbf{R}$ is the velocity variable and $t$ the time.

The time evolution of $f$ and $E$ is described by the Vlasov-Maxwell (VM) system

$$\frac{\partial f}{\partial t} + v\frac{\partial f}{\partial x} - E\frac{\partial f}{\partial v} = 0 \tag{2.1.1a}$$

$$\frac{\partial E}{\partial x} = 1 - \rho(x, t) \tag{2.1.1b}$$

$$\frac{\partial E}{\partial t} = u(x, t) \tag{2.1.1c}$$

$$\rho(x, t) = \int f \tag{2.1.1d}$$

$$u(x, t) = \int vf \tag{2.1.1e}$$

(where $x$ is measured in units of $\lambda_D = \sqrt{T/(4\pi ne^2)}$, $v$ in units of $v_{th} = \sqrt{T/m}$, $t$ in units of $\omega_p^{-1} = \sqrt{m/(4\pi ne^2)}$, $f$ in units of $n/v_{th}$ and $E$ in units of $4\pi en\lambda_D$, where $n$ is the plasma density, $T$ the temperature, $e$ the charge and $m$ the mass of the electron, and we adopt the convention $\int \equiv \int_{-\infty}^{\infty}(.)\,dv$), with the initial condition

$$f(x, v, 0) = g(x, v) \tag{2.1.2}$$

and boundary conditions $f(0, v, t) = f(L, v, t)$, $E(0, t) = E(L, t)$, and $lim_{|v|\to\infty} f(x, v, t) = 0$.

Under certain conditions, which we shall immediately specify, (VM) is equivalent to the Vlasov-Poisson (VP) system, i.e. eqs. (2.1.1a) and (2.1.1b) only.

Note, first, that (VP) leaves the boundary values or, alternatively, the space average of the electric field

$$< E(x,t) > \equiv \frac{1}{L}\int_0^L E(x,t)\,dx$$

undetermined. Therefore, if (VP) only has to be considered, it has to be specified under what conditions for $< E(x,t) >$ (or $E(0,t)$) the equations ought to be solved. Moreover, the assignement for $< E(t) >$ should not violate (2.1.1c), otherwise unphysical solutions would be obtained. Before investigating under what conditions on $< E(t) >$ (which actually amounts to a condition on the initial distribution) (VP) is equivalent to (VM), note that, if (2.1.1a) and (2.1.1c) hold for all $t$ and (2.1.1b) holds at $t = 0$, then (2.1.1b) holds for all $t$, since

$$\frac{\partial}{\partial t}(\frac{\partial E}{\partial x} - 1 + \rho) = \frac{\partial u}{\partial x} + \frac{\partial \rho}{\partial t} = 0$$

as follows from (2.1.1a) after integrating over $v$. In order to show the conditions under which (2.1.1a) and (2.1.1b) imply (2.1.1c), we first space-average (2.1.1c), which gives

$$\frac{\partial < E >}{\partial t} = < u > \qquad (2.1.3a)$$

Then, from (2.1.1a), multiplying by $v$, space averaging, substituting from (2.1.1b) and exploiting the periodicity of the boundary conditions we have

$$\frac{\partial < u >}{\partial t} = - < E > \qquad (2.1.3b)$$

A solution for $< u > (t)$ and $< E > (t)$ can be obtained from (2.1.3a) and (2.1.3b):

$$< u > (t) = < u > (0)\cos t - < E > (0)\sin t \qquad (2.1.4a)$$

$$< E > (t) = < u > (0)\sin t + < E > (0)\cos t \qquad (2.1.4b)$$

i.e. $< u(t) >$ and $< E > (t)$ perform harmonic motion (see also [25], where the problem is discussed in the more general framework of non-periodic boundary conditions). Equation (2.1.4b) gives the correct value for $< E > (t)$ to be used in (VP). In particular, it is immediately evident that, if (VP) is to be solved with $< E > (t) = 0$ for all times, it is not sufficient to demand that $< E > (0) = 0$, but $< u > (0) = 0$ is also required, which is satisfied by any equilibrium distribution which is symmetric in $v$. Therefore, if, as it is very often done in the literature, (VP) with $< E > (t) = 0$ for all $t$ is used to investigate the evolution of a perturbation to a spatially homogeneous non-symmetric equilibrium distribution, chosen such as $< u > (0) \neq 0$, (e.g., the one sided bump-on-tail), eq. (2.1.1c) is violated and the solution is unphysical. However, even in the presence of distributions that violate (2.1.1c), (VP) is still a consistent set of equations for $f$ and $E$ and, for the sake of comparison with other people's work and of a better formal understanding of the equations, we shall not exclude those cases from our investigations.

One might be tempted to look for solutions of (VM) by just solving (VP) and prescribing $< E > (t)$ from (2.1.4b) for all times. For a bump-on-tail distribution we would have

$$\begin{aligned}
< u > (0) &= L \int v f_0(v) \\
&= L \frac{1}{\sqrt{2\pi}} \int v \{ n_p e^{-\frac{v^2}{2}} + n_b e^{-\frac{1}{2}(\frac{v-V_0}{v_t})^2} \} \\
&= L \frac{n_b}{\sqrt{2\pi}} \int v e^{-\frac{1}{2}(\frac{v-V_0}{v_t})^2} \\
&= L \frac{n_b}{\sqrt{2\pi}} v_t \int_{-\infty}^{\infty} dx (x v_t + V_0) e^{-\frac{x^2}{2}} \\
&= L n_b v_t V_0
\end{aligned}$$

Here, $n_p$ and $n_b$ are the plasma and the beam densities and $v_t$ and $V_0$ the thermal and drift velocities of the beam respectively. Typical values (see Chapter 5) of the

parametrs would give

$$< u > (0) \approx 20 \times 0.2 \times 0.5 \times 4.5 = 9$$

which is much larger (by at least one order of magnitude) than the amplitude of any of the non-zero Fourier modes of the electric field (see again Chapter 5) during a whole simulation. Such a large electric field would make the numerical solution impossible with a realistically small grid.

### 2.1.1 The characteristics and the formal solution of (VP).

The Vlasov-Poisson system can formally be solved by the method of characteristics. The characteristic system for (VP) is

$$\dot{x} = v$$

$$\dot{v} = -E(x,t)$$

whose solution can be written as

$$x'(t') = \chi(t,t',x,v)$$

$$v'(t') = \eta(t,t',x,v)$$

with the boundary conditions

$$\chi(t,t,x,v) = x$$

$$\eta(t,t,z,v) = v$$

Vlasov's equation expresses the fact that the distribution function is constant along the characteristics. This allows one to write the formal solution of (VP) as

$$f(x,v,t) = f(\chi(t,0,x,v),\eta(t,0,x,v),0) \qquad (2.1.5)$$

with the electric field $E(x,t)$ given by Poisson's law. Using the formal solution (2.1.5) and the contraction principle, Batt [26] proved existence and uniqueness of the solution in 1963. A proof of existence and uniqueness for the whole (VM) system has been given by Klimas and Cooper [27] in 1972 and, again, by Klimas [28] in 1979.

According to the formal solution of (VP) written above, to obtain the value of the distribution function at the point $(x, v)$ of the phase space at the time $t$, we have to trace back to $t = 0$ the characteristic curve passing through $(x, v)$ at the time $t$; the projection of the characteristics on the phase space, therefore, coincides with the level curves of $f$. Of course, nothing more than the formal solution can be written analytically, but this is the method used in our simulations for the numerical integration of (VP). The numerical scheme will be descibed in Chapter 4.

The knowledge of the characteristic curves is important in that most of the physics described by (VP) lies in their structure. Since in most of the cases that we shall consider the electric field $E(x, t)$ is well represented by a sinusoid in space with a slowly varying time dependent amplitude, the form of the characteristics for $E(x, t) = E_0 \sin kx$ quite often plays a very important role in the physics; therefore, we want to look at them in some detail. Of course, this problem is completely analogous to the nonlinear harmonic oscillator.

Since we are dealing with a time independent electric field, the single particle energy

$$\mathcal{E} = \frac{v^2}{2} - \phi(x)$$

is a constant of motion; here

$$\begin{aligned} \phi(x) &\equiv -\int_0^x E(x')dx' \\ &= \frac{E_0}{k}\cos kx \\ &\equiv \phi_0 \cos kx \end{aligned}$$

is the electric potential and $\phi(x = 0) = 0$ has been chosen. Then we have for the velocity

$$v = \pm\sqrt{2(\mathcal{E} + \phi_0 \cos kx)}$$

leading to two distinct families of trajectories:

*(i)* open curves characterized by $\mathcal{E} > \phi_0$, for which any value of $x$ is allowed;

*(ii)* closed curves characterized by $-\phi_0 < \mathcal{E} < \phi_0$, for which there are two turning points, namely the solutions of $\cos kx = -\mathcal{E}/\phi_0$.

Electrons with energy $\mathcal{E} > \phi_0$ are on the open curves, so they are untrapped and can move anywhere in the physical space. On the contrary, electrons with energy $\mathcal{E} < \phi_0$ are trapped by the potential and just travel back and forth between the turning points. These last electrons are the ones which most effectively exchange energy with the wave and are responsible for the nonlinear damping or growth of the electric field amplitude. The two curves with $\mathcal{E} = \pm\phi_0$ are the separatrices of the two families of trajectories. The characteristics for $E(x,t) = E_0 \sin kx$ are shown in fig. 2.1; due to the particular shape of the closed orbits and of the separatrices, this particular pattern is called "cat's eye". If we had chosen $k = 2\pi m/L$, with $m > 1$, then we would see $m$ cat's eyes.

In the solution of (VP), higher harmonics will give non zero contributions to the electric field, so the characteristics will be deformed – although in most cases only slightly – with respect to the cat's eyes structure. Moreover, the amplitude of the electric field will change in time and so, since the electrons will see a slowly time-varying potential, their phase space orbits will not close but will somehow spiral in or out; this explains how the cat's eyes turn into vortices in phase space, as is known from already existing numerical results and from the ones we have obtained.

## 2.2 On some symmetry properties of the solutions of (VP).

It is often the case that the initial condition $g(x,v)$ (see (2.1.2)) is chosen of the form

$$g(x,v) = f_0(v)(1+\epsilon\cos kx) \tag{2.2.1}$$

where $f_0(v)$ is a spatially homogeneous equilibrium solution of (VP), $\epsilon \ll 1$ and $k$ is the wave number, satisfying $kL = 2\pi m$, with $m$ the mode number. If we assume that $f_0(v) = f_0(-v)$, then

$$g(x,v) = g(L-x,-v) \tag{2.2.2}$$

and we now show that this symmetry property is preserved by (VP). By the transformation

$$y = L - x$$

$$u = -v$$

$$h(y,u,t) = f(x,v,t)$$

$$K(y,t) = E(x,t)$$

(VP) becomes

$$\frac{\partial h}{\partial t} + u\frac{\partial h}{\partial y} + K\frac{\partial h}{\partial u} = 0$$

$$-\frac{\partial K}{\partial y} = 1 - \int h\,du$$

Therefore, we note by inspection that, if the pair of functions $(f,E)$ is a solution of (VP), also $(h,-K)$ is. Since at $t=0$ $h=f$ and $K=-E$, the uniqueness of the solution [26] requires that $f(x,v,t) = f(L-x,-v,t)$ and $E(x,t) = -E(L-x,t)$ at all times, provided it is true at $t=0$.

Note that, because of this symmetry property, the implication

$$< f(x,v,0) >=< f(x,-v,0) > \Rightarrow < f(x,v,t) >=< f(x,-v,t) >$$

follows:

$$
\begin{aligned}
&< f(x,-v,t) > \\
&= \frac{1}{L}\int_0^L f(x,-v,t)\,dx \\
&= \frac{1}{L}\int_0^L f(L-x,-v,t)\,dx \\
&= \frac{1}{L}\int_0^L f(x,v,t)\,dx \\
&=< f(x,v,t) > .
\end{aligned}
$$

If the initial perturbation is chosen such that $E(0,0) = E(L,0) = E(L/2,0) = 0$, then $E(0,t) = E(L,t) = E(L/2,t) = 0$ at all times, i.e. the nodes of the electric field do not propagate. This remains true if, instead of having $g(x,v) = f_0(v)(1+\epsilon\cos kx)$, we choose $g(x,v) = f_0(v)(1+\epsilon\sin kx)$, since this is just a space translation by $\pi/(2kL)$. Therefore, we do not expect to see travelling wave type solutions (see Section 2.5) when starting with these initial conditions.

### 2.3 Conservation laws.

The usual conservation laws for number of particles, $n(t)$, total momentum $p(t)$ and total energy $W(t)$ hold for (VM) and for (VP) with $< E > (t) = 0$. Define (in our dimensionless units):

$$
\begin{aligned}
n(t) &= \int_0^L dx \int f \\
p(t) &= \int_0^L dx \int vf \\
W(t) &= \int_0^L dx \left[E(x)^2 + \int v^2 f\right]
\end{aligned}
$$

Then we have:

$$\begin{aligned}\frac{dn}{dt} &= \int_0^L dx \int v\frac{\partial f}{\partial t} \\ &= \int_0^L dx \int (-v\frac{\partial f}{\partial x} + E\frac{\partial f}{\partial v}) \\ &= -\int_0^L dx\frac{\partial u}{\partial x} + \int_0^L dxE \int \frac{\partial f}{\partial v} \\ &= 0\end{aligned}$$

for the conservation of particles,

$$\begin{aligned}\frac{dp}{dt} &= \int_0^L dx \int v\frac{\partial f}{\partial t} \\ &= \int_0^L dx \int v(-v\frac{\partial f}{\partial x} + E\frac{\partial f}{\partial v}) \\ &= -\int_0^L dx\frac{\partial \int v^2 f}{\partial x} + \int_0^L dxE \int v\frac{\partial f}{\partial v} \\ &= -\int_0^L dxE\rho \\ &= -\int_0^L dxE(1 - \frac{\partial E}{\partial x}) \\ &= L < E > \\ &= 0\end{aligned}$$

for the conservation of momentum and

$$\begin{aligned}\frac{dW}{dt} &= \int_0^L dx(2E\frac{\partial E}{\partial t} + \int v^2\frac{\partial f}{\partial t}) \\ &= \int_0^L dx\{2E\frac{\partial\left[\int_0^x (1-\rho(y))dy\right]}{\partial t} + \int v^2(-v\frac{\partial f}{\partial x} + E\frac{\partial f}{\partial v})\} \\ &= \int_0^L dx\left[2E(-\int_0^x \frac{\partial\rho(y)}{\partial t}dy) - \int v^3\frac{\partial f}{\partial x} + E\int v^2\frac{\partial f}{\partial v}\right] \\ &= 2\int_0^L dxE\int_0^x \frac{\partial u(y)}{\partial y}dy - 2\int_0^L dxE\int vf \\ &= 2\int_0^L dxE\left[u(x) - u(0)\right] - 2\int_0^L dxEu(x) \\ &= -2u(0)\int_0^L dxE \\ &= -2Lu(0)L < E >\end{aligned}$$

for the conservation of energy. We see that conservation of momentum and conservation of energy require the condition $< E > (t) = 0$, while conservation of particles does not. Also, since no dissipation is present in the system, (VP) conserves the total entropy

$$S(t) = \int_0^L dx \int f ln f$$

without any constraint on $< E > (t)$:

$$\begin{aligned}
\frac{dS}{dt} &= \int_0^L dx \int (lnf + 1)\frac{\partial f}{\partial t} \\
&= \int_0^L dx \int (lnf + 1)(-v\frac{\partial f}{\partial x} + E\frac{\partial f}{\partial v}) \\
&= \int_0^L dx(-\frac{\partial u}{\partial x} + E\int \frac{\partial f}{\partial v}) - \int v \int_0^L dx \frac{\partial f}{\partial x} lnf + \int_0^L dx E \int \frac{\partial f}{\partial v} lnf \\
&= \int v \int_0^L dx \frac{\partial f}{\partial x} - \int_0^L dx E \int \frac{\partial f}{\partial v} \\
&= 0
\end{aligned}$$

These conservation laws will be used in our code as a benchmark for the validity of the numerical solution.

### 2.4 Stability.

Being the solution of (VP) constant along characteristics, the distribution function remains bounded for all times, provided it is bounded at $t = 0$. This property, however, which is sometimes referred to as global stability, does not provide any information about the stability of equilibrium solutions of (VP), for which other definitions have to be adopted. In particular, one would like to know if a given small perturbation to an equilibrium state grows in time, driving the system away from that equilibrium, or if it decays, driving the system back to the equilibrium state and possibly oscillating about it. However, while the stability analysis of many mechanical systems (e.g., a simple pendulum) can be carried out in the framework

of a linear appriximation, this method could lead to quite misleading conclusions in the present case. In the case of a simple pendulum, for example, if the system is given a very small perturbation about a stable equilibrium, a linearized model describes various properties of the time evolution with very good approximation for arbitrarily long times; moreover, the smaller the initial perturbation, the better the linear approximation describes the behaviour of the system, without nonlinear effects ever coming into play. A quite different situation is encountered when analysing the stability of Vlasov equilibria. As we shall see in the next chapter, the linear approximation breaks down after a finite time, no matter how small a perturbation the system is given, and therefore it cannot be used in order to predict the long time behaviour of the solutions. For this reason, we have to distinguish between the concepts of stability and linear stability. We shall call an equilibrium solution of (VP) linearly stable if any given perturbation is predicted to decay in time by linear theory and linearly unstable if there exist perturbations that linear theory predicts to grow in time. More generally, if $f_0(v)$ is a spatially homogeneous solution of (VP), it will be called stable if, for each neighbourhood $U$ of $f_0$, there exists a neighbourhood $V$ of $f_0$ such that, if $f(x,v,0) \in V$ then $f(x,v,t) \in U$ for all $t$. This definition can obviously be extended to spatially inhomogeneous equilibria, but since linear theory for spatially inhomogeneous equilibria is not well developed, we shall be concerned only with spatially homogeneous equilibria.

Rigorous mathematical results on the relationship between stability and linear stability are still lacking, the only achievement so far being due to Marchioro and Pulvirenti [8], who proved the stability of spatially homogeneous distributions which are monotonically decreasing functions of the single particle energy. We shall try to draw some conclusions about this question from our numerical results.

## 2.5 Exact nonlinear solutions (BGK equilibria).

A class of solutions of the Vlasov Poisson system has been found by Bernstein, Green and Kruskal in 1957 [9]. First, let us state the invariance of the (VP) system under a galileian transformation. If $f(x,v,t)$ and $E(x,t)$ are solutions of (2.1.1a) and (2.1.1b) then, for an arbitrary $V \in \mathbb{R}$, define $f'(x,v,t) \equiv f(x',v',t)$ and $E'(x,t) \equiv E(x',t)$, with $x' = x - Vt$ and $v' = v - V$. Then we have:

$$\frac{\partial f'}{\partial t} = \frac{\partial f}{\partial t} - V\frac{\partial f}{\partial x}$$
$$\frac{\partial f'}{\partial v'} = \frac{\partial f}{\partial v}$$
$$\frac{\partial f'}{\partial x'} = \frac{\partial f}{\partial x}$$
$$\frac{\partial E'}{\partial x'} = \frac{\partial E}{\partial x}$$
$$\frac{\partial E'}{\partial t} = \frac{\partial E}{\partial t} - V\frac{\partial E}{\partial x}$$
$$\int f'dv' = \int f dv$$
$$\int v'f'dv' = \int vf dv - V\int f dv$$

Therefore

$$\begin{aligned}
&\frac{\partial f'}{\partial t} + v'\frac{\partial f'}{\partial x'} - E'\frac{\partial f'}{\partial v'} \\
&= \frac{\partial f}{\partial t} - V\frac{\partial f}{\partial x} + (v+V)\frac{\partial f}{\partial x} - E\frac{\partial f}{\partial v} \\
&= \frac{\partial f}{\partial t} + v\frac{\partial f}{\partial x} - E\frac{\partial f}{\partial v} \\
&= 0
\end{aligned}$$

and

$$\frac{\partial E'}{\partial x'} = \frac{\partial E}{\partial x} = 1 - \int f dv = 1 - \int f'dv'$$

i.e. $E'$ and $f'$ are a solution of (VP) as well. Therefore, from any solution of (VP), one can construct an infinite family of them by applying a galileian transformation. In particular, once a spatially periodic stationary solution of (VP) is given, an infinite

family of spatially periodic travelling waves can be found. These are the solutions considered by Bernstein, Green and Kruskal in their paper; from the names of the authors such solutions are called BGK equilibria. Hence, BGK equilibria are solutions of (VP) such that there exists a galileian transformation into a coordinate system in which $f$ and $E$ are time independent. In other words, $f$ and $E$ must be of the form $f(x,v,t) = f'(x - Vt, v)$ and $E(x,t) = E'(x - Vt)$ for some real $V$.

Consider the stationary Vlasov-Poisson system:

$$v\frac{\partial f}{\partial x} - E\frac{\partial f}{\partial v} \tag{2.5.1a}$$

$$\frac{\partial E}{\partial x} = 1 - \int f \tag{2.5.1b}$$

In order to describe BGK equilibria, it turns out more convenient to work with the electric potential

$$\phi(x) = -\int_0^x E(x')dx'$$

where $\phi(0) = 0$ has been chosen and the time dependence of the functions has now been dropped. In terms of the potential, (2.5.1a) and (2.5.1b) become

$$v\frac{\partial f}{\partial x} + \frac{d\phi}{dx}\frac{\partial f}{\partial v} = 0 \tag{2.5.2a}$$

$$-\frac{d^2\phi}{dx^2} = 1 - \int f \tag{2.5.2b}$$

Since the electrons feel a time independent potential, the single particle energy

$$\mathcal{E} \equiv \frac{v^2}{2} - \phi(x)$$

is a constant of motion; therefore, a function of the single particle energy is a solution

of (2.5.2a) and (2.5.2b): if $f(x,v) = F(\mathcal{E})$ we have

$$\begin{aligned} & v\frac{\partial f}{\partial x} + \frac{d\phi}{dx}\frac{\partial f}{\partial v} \\ &= v\frac{dF}{d\mathcal{E}}\frac{\partial \mathcal{E}}{\partial \S} + \frac{d\phi}{dx}\frac{dF}{dx}\frac{\partial \mathcal{E}}{\partial \sqsubseteq} \\ &= \frac{dF}{d\mathcal{E}}(-v\frac{d\phi}{dx} + v\frac{d\phi}{dx} \\ &= 0 \end{aligned}$$

Some of the electrons will be trapped in the potential well and some will be untrapped; namely, from

$$v = \pm\sqrt{2(\mathcal{E} + \phi(x))}$$

we have that electrons having energy $\mathcal{E} \in [-\phi_{max}, -\phi_{min}]$ are trapped, while electrons with $\mathcal{E} > -\phi_{min}$ are untrapped. This enters in transforming the integral in (2.5.2b) from the velocity variable to the energy:

$$\begin{aligned} \int f dv &= \int_{-\phi(x)}^{\infty} d\mathcal{E}\frac{F(\mathcal{E})}{\sqrt{2(\mathcal{E} + \phi(x))}} \\ &= \int_{-\phi(x)}^{\phi_{min}} d\mathcal{E}\frac{F(\mathcal{E})}{\sqrt{2(\mathcal{E} + \phi(x))}} + \int_{-\phi_{min}}^{\infty} d\mathcal{E}\frac{F(\mathcal{E})}{\sqrt{2(\mathcal{E} + \phi(x))}} \end{aligned}$$

and therefore

$$-\frac{d^2\phi}{dx^2} = 1 - \int_{-\phi(x)}^{-\phi_{min}} d\mathcal{E}\frac{F(\mathcal{E})}{\sqrt{2(\mathcal{E} + \phi(x))}} + \int_{-\phi_{min}}^{\infty} d\mathcal{E}\frac{F(\mathcal{E})}{\sqrt{2(\mathcal{E} + \phi(x))}}$$

the first integral being over the trapped electrons and the second over the untrapped ones. It follows that one can prescribe, for example, the potential $\phi(x)$ and the distribution of the untrapped electrons and then solve for the trapped electron distribution. Alternatively, one can solve for the distribution of the trapped electrons or the one of the untrapped electrons.

The class of BGK equilibria is quite large (we don't want to dwell on the precise meaning of "large"), since, as shown in the original paper, almost any potential wave

form with continuous second derivatives can be achieved, by properly prescribing the distribution of the untrapped electrons. Note also that, while for the trapped electrons the distribution must be the same for both signs of velocity (because $f$ must be independent of time), this is not required for the untrapped electrons: therefore, given a periodic potential of a certain wave length, it is possible (via a galileian transformation) to obtain waves travelling with arbitrary phase velocity, keeping the average velocity of the plasma equal to zero by rearranging the distribution of the untrapped electrons between the two directions of velocity. It follows that a dispersion relation in the sense of a one-to-one correspondance between phase velocity and wave length does not exist for BGK modes.

The importance of BGK equilibria lies mainly in the fact that they are easier to analyse than other types of solutions. As we shall see in Chapter 5, there are not many cases in which the system evolves towards a BGK equilibrium starting from a given distribution, and the problem of how BGK equilibria can be reached is completely open.

In recent years, by using Lie groups techniques, several authors have found canonical transformations which, under the condition that the potential can be written in a specific form, allow to reduce Vlasov's equation to a partial differential equation in two variables. Namely, if new time, position and velocity coordinates are introduced, the transformed distribution and the transformed electric field are independent of time (in the new variables); the resulting equations in the new coordinates are therefore of the BGK type and are called generalized BGK equilibria. Several solutions have been found [29-30-31-32-33-34] for several forms of the potential; however, there seems to be still a long way before the solution to the initial value problem (in the laboratory coordinates) can be given by using these methods.

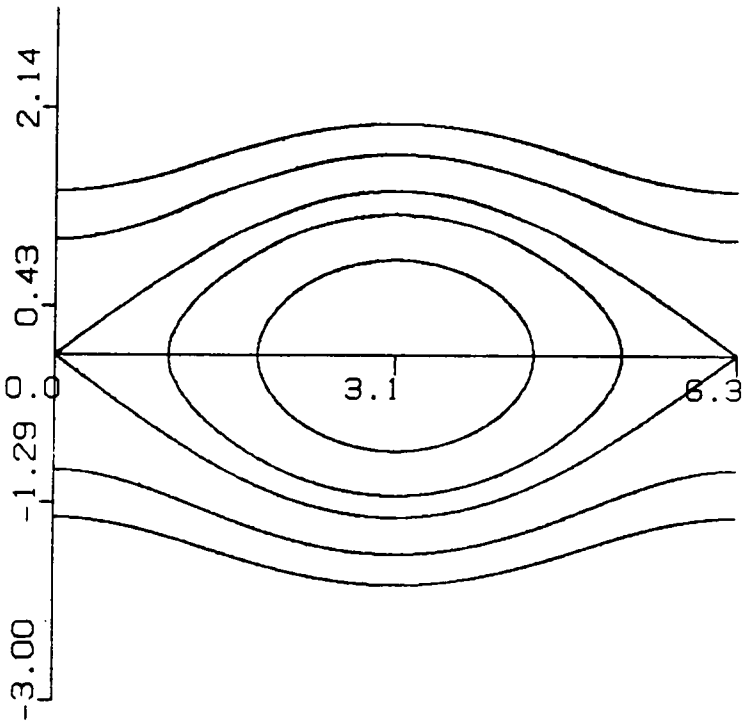


Fig. 2.1 Characteristics for sinusoidal electric field.

## Chapter 3: The Linearized Vlasov-Poisson System

### 3.1 Introduction.

For small perturbations about a spatially homogeneous equilibrium, a linearized model is appropriate to describe the evolution of the system. In the linearized model the orbits of the electrons are assumed to be straight lines; when the actual characteristics of (VP) (see Section 2.2.1 and the example there described) start influencing significantly the motion of the electrons, so that it doesn't occur along unperturbed trajectories any more, the linearization breaks down and nonlinear effects must be taken into account in the solution. Thus, the amplitude of the perturbation being small is not the only requirement for the linear approximation to remain valid. However, some of the information given by linear theory about the time evolution of the system bears a broader validity than it is usually assumed. We shall discuss this point when the results of our numerical investigations will be presented.

The linearized Vlasov-Poisson system (LVP) has been extensively studied, its solution has been known for long time and it has been obtained in at least three different ways, two of which we shall illustrate in the next section, without dwelling on well known technical details.

### 3.2 The linearized equations.

A function of $v$ only, say $f_0(v)$, is an equilibrium solution of (VP) with no electric field. Let's write the distribution function as

$$f(x,v,t) = f_0(v) + \epsilon \tilde{f}(x,v,t) \tag{3.2.1}$$

with $\epsilon \ll 1$. Then, since

$$\frac{\partial E}{\partial x} = 1 - \int f = -\epsilon \int \tilde{f},$$

the electric field is $O(\epsilon)$, i.e. $E(x,t) = \epsilon\tilde{E}(x,t)$. To $O(\epsilon)$ (VP) becomes

$$\frac{\partial \tilde{f}}{\partial t} + v\frac{\partial \tilde{f}}{\partial x} - \tilde{E}\frac{\partial f_0}{\partial v} = 0$$
$$\tilde{E} = -\int \tilde{f}$$

Fourier transforming according to

$$\tilde{f}(x,v,t) = \sum_k f_k(v,t)e^{ikx}$$
$$\tilde{E}(x,t) = \sum_k E_k(t)e^{ikx}$$

(LVP) becomes, for each mode $k \neq 0$,

$$\frac{\partial f_k}{\partial t} + ikvf_k - E_k\frac{\partial f_0}{\partial v} \qquad (3.2.2a)$$
$$ikE_k = -\int f_k \qquad (3.2.2b)$$

Note that the $k = 0$ mode corresponds to the space average of the functions, so we have

$$E_0(t) =< E(x,t) >= 0$$

$$f_0(v,t) =< \tilde{f}(x,v,t) >= 0$$

which makes clear that (LVP) does not take into account the time dependence of the space averaged distribution. This time dependence can be calculated explicitely in quasilinear approximation; by allowing for a time dependence in $f_0$, i.e. $f_0 = f_0(v,t)$ in (3.2.1), with $f_0(v, t=0) = f_0(v)$, the space average of (VP) yields

$$\frac{\partial f_0(v,t)}{\partial t} = \epsilon^2 < \tilde{E}(x,t)\frac{\partial \tilde{f}(x,v,t)}{\partial v} >$$

which shows that $\partial f_0/\partial t$ is $O(\epsilon^2)$ and cannot be included in a linearized model.

It should be mentioned here that, in linearizing Vlasov's equation, in addition to assuming that the perturbation is small compared to the equilibrium distribution, one implicitly assumes that the perturbation itself does not have large velocity gradients,

since the term $\epsilon^2 \tilde{E} \partial \tilde{f} / \partial v$ is assumed to be $O(\epsilon^2)$. Therefore, we do not expect linear theory to be valid if an initial distribution with large velocity gradients is chosen.

### 3.3 The Landau and the Case solutions.

Substituting (3.2.2b) in (3.2.2a) one obtains

$$\frac{\partial f_k}{\partial t} + ikvf_k - \frac{i}{k}\frac{\partial f_0}{\partial v}\int f_k = 0 \tag{3.3.1}$$

which has to be solved subject to the initial condition $f_k(v, t = 0) = f_k(v, 0)$. If we look at solutions of the form $f_k \sim e^{-i\omega t}$, we find that

$$1 + \frac{1}{k^2}\int \frac{\partial f_0/\partial v}{v - \omega/k} = 0 \tag{3.3.2}$$

is a necessary condition for nontrivial solutions to exist. The integral in (3.3.2) becomes singular if $Im\omega = 0$ and a prescription is needed to deal with this singularity. In the approach used by Landau [3], Laplace transforms are used to solve (3.3.1) as an initial value problem. Then, the solution can be written as

$$f_k(v, t) = f_k(v, 0)e^{-ikvt} - \frac{1}{k^2}\sum_j q_j \frac{\partial f_0/\partial v}{v - \nu_j} e^{-ik\nu_j t} \tag{3.3.3}$$

Here, the $\nu_j$'s are the complex solutions of

$$\Lambda_k(\nu) \equiv 1 + \frac{1}{k^2}\int_L \frac{\partial f_0/\partial v}{v - \nu} \tag{3.3.4}$$

where the contour L (called Landau contour) is shown in figs. 3.1a, 3.1b and 3.1c for $Im\nu > 0$, $Im\nu = 0$ and $Im\nu < 0$ respectively and

$$q_j = \left(\lim_{\nu \to \nu_j} \frac{\Lambda_k(\nu)}{\nu - \nu_j}\right)^{-1} \int \frac{f(v, 0)}{v - \nu_j} \tag{3.3.5}$$

In (3.3.5), it has been assumed that $\Lambda_k(\nu)$ has only simple roots. Roots with greater multiplicity present a problem, which has been addressed and solved in [6], where a

different approach to the linearized problem was used. We will never consider cases where multiple roots appear, so we shall neglect this difficulty.

The function $\Lambda_k(\nu)$ defined in (3.3.4) is analytic in the complex $\nu$ plane and its roots determine the linear stability properties of the solution. In (3.3.3), the first term is the free-streaming contribution to the distribution function and becomes more end more oscillatory in velocity space as time proceeds. It does not contribute to the moments of the distribution, but its presence gives rise to serious difficulties in the numerical approach to Vlasov's equation, as we shall see in the next chapter. When the Fourier modes that enter the time evolution of the system form a continuous spectrum, with roughly uniform energy density, contributions coming from different parts of the spectrum will phase mix to zero; this fact plays a crucial role in the derivation of the quasilinear equations. When a finite system is considered, as is done here, the spectrum is discrete and, in many cases, one of the modes dominates. In this last case, the action of the first term in (3.3.3) is simply that of twisting the wavelike structure from the physical space, where it initially lives, into the velocity space, rapidly causing the formation of large velocity gradients. The nature of the other terms depends on the location of the roots of the dispersion relation (3.3.4) in the complex $\nu$ plane. Terms corresponding to roots with positive imaginary part (unstable roots) grow exponentially with time giving rise to (linear) instability, while terms corresponding to roots with negative imaginary part (stable roots) are exponentially damped in time. This is called Landau damping. It is the nature of of the equilibrium distribution and the wave number of the perturbation which determine the location of the roots of (3.3.4) in the complex $\nu$ plane. For some equilibrium distributions there are no unstable roots, so the equilibrium is stable against any perturbation, while other equilibria are unstable against perturbations in a certain range of wave

numbers. Finally, for roots with zero imaginary part, linear theory predicts steady-state oscillations.

Note that, in the Landau approach, the initial distribution function must be analytic in the region of the complex plane where the Landau contour lies. This is not a serious restriction from the physical point of view, since all the physically relevant distributions can be extended analytically to the entire complex plane. This analyticity assumption is not needed in the approach adopted by Case [5], which makes use of an expansion in singular eigenfunctions. Equation (3.3.1) can be rewritten as

$$\frac{\partial f_k}{\partial t} = L_k f_k \tag{3.3.6}$$

where the linear operator $L_k$ is defined as

$$L_k f_k = (-ikv + \frac{i}{k}\frac{\partial f_0}{\partial v}\int) f_k$$

Then, looking for solutions of the form $f_k \sim e^{-i\omega t}$ is equivalent to studying the spectrum of $L_k$:

$$L_k \phi_\lambda = \lambda \phi_\lambda$$

where $\lambda \equiv -i\omega$. According to Case's result, the spectrum of $L_k$ has a continuous part, $\sigma_c(L_k) = \mathbb{R}$ and a discrete part, $\sigma_d(L_k) = \{\lambda_j\}$, where $\lambda_j$ is a solution of

$$\Lambda_k(\nu) \equiv 1 + \frac{1}{k^2}\int \frac{\partial f_0/\partial v}{v - \nu} = 0 \tag{3.3.7}$$

with $\nu = i\lambda/k$. The function $\Lambda_k(\nu)$ is analytic in the cut plane $\mathbb{C} \setminus \mathbb{R}$, with continuous boundary values $\Lambda_k^{\pm}(\nu)$ evaluated on the branch cut $\mathbb{R}$ from above and from below. For $Im\nu > 0$, $\Lambda_k(\nu)$ coincides with the Landau dispersion function; in the lower half plane ($Im\nu \leq 0$) the Landau dispersion function is the analytic continuation of (3.3.7). Note that, since $\Lambda_k(\nu^*) = [\Lambda_k(\nu)]^*$, the roots of (3.3.7) occur in complex

conjugate pairs. The eigenfunctions $\phi_\lambda$ are

$$\phi_\lambda = \frac{1}{k^2}\frac{\partial f_0/\partial v}{v-\nu} + \xi(v)\delta(v-\nu), \lambda \in \sigma_c \tag{3.3.8a}$$

$$\phi_{\lambda_j} = \frac{1}{k^2}\frac{\partial f_0/\partial v}{v-\nu_j}, \lambda_j \in \sigma_d \tag{3.3.8b}$$

and form a complete set of orthonormal functions.Then, the solution can be written as

$$f_k(v,t) = \int A_\lambda \phi_\lambda(v) e^{\lambda t} d\lambda + \sum_j a_j \phi_{\lambda_j} e^{\lambda_j t} \tag{3.3.9}$$

where the coefficients $A_\lambda$ and $a_j$ can be computed using orthogonality; e.g.,

$$a_j = (\int \tilde{\phi}_\lambda \tilde{\phi}_{\lambda_j})^{-1} \int \tilde{\phi}_{\lambda_j} f_0$$

with the adjoint eigenfunctions $\tilde{\phi}_{\lambda_j} = -1/(v-\nu_j) + \tilde{\xi}(v)\delta(v-\nu_j)$. Here, $\xi(v) = [\Lambda_k^+(v) + \Lambda_k^-(v)]/2$ and $\tilde{\xi}(v)$ is arbitrary.

Case's result is equivalent to Landau's result, as shown in [5]. However, the singular eigenfunction approach has the advantage that no analyticity assumption on the initial data is needed; moreover, the way linearly stable and unstable cases are dealt with differs in the two methods. Since the roots of Case's dispersion relation, $\Lambda_k(\nu) = 0$, occur in complex conjugate pairs, the presence of a root with nonvanishing imaginary part automatically guarantees linear instability, so it is the continuous spectrum which gives the damped solutions. For example, in the case of a single-humped equilibrium distribution, all the roots of (3.3.4) have negative imaginary part, while (3.3.7) has no roots and the discrete sum in (3.3.9) is absent.

As shown in [35], the Landau dispersion relation has infinitely many stable roots, and a finite number (possibly zero) of unstable roots. It is obviously the root with the largest imaginary part that determines the behaviour of the solution for large times (always within the validity of the linear approximation); in case of stable equilibria,

this root has to be found using the Landau dispersion relation, so we shall always make use of (3.3.4) in our computations.

Finally, we want to recall the results of the linear stability analysis for some relevant spatially homogeneous equilibrium distributions. Since they can be found in almost any plasma physics textbook, we don't go into the details of their derivation.

Single humped distributions (such as maxwellians, shifted or not) are always stable, i.e. the Landau dispersion relation has no roots in the upper half plane. For an equilibrium distribution to be linearly unstable there must exist, in the refernce frame consistent with the bulk velocity of the electrons, an interval in the velocity variable where $v\partial f/\partial v > 0$. In other words, looking at positive (negative) velocities. the distribution must have a rising (falling) portion. Then, the distribution will be unstable against perturbations having wave number $k$ such that $v_\phi \equiv \omega_r/k$ falls in the rising (falling) portion of the distribution. Here, $\omega_r$ is the real part of the frequency given by the linear dispersion relation. Electrons having $v \approx v_\phi$ exchange energy with the wave; the ones travelling slightly slower than the wave take energy from it while the ones travelling slightly faster give energy to the wave. Therefore, if the phase velocity of the wave falls in the rising (falling) portion of the distribution there are more electrons giving energy to than electrons taking energy from the wave, giving rise to instability. Of course, this picture is modified when nonlinear effects start playing a role. Typical examples of spatially homogeneous equilibrium distributions which are unstable against perturbations in a certain range of wave numbers are the bump-on-tail (symmetric or not), the two stream and the lorentzian. Although analytical studies about this last distribution do exist, its rate of decay at infinity is so slow that it makes numerical investigations impractical. Therefore, we shall consider only maxwellian, bump-on-tail and two-stream type distributions.

### 3.4 Numerical solutions of the Landau dispersion relation.

There are few equilibrium distributions for which (3.3.4) can be solved analytically. For the equilibria of our concern, however, a numerical solution can be easily obtained. It is convenient to introduce the plasma dispersion function [36]

$$Z(\nu) = \frac{1}{\sqrt{\pi}} \int_{-\infty}^{\infty} \frac{e^{-x^2}}{x - \nu} dx, \; Im\nu > 0 \tag{3.4.1}$$

with analytic continuation in the lower half plane. The plasma dispersion function is related to the error function $erf(z)$ by $Z(\nu) = i\sqrt{\pi} e^{-\nu^2}[1 - erf(-i\nu)]$ and is therefore easily computable with very high accuracy using library subroutines available with most computers. The Landau dispersion function, $\Lambda_k(\nu)$. can be written in terms of the plasma dispersion function for a number of physically interesting distributions. Here are the expressions for the cases of our concern:

($i$): Maxwellian distribution

$$f_0(v) = \frac{1}{\sqrt{2\pi}} e^{-\frac{v^2}{2}}$$

$$\Lambda_k(\nu) = 1 + \frac{1}{k^2}[1 + \nu Z(\nu)]$$

($ii$): Drifted maxwellian

$$f_0(v) = \frac{1}{\sqrt{2\pi}} e^{-\frac{1}{2}(\frac{v - v_0}{v_t})^2}$$

$$\Lambda_k(\nu) = 1 + \frac{1}{k^2} \frac{1}{v_t}[1 + \nu_- Z(\nu_-)]$$

($iii$): Two-stream distribution

$$f_0(v) = \frac{1}{\sqrt{2\pi}} v^2 e^{-\frac{v^2}{2}}$$

$$\Lambda_k(\nu) = 1 + \frac{1}{k^2}\{1 - 2(1 - \nu^2)[1 + \nu Z(\nu)]\}$$

($iv$): One sided bump-on-tail

$$f_0(v) = \frac{N}{\sqrt{2\pi}} e^{-\frac{v^2}{2}} + \frac{n}{\sqrt{2\pi}} e^{-\frac{1}{2}(\frac{v - v_0}{v_t})^2}$$

$$\Lambda_k(\nu) = 1 + \frac{1}{k^2}\{N[1 + \nu Z(\nu)] + \frac{n}{v_t}[1 + \nu_- Z(\nu_-)]\}$$

$(v)$: Symmetric bump-on-tail

$$f_0(v) = \frac{N}{\sqrt{2\pi}} e^{-\frac{v^2}{2}} + \frac{n}{\sqrt{2\pi}} \{ e^{-\frac{1}{2}(\frac{v-V_0}{v_t})^2} + e^{-\frac{1}{2}(\frac{v+V_0}{v_t})^2} \}$$

$$\Lambda_k(\nu) = 1 + \frac{1}{k^2} \{ N[1 + \nu Z(\nu)] + \frac{n}{v_t} [2 + \nu_- Z(\nu_-) + \nu_+ Z(\nu_+)] \}$$

In $(iv)$ and $(v)$, $N$ is the plasma density, $n$ the density, $v_t$ the thermal velocity and $V_0$ the drift velocity of the beam(s). Because of the normalization condition $\int f_0 = 1$ we must have $N = 1 - nv_t$ in the one sided case and $N = 1 - 2nv_t$ in the symmetric case. Finally, $\nu_\pm = \nu \pm V_0/(v_t\sqrt{2})$.

For the numerical solution of (3.3.4) we used Nyquist diagrams methods [1] (mainly to approximately locate the roots) in combination with Mueller's method to find the zeros of an analytic function.

The numerical solution of the Landau dispersion relation for these "classical" equilibrium distributions will be used to obtain the real and imaginary parts of the frequency, with which the values resulting from our numerical simulations have to be compared.

### 3.4.1 Numerical solution for a dataset function.

We shall be interested in calculating the roots of the Landau dispersion relation for the spatially averaged distribution function $< f >$ that results from the numerical solution of (VP). Then, an explicit expression for this function is not available, but the function itself is known only on a finite number of points in velocity space. Assuming, at the outset, that $< f >$ has an analytic continuation in the complex plane, the problem is to find this analytic continuation and then use it in order to solve (3.3.4). Obviously, since $< f >$ is only known on a set of points on the real line, the approximation to its analytic extension will be good only near the real axis; mainly for this reason, we shall use this method only when the roots of (3.3.4) are on

the real axis or very close to it.

Let $\{f_j\}$ be the known values of $< f >$ on the set of points $\{v_j\}$, $j = 1, \ldots, M$. The most natural way of obtaining an approximation to the analytic extension of $< f >$ is to make an analytic fit, i.e. to have an analytic function passing through the $M$ points $v_1, v_2, \ldots, v_M$. Also, for our type of problem, the most natural choice for the analytic function is a maxwellian or a sum of maxwellians. In this spirit, we write for the analytic continuation $\Phi(v)$:

$$\Phi(v) = \sum_{j=1}^{M} \frac{1}{\sqrt{2\pi}} d_j e^{-\frac{1}{2}(\frac{v-V_j}{\alpha \Delta v})^2}$$

where $\Delta v$ is the step size in velocity. Moreover, we choose $\{V_j\} = \{v_j\}$, with $v_j = -\Delta v/2 + \Delta v(j - M/2)$ (see the description of the code in Chapter 4). Because of the normalization condition $\int \Phi = 1$ we must have $\sum_{j=1}^{M} d_j \alpha \Delta v = 1$. By imposing that $\Phi(v)$ passes through the points $(v_j, f_j)$ we have the linear system for the coefficients $\{d_j\}$

$$\sum_{j=1}^{M} \frac{1}{\sqrt{2\pi}} d_j e^{-\frac{1}{2}(\frac{i-j}{\alpha})^2} = f_i$$

where $v_i - v_j = \Delta v(i - j)$ has been used. The Landau dispersion function for $< f >$ can now be written as

$$\Lambda_k(\nu) = -\sum_{i=1}^{M} \frac{d_i}{\alpha \Delta v}[1 + \nu_i Z(\nu_i)]$$

with $\nu_i = \frac{\nu - V_i}{\alpha \Delta v \sqrt{2}}$. The parameter $\alpha$ controls the width of the maxwellians with respect to the grid spacing. It turns out that the accuracy of the approximation is very sensitive to both $\alpha$ and $M$. Unfortunately, if the approximation appears to be good for some $M$, increasing the number of points does not bring any improvement, but it rather makes the situation worse. We checked the validity of the method by using a maxwellian distribution, for which the analytic extension is obviously known.

With $\nu = 1 - 0.5i$ and $M = 64$ we found for the relative error in $\Lambda_k(\nu)$ as function of $\alpha$ the values shown in Table 3.1. Note that in the range $1.5 < \alpha < 2.2$ the relative error stays small and constant, while it becomes unacceptably large immediately outside this interval. For the same values of $\alpha$ and $\nu$ but with $M = 128$ we could never find a relative error smaller than 6. As $\nu$ is let to approach the real axis, errors become much smaller and they remain small on a wide range of values for $\alpha$ and $M$. Since we shall be interested in finding the roots of (3.3.4) when $\nu$ is very close to the real axis ($Im\nu \sim 10^{-2}$ or smaller) we shall be satisfied with the use of this method.

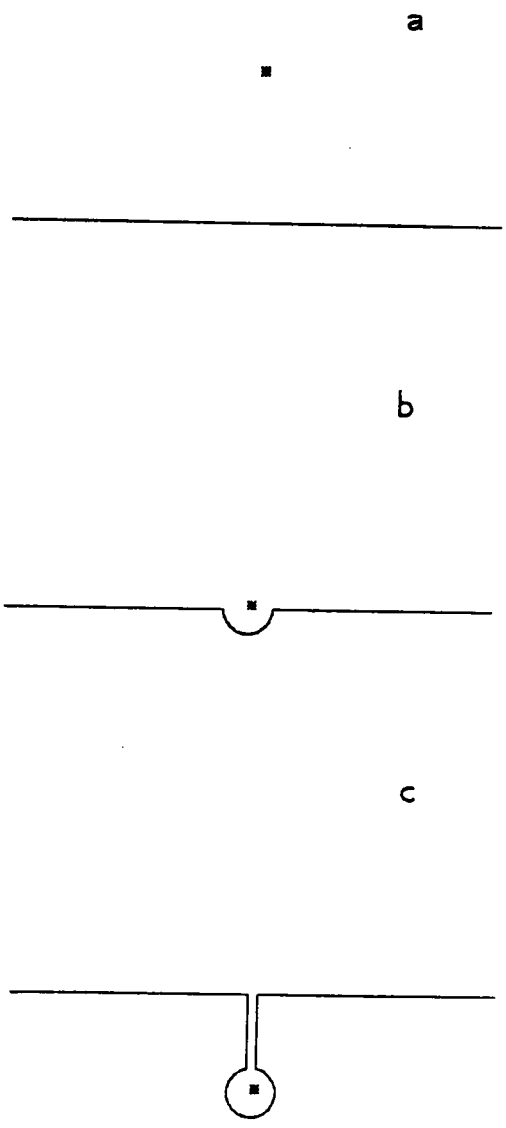


**Fig. 3.1** Landau contour for (a) $Im\nu > 0$, (b)$Im\nu = 0$ and (c) $Im\nu < 0$.

Table 3.1 Relative error in $\Lambda_t$ as function of $\alpha$.

| ALFA | RELATIVE ERROR |
|---|---|
| 0.10 | 1.0 E+114 |
| 0.50 | 1.0 E+7 |
| 1.00 | 2.5 |
| 1.50 | 2.4 E-3 |
| 1.75 | 2.4 E-3 |
| 2.00 | 2.4 E-3 |
| 2.20 | 2.9 E-3 |
| 3.00 | 1.0 E+6 |

# Chapter 4: The numerical approach

## 4.1 General remarks

Various numerical techniques have been used for the solution of (VP) [15-16-17-18-19-37]. In early numerical codes, methods based upon expanding the distribution function in classical polynomials, such as Hermite or Chebyshev, were adopted; expansion in Fourier modes was also used. These methods are impractical if one wants to follow the solution for long times with very high accuracy, because of the large number of terms that need to be retained. They have been made obsolete by the appearance of the splitting scheme, which allows the computation of the Vlasov solution with high accuracy for long times. Only the Fourier transforms method has received new consideration because it is very well suited to introduce filtered distributions, as we shall discuss later. The main numerical difficulty in this problem lies in that a finer and finer structure in phase space is formed in the distribution function as time proceeds. This phenomenon is called filamentation. As mentioned in Chapter 3, it is the free streaming contribution to the solution which is responsible for this formation of fine structure, with the development of larger and larger velocity gradients as time proceeds. If the phase space is discretized for the numerical computation, at some time $T_R$ (called recursion time) the fine structure of $f$ reaches the size of the grid and the numerical solution no longer represents the mathematical solution of (VP) for those particular initial data. In some numerical simulations, particularly in those where Landau damping is negligible with respect to nonlinear effects, it is observed that the filamentation process stops and, subsequently, the fine structure of the distribution becomes smoother and smoother as time proceeds. Moreover, no pathological behaviour is observed in the averaged quantities, such as density and electric field, at $t \sim T_R$ and later. Probably, this smoothing is a purely numerical

effect; in a sense, the finite size of the grid in phase space performs a coarse-grain average of the distribution, weighing among neighbouring mesh points. How big is the error induced by this spurious diffusion on the averaged quantities is still an open problem. However, the reliability of the results can always be checked by reducing the size of the grid in phase space. A possible explanation for the insensitivity of the averaged quantities to this spurious smoothening will be offered in Chapter 5, where the numerical results are presented.

Two numerical Vlasov codes have become increasingly popular in recent years: the splitting scheme by Cheng and Knorr [19] and the Fourier-Fourier transform method by Klimas [37]. The splitting scheme is the most accurate algorithm that has been devised so far for the numerical solution of (VP) and it is well suited for being used on a vector computer. It performs the integration of (VP) along the characteristics with an interpolation procedure, it is very stable and one only has to worry about recursion. Since this is the algorithm that we used in our numerical simulations, we shall describe it in greater detail in a further section.

Simulations of one-dimensional unmagnetized plasmas are being carried out with particle simulation codes as well. Since none of these codes actually solves the Vlasov-Poisson system, we shall never make comparisons with the results generated by them. We shall only mention, in the next chapter, the algorithm devised by Denavit [18], which combines Vlasov code techniques with particle simulation techniques; this code has been used twice to address the question of the saturation amplitude for weakly unstable modes, a question that we addressed using the splitting scheme (see Section 5.4).

## 4.2 The recursion time.

Being due to the free-streaming contribution to the Vlasov solution, the recursion time $T_R$ can be calculated a priori. Consider Vlasov's equation with no electric field

$$\frac{\partial f}{\partial t} + v\frac{\partial f}{\partial x} = 0$$

with periodic boundary conditions and the initial condition (see (2.21))

$$g(x, v) = \epsilon \frac{1}{\sqrt{2\pi}} e^{-\frac{v^2}{2}} \cos kx.$$

Then the solution is known:

$$f(x, v, t) = f(x - vt, v, 0) = \epsilon \frac{1}{\sqrt{2\pi}} e^{-\frac{v^2}{2}} \cos k(x - vt)$$

which gives for the density

$$\rho(x, t) = 1 - \int f\, dv = \epsilon e^{-\frac{k^2 t^2}{2}} \cos kx.$$

In a possible numerical simulation, suppose that the velocity space is restricted to $v \in [-V, V]$ and that $M$ points are used for the grid. Then we will have for the density (using the trapezoidal rule; but the result applies to any other integration algorithm)

$$\begin{aligned} \rho(x, t) &= \sum_{j=1}^{M} f(x - v_j t, v_j, 0)\Delta v \\ &= \frac{\epsilon \Delta v}{\sqrt{2\pi}} \sum_{j=1}^{M} e^{-\frac{v_j^2}{2}} \cos k(x - v_j t) \end{aligned}$$

where $v_j = -V + (j-1)\Delta v$. Then $\rho$ is a periodic function of time, with period

$$T_R = \frac{2\pi}{k\Delta v}.$$

Therefore, the numerical solution of a Vlasov simulation, which has to use a discretized phase space (like the splitting scheme algorithm) can be made accurate for

an arbitrarily large time, provided $\Delta v$ is chosen small enough so that $T_R$ becomes sufficiently large.

Recursion can also be understood by considering the continuous spectrum of the linearized Vlasov operator (see Sect. 3.3). As the velocity space is discretized, the continuous spectrum is replaced by a finite number of discrete eigenvalues and the integration over $v$ leads to periodicity in time. When polynomial representations are used, the effect arises from the truncation of infinite matrices.

Sometimes, one is interested in following the solution of (VP) for very long times and is therefore bound to choose a very small $\Delta v$, possibly so small that the required computational effort becomes too big. A method of resolving the filamentation without increasing the computational effort, which has been extensively used in various forms, is the introduction of filtered distributions. In this approach, certain averages of the distribution function with respect to suitably chosen weight functions are performed. These weight functions are usually chosen such that the first few moments of the distribution function are conserved. However, a significant loss of information can occur, and the accumulated error can become large after some time. In a different approach, a small collision term is sometimes added to Vlasov's equation in order to avoid recursion; this method has often been used in connection with polynomial representation solutions of (VP). In both cases, the system described by these smoothened distributions looses its hamiltonian character and its entropy is not any more conserved. We shall not dwell on this topic, since neither will we ever make use of filtered distributions nor will we use collisions to emulate the hamiltonian system. However, it should be mentioned that among all the models which have been proposed and used to smoothen the distribution, only the one proposed by Klimas [22] has been proved analytically to give for the averaged quantities the same result

as given by the unfilterd Vlasov solution, so that no error is introduced by the filtering procedure. This is done by considering the evolution equation obeyed by the filtered distribution and then solving numerically this last equation rather than (VP). Consider the filtered distribution

$$\overline{f}(x,v,t) = \frac{1}{v_0\sqrt{2\pi}} \int e^{-\frac{1}{2}(\frac{x-vt}{v_0})^2} f(x,vt,t)$$

where $v_0$ is the width of the filter and can be chosen arbitrarily. It is easily seen that $\int \overline{f} = \int f$ , $\int v\overline{f} = \int vf$ and that $\overline{f}$ obeys

$$\frac{\partial \overline{f}}{\partial t} + v\frac{\partial \overline{f}}{\partial x} - E(x,t)\frac{\partial \overline{f}}{\partial v} = -v_0^2 \frac{\partial^2 \overline{f}}{\partial x \partial v} \tag{4.2.1}$$

with the electric field given by

$$\frac{\partial E}{\partial x} = 1 - \int \overline{f}$$

The loss of information due to the higher moments of $f$ not being conserved is now accounted for in the diffusive term on the right hand side of (4.2.1). Moreover, an *a priori* bound on $\partial \overline{f}/\partial v$ exists, namely

$$|\frac{\partial \overline{f}(x,v,t)}{\partial v}| \leq \sqrt{\frac{2}{\pi}} \frac{1}{v_0} M_{f_0}$$

(where $M_{f_0}$ is the maximum value taken by $f(x,v,0)$ in the phase space) while $\partial f/\partial v$ is unbounded. The width of the filter, $v_0$, is to be chosen according to how much information about the details of the distribution function one wishes to retain.

Unfortunately, there seems to be no easy way to introduce the Klimas filamentation filter in a code that uses the splitting scheme algorithm with low noise, while it becomes a rather trivial operation, with virtually no extra computational effort, in a code that uses the Fourier-Fourier transform method. This latter algorithm is based upon Fourier transforming the distribution function in both the space and the

velocity variable; unfortunately, it is plagued by numerical instabilities that need to be detected and filtered out before they significantly affect the solution. Moreover, while with the splitting scheme one can easily discretize the space variable with $\sim 100$ points, retaining more than $\sim 10$ Fourier modes becomes impractical (for computational reasons) with the Fourier-Fourier transform method. For these reasons, we opted for the use of the splitting scheme to carry out our numerical simulations. It is certainly desirable to find a way to implement the Klimas filamentation filter in such a code.

## 4.3 The splitting scheme algorithm.

### 4.3.1 The discretized phase space.

The distribution function $f(x, v, t)$ is defined on the phase space $[0, L] \times \mathbf{R}$. For the numerical solution the phase space has to be discretized and the distribution function will be obtained on a finite number of points. In particular, a cutoff has to be introduced in the velocity variable, which, in principle, modifies the boundary conditions on $f$. If $V$ is the cutoff speed, then the phase space becomes $[0, L] \times [-V, V]$ and we have for $f(x, v, t) = 0$ for $|v| \geq V$. The cutoff has to be sufficiently large so that no information is lost through the velocity boundary. With distributions that decay exponentially as $|v| \to \infty$ a cutoff velocity $V \sim 8$ or 10 can be used, which gives typically 10000 to 50000 points for the phase space. Unfortunately, this rules out the possibility of using the code with lorentzian distributions, which decay as $1/v^2$ at infinity. A realistic choice for the cutoff velocity would be $V \sim 10000$ or even larger, which couldn't be handled numerically.

Let $\{x_i, v_j\}$, $i = 1, N+1$; $j = 1, M$ be the discretized phase space, with $x_1 = 0$, $x_N = L$, $v_1 = -V$, $v_M = V$, $x_{i+1} = x_i + \Delta x$, $v_{j+1} = v_j + \Delta v$, $\Delta x = L/(N-1)$

and $\Delta v = 2V/(M-1)$. At each time $t$, the $M \times (N+1)$ values for the distribution function at each mesh point, $f(x_i, v_j, t) = f_{ij}(t)$, $i = 1, N+1$; $j = 1, M$, have to be calculated, with the boundary conditions

$$f_{N,j}(t) = f_{1,j}(t)$$

$$f_{N+1,j}(t) = f_{2,j}(t)$$

$$f_{i,M}(t) = f_{i,1}(t) = 0$$

### 4.3.2 The splitting of Vlasov's equation.

The splitting scheme performs the integration of (VP) along the characteristics using interpolation methods. Suppose that the values of $f$ at the time $t$ on the mesh points, $f_{i,j}(t)$, are known. First, the free streaming part of Vlasov's equation is solved for half time step:

$$\frac{\partial f^{(1)}}{\partial t} + v\frac{\partial f^{(1)}}{\partial x} = 0. \tag{4.1}$$

whose solution is $f^{(1)}_{i,j} = f(x_i - v_j \Delta t/2, v_j, t)$. The value for $f(x_i - v_j \Delta t/2, v_j, t)$ is found by using one-dimensional cubic spline interpolation with periodic boundary conditions on the values $f_{i,j}(t)$. At this point, the electric field can be calculated from the new distribution $f^{(1)}_{i,j}$ by first integrating over $v$ to obtain the density $\rho(x) = \int f$ and then integrating in $x$ to calculate the electric field

$$E(x) = \int_0^x [1 - \rho(y)]\, dy. \tag{4.2}$$

We shall comment about these two integrations later. Once the electric field $E(x_i) = E_i$ is obtained on the mesh points, the equation

$$\frac{\partial f^{(2)}}{\partial t} - E(x,t)\frac{\partial f^{(2)}}{\partial v} = 0$$

is solved for the second half time step. In this case the solution is $f^{(2)}_{i,j} = f^{(1)}(x_i, v_j + E_i \Delta t)$. Again, the value for $f^{(2)}_{i,j} = f^{(1)}(x_i, v_j + E_i \Delta t)$ is found by using one-dimensional cubic spline interpolation with zero boundary conditions on the values $f^{(1)}_{i,j}$.

Finally, eq. (4.1) is solved again for half time step, so that

$$f_{i,j}(t+\Delta t) = f^{(2)}(x_i - v_j \frac{\Delta t}{2}, v_j)$$

is the desired solution at the time $t + \Delta t$. It has been shown [19] that this scheme gives the solution correct to second order in $\Delta t$, although nothing is known about the dependence of the error on $\Delta x$ and $\Delta v$.

### 4.3.3 The integrations in $x$ and $v$.

The integration over $v$, which gives the density, is performed with Simpson's 3/8 rule, so that

$$\rho(x_i) \equiv \rho_i = \frac{\Delta v}{8}\{3f_1+9f_2+9f_3+6f_4+9f_5+\cdots+9f_{N-4}+6f_{N-3}+9f_{N-2}+9f_{N-1}+3f_N\}$$

This method would prove far too inaccurate for the integration over $x$, which gives the electric field. Also, when the initial distribution does not obey the symmetry property illustrated in Sect. 2.2 at least at one point $E(x)$ has to be calculated with the very inaccurate trapezoidal rule. Since our functions are periodic in $x$, the most effective way of performing the integration over $x$ is by using Fourier transforms. Since $\partial E/\partial x = 1 - \rho$, $E_k = -i(\delta_{k,0} - \rho_k)/k$ where $E_k$ and $\rho_k$ are the Fourier transforms of $E$ and $\rho$. Then, $E(x)$ can be reconstructed from its Fourier components. The efficient Fast Fourier Transform (FFT) routines CRFFT2 and RCFFT2 of the mathematical library of the Pittsburgh Supercomputing Center have been used.

As an example, In Table 4.1 the values for the electric field at $t = 0$ and at $t = 50$ are given, using both Simpson's rule and Fast Fourier Transforms. The initial condition is chosen of the form (2.2.1), with $f_0(v)$ a maxwellian. Therefore, $E(x, t = 0) = -(\epsilon/k)\sin kx$ and the error in the electric field at $t = 0$ can be computed from the exact solution. At $t = 50$ the symmetry property $E(x) = E(L - x)$ has been

checked and the values for $\epsilon_S = |E(x)+E(L-x)|/|E(x)|$ (relative error with Simpson's rule) and $\epsilon_{FT} = |E(x)+E(L-x)|/|E(x)|$ (relative error with Fast Fourier Transforms) are given, making it clear how much more accurate the Fourier transforms method is.

### 4.3.4 The interpolation.

Both for the interpolation in $x$ and in $v$ cubic splines have been used, following the prescription in [19]. However, while for the interpolation in $x$ the points at which the distribution function is required are known and are the same at each time step, this is not so for the interpolation in $v$, which depends on the value of the electric field. Since the value for the distribution which has been found by interpolation at some point $(\overline{x}_i, \overline{v}_j)$ has to replace the value of the function at some given mesh point $(x_i, v_j)$, it is desirable that $|\overline{x}_i - x_i| \leq \Delta x$ and $|\overline{v}_j - v_j| \leq \Delta v$. Obviously, while this condition can always be met for the interpolation in $x$ – provided $V\Delta t/2 \leq \Delta x$ –, one cannot predict *a priori* the maximum amplitude of the electric field and so that condition might not be met in the $v$ interpolation. We included a check in the code, so that $J \equiv max_j\,[|\overline{v_j} - v_j|/\Delta v]$ is monitored at each time step. As long as this quantity remains small (typically $\approx 2$ or $\approx 3$) virtually no error is included in the computation, provided $f(x, v, t)$ decays rapidly enough as $|v| \to \infty$. When $J$ becomes larger ($J \approx 10$) then we stopped the computation and re-ran with a smaller $\Delta t$.

It is worth mentioning that, for long simulations, about 85% of the CPU time is spent by the code in the subroutine MXV, which performs a matrix ×vector product to calculate the spline coefficients. This subroutine is already vectorized and optimized, therefore the code has been used in the most efficient possible way. In Table 4.2 the total CPU time per time step is given for several values of N and M. These values for the CPU time refer to the Cray X-MP of the PSC, on which machine most

of our simulations have been run. The total CPU time is proportional to the number of time steps required, but the vectorization properties of the Cray X-MP (including possible memory bank conflicts) make the relationship nonlinear in $N$ and $M$.

### 4.3.5 Recursion with the splitting scheme.

Finally, we briefly illustrate the effect of recursion on the solution in the linear Landau damping case. Figs. 4.2a and 4.2b show the amplitude of the fundamental mode of the electric field as function of time for two different values of the step size in the velocity variable; the initial distribution is

$$f(x, v, 0) = f_0(v)(1 + \epsilon \cos kx)$$

with

$$f_0(v) = \frac{1}{\sqrt{2\pi}} e^{-\frac{v^2}{2}}$$

$\epsilon = 0.1$, $k = 0.5$ and $m = 1$. Here, $\Delta t = \frac{1}{8}$, $N = 9$ while $M = 32$ in fig. 4.2a and $M = 64$ in fig. 4.2b. The recursion time for the two cases is $T_R \approx 48$ and $T_R \approx 64$ respectively. Note how the solution is heavily affected by recursion at $t \approx \frac{1}{4} T_R$. By no means could we reproduce fig. 3 of Cheng and Knorr [19], where the effect due to recursion is effectively seen only at $t \approx T_R$.

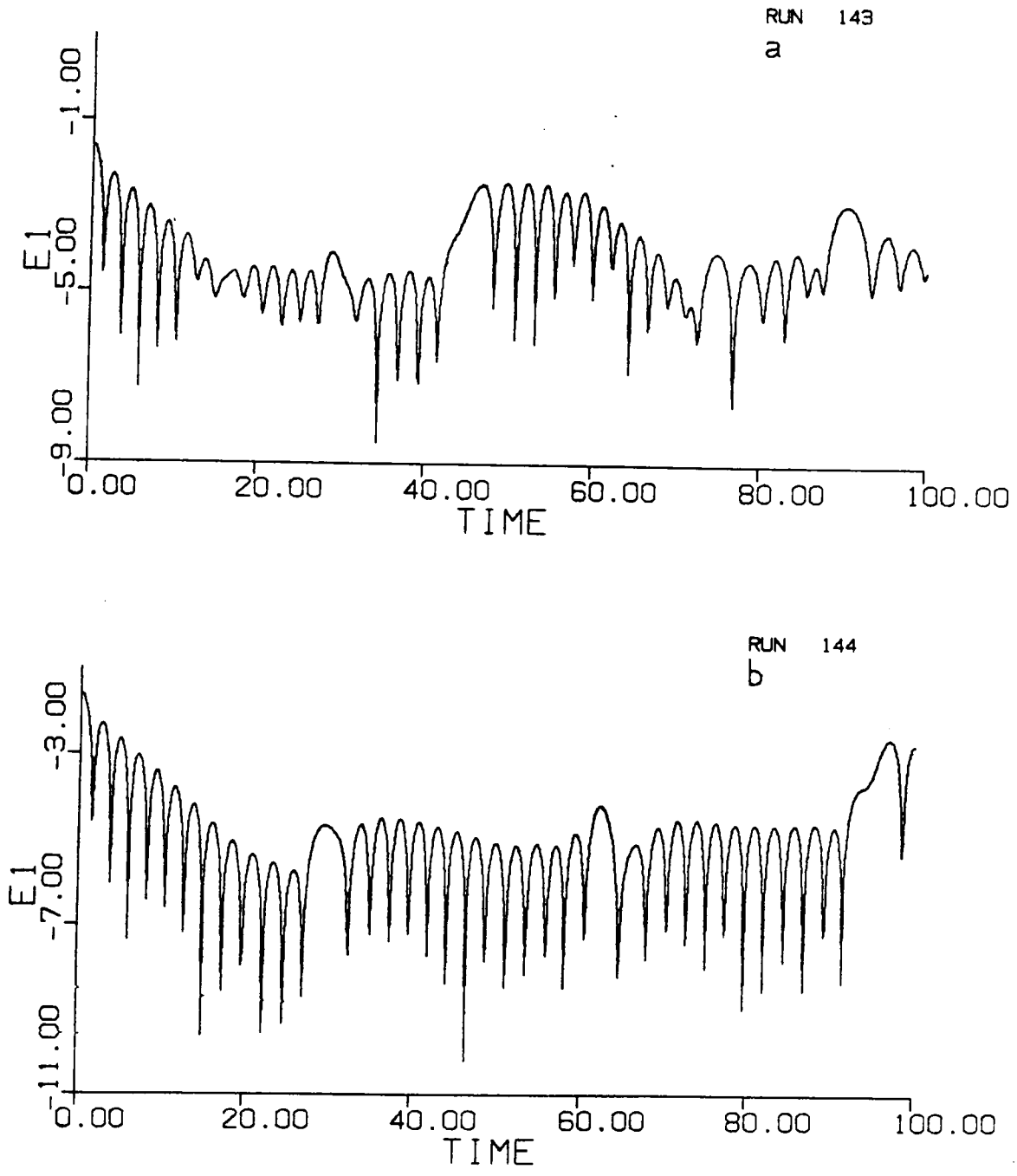


Fig. 4.1 The effect of recursion on the linear Landau damping solution: (a) $M = 32$ and (b) $m = 64$.

Table 4.1 Electric field with Simpson's rule and FFT.

time = 0.0000000E+00

| E(x) FFT | E(x) Simps. | eps. FFT | eps Simps. |
|---|---|---|---|
| -3.2672E-02 | -3.2646E-02 | 0.0000E+00 | 8.0327E-04 |
| -1.5713E-01 | -1.5701E-01 | 9.4832E-08 | 8.0323E-04 |
| -2.5767E-01 | -2.5746E-01 | 1.1566E-07 | 8.0326E-04 |
| -3.1898E-01 | -3.1872E-01 | 0.0000E+00 | 8.0331E-04 |
| -3.3173E-01 | -3.3146E-01 | 8.9840E-08 | 8.0326E-04 |
| -2.9397E-01 | -2.9374E-01 | 1.0138E-07 | 8.0321E-04 |
| -2.1146E-01 | -2.1129E-01 | 1.4093E-07 | 8.0318E-04 |
| -9.6762E-02 | -9.6684E-02 | 7.6999E-08 | 8.0341E-04 |

time = 50.00000

| E(x) FFT | E(x) Simps. | eps. FFT | eps Simps. |
|---|---|---|---|
| -1.7753E-02 | -1.8007E-02 | 1.0492E-07 | 9.9589E-03 |
| -8.5778E-02 | -8.7057E-02 | 8.6859E-08 | 2.0339E-03 |
| -1.4000E-01 | -1.4211E-01 | 0.0000E+00 | 1.1197E-03 |
| -1.7184E-01 | -1.7429E-01 | 0.0000E+00 | 8.2485E-04 |
| -1.7590E-01 | -1.7822E-01 | 0.0000E+00 | 6.8236E-04 |
| -1.5201E-01 | -1.5399E-01 | 0.0000E+00 | 6.6091E-04 |
| -1.0788E-01 | -1.0929E-01 | 0.0000E+00 | 7.3455E-04 |
| -4.9159E-02 | -4.9798E-02 | 0.0000E+00 | 1.4408E-03 |

Table 4.2 CPU time per time step as function of $M$ and $N$.

| NV / NX = | 9 | 33 | 65 |
|---|---|---|---|
| 128 | 0.01 | 0.03 | 0.08 |
| 256 | 0.02 | 0.08 | 0.20 |
| 512 | 0.07 | 0.25 | 0.56 |

# Chapter 5: Numerical results

## 5.1 Introduction

While the linearized Vlasov-Poisson system has been extensively studied and its solution - in one form or in another - has been known for many years, not much is known analytically about the nonlinear behaviour of the solutions and about the asymptotic state that they approach. Discrepancies appear among different theoretical models that deal with the saturation of weakly unstable modes and the numerical simulations performed so far leave a good deal of uncertainty about their solution. Only in the last ten years the techniques developed for the numerical solution of (VP) have allowed simulations long enough in time for the understanding of the asymptotic states. Of course, no ultimate and definitive conclusions about asymptotic states can be drawn from numerical results alone; however, in several cases the numerical indications can be combined with physical intuition (alas, not so often with analytical results) and a good level of confidence can be achieved in the description of these asymptotic states.

In this chapter we shall present and discuss the results of our numerical simulations on the full nonlinear Vlasov-Poisson system. Our emphasis will be on understanding the asymptotic state towards which the system evolves and on how much information about this state is contained in the solution of the linearized problem. Some of these results have already been obtained in the literature by means of the same numerical algorithm; however, since our understanding about the asymptotic state sometimes conflicts with the conclusions drawn by other authors (although it is not yet clear whether the discrepancy is only at a semantical level or if it is more profound), we shall repeat those results in the present work, with display of some

more details to support our assertions.

In many cases the system will be perturbed about a spatially homogeneous equilibrium by the excitation of a single mode, with the initial perturbed distribution of the form

$$f(x, v, 0) = f_0(v)(1 + \epsilon \cos kx) \tag{5.1.1}$$

where $k = 2\pi m/L$ is the wave number, $m$ the mode number and $\epsilon \ll 1$. The function $f_0(v)$ is an equilibrium solution of (VP), normalized so that $\int f_0 = 1$. Then, from Poisson's equation, we have for the electric field

$$E(x, 0) = -\frac{\epsilon}{k} \sin kx.$$

Note that, if $f_0(v)$ is symmetric in $v$, the distribution (5.1.1) obeys the symmetry property shown in Sect. 2.2, so the electric field behaves like a standing wave and never like a travelling wave. As we shall see in the next section, this situation is incompatible with a BGK equilibrium, so our interpretation of the asymptotic state approached by the system starting from (5.1.1) when $f_0(v)$ is symmetric in $v$ differs from the one given in [20-21] where it is claimed that BGK equilibria can be approached, for example, when a maxwellian equilibrium distributions is perturbed according to (5.1.1).

While the dispersion relation given by linear theory is largely independent of the shape of the initial perturbation (as long as it is small compared to the equilibrium distribution), the actual form of the solution (even in the linearized model) is not, and we might expect to find a different behaviour in the nonlinear evolution of the system if different perturbations are chosen. Therefore, besides the particular function shown in (5.1.1) we shall consider more general types of perturbations, namely

$$f(x, v, 0) = f_0(v) + \epsilon \tilde{f}(x, v) \tag{5.1.2}$$

with $0 < \epsilon \ll 1$ and $\lim_{|v|\to\infty} \tilde{f} = 0$. Moreover, since we are mainly interested in exciting with a single mode, a wavelike behaviour $\sim \sin kx$ or $\sim \cos kx$ in the space variable will always be assumed. Allowing for more general types of perturbations opens the possibility of breaking the symmetry property mentioned in Section 2.2 in presence of symmetric equilibrium distributions, so that travelling-wave-like solutions can now be sought. Since we must have $f(x, v, 0) > 0$ for all $x$ and $v$, and explicitely choosing $\cos kx$ for the space dependence, we can rewrite (5.1.2) as

$$f(x, v, 0) = f_0(v)\{1 + \tilde{\epsilon}(v) \cos kx\} \tag{5.1.3}$$

with $|\tilde{\epsilon}(v)| \ll 1$. Simulations with these more general type of perturbations have never been produced before and our results are the first to appear.

## 5.2 Maxwellian equilibrium

A maxwellian equilibrium distribution,

$$f_0(v) = \frac{1}{\sqrt{2\pi}} e^{-\frac{v^2}{2}}$$

is predicted to be stable by linear theory. The only analytical result which describes the nonlinear evolution of the system after perturbing the maxwellian has been obtained twenty years ago by O'Neal [10], in a theory that takes into account the effect of the trapped particles on the distribution in the resonant region. In this model, the form of the electric field is prescribed, namely $E(x, t) = A(t) \sin kx$ with $A(t)$ varying only on a much slower time scale than the one characterized by the inverse damping rate. Under this assumption, the electrons see an approximately time independent potential over many plasma periods and they obey the equation of motion

$$\ddot{x} = -A(t) \sin kx$$

with $A \approx constant$. For those electrons which are trapped near the bottom of the

potential well this equation can be linearized, giving

$$\ddot{x} = -Akx$$

i.e. these electrons exhibit oscillatory motion with frequency $\omega_t = \sqrt{Ak}$, called the trapping frequency. Keeping $A(t) \approx constant$, we have seen in Section 2.1.1 how the characteristics look like for this case: following the motion of a trapped electron along the characteristic, we see that the trapping frequency is related to the time it takes for this electron to complete the entire closed orbit, i.e. $\omega_t^{-1}$. Therefore, if a trapping time $\tau \equiv 2\pi/\omega_t$ is introduced, linear theory is expected to be applicable only for $t \ll \tau$. In order to exhibit an analytical expression for the solution which is valid for longer times, O'Neal introduced a time dependent damping rate $\gamma(t)$; by solving exactly Vlasov's equation in the resonant region, O'Neil found that $\gamma(t)$ coincides with the value given by the linear dispersion relation for $t \ll \tau$, then it oscillates for $t \sim \tau$ and tends to zero as $t \to \infty$. From this result, one expects the amplitude of the electric field to exhibit Landau damping for $t \ll \tau$, then to oscillate for $t \sim \tau$, with alternating growing and damping phases, reaching some constant value as $t \to \infty$. The frequency of these (damped) amplitude oscillations, $\omega_A$, is approximately proportional to $\omega_t$, although not necessarily equal (since the amplitude of the electric field changes in time, we wouldn't know what to use for $A$). O'Neal's result is obtained in a reference frame travelling with the wave speed, $\omega_r/k$; therefore, in the laboratory frame, these amplitude oscillations simply modulate the more rapid oscillations at the linear frequency. A numerical simulation, carried out by Shoucri and Gagne' [20] using the splitting scheme, confirms O'Neal's model. We have repeated the simulation, obtaining results which are consistent with theirs. For this case, the initial distribution is chosen as in (5.1.1), with $k = 0.3$, $m = 1$, $\epsilon = 0.1$, $N = 65$, $M = 256$ and $\Delta t = 1/16$. In figs. 5.1a-d the amplitude of the fundamental

mode of the electric field, the first two harmonics and the electric field energy are shown as functions of time. To be more definite, let

$$E(x,t) = \sum_l E_l(t) e^{ilx}$$

Then, $|E_1|$ is shown in fig. 5.1a, while $|E_2|$ and $|E_3|$ are shown in figs. 5.1b and 5.1c, respectively. The electric field energy, shown in fig. 5.1d, is defined as

$$W(t) \equiv \int_0^L dx\,[E(x,t)]^2$$

The electric field, as function of $x$, is shown at selected times in figs. 5.4a-l. From these results, it is clear that the mode $m = 1$ remains dominant at all times, so the electric field remains approximately sinusoidal throughout the whole simulation. Moreover, the nodes of the electric field remain fixed at $x = 0$, $x = L$ and $x = L/2$. Therefore, $E(x,t)$ behaves like a standing wave. As it appears from fig. 5.1a, the electric field follows closely the predictions os O'Neil's model, with the initial linear Landau damping followed by the amplitude oscillations, which modulate the oscillations at the linear frequency, and which appear to be damped. The linear dispersion relation gives for this case $\omega = 1.1598 - 0.01262i$; from our simulation we have $\omega \approx 1.15 - 0.013i$, in agreement with the theoretical value. The frequency of the amplitude oscillations from the numerical result is $\omega_A \approx 0.135$; extending heuristically O'Neil's model, we expect $\omega_A \propto \sqrt{k\epsilon/k} = \sqrt{\epsilon}$. Therefore, we ran another simulation with $\epsilon = 0.01$; the amplitude $|E_1|$ for this latter case is shown in fig. 5.6. The frequency of the amplitude oscillations is $\omega_A \approx 0.04$, giving $\omega_A(\epsilon = 0.1)/\omega_A(\epsilon = 0.01) \approx 3.37$, close to the predicted value $\sqrt{0.1/0.01} = \sqrt{10}$. The amplitude of the asymptotic oscillations, $|E_1|_\infty$, appears to be roughly 1/10 of the one for the case with $\epsilon = 0.1$ ($|E_1|_\infty \approx 0.013$ and $|E_1|_\infty = 0.18$ respectively).

The distribution function is shown in figs 5.2a-h (level curves of $f(x,v,t)$ at selected times) and 5.3a-l (spatially averaged distribution $< f(x,v,t) >$ at selected

times). The initial wavelike perturbation in $x$ has been "twisted" and has caused the formation of two vortices in phase space; these vortices are centered at $v_\phi$ and $-v_\phi$ respectively and they move, parallel to the space axis, with velocity $v_\phi$ and $-v_\phi$ respectively. Here, $v_\phi \equiv \omega_r/k$ is the phase velocity of the wave. In figs. 5.5a-d we have the level curves for the same case, but the perturbation has been chosen with mode number $m = 3$. Now we have three vortices at positive velocities and three at negative velocities, as expected, since we would have three "cat's eyes" for the characteristics of Vlasov's equation with a purely sinusoidal electric field. Looking at the space averaged distribution,we see that a very small bump has formed in the resonant region; this bump oscillates in size and position, in response to the variations in the electric field amplitude, and seems to settle asymptotically to a shape such that the minimum of $< f >$ lies exactly at the phase velocity $v_\phi$. When considering the case with $\epsilon = 0.01$, this bump in the space averaged distribution is significantly smaller. Unfortunately, simulations with very small perturbations would be affected very soon by recursion effects (we shall comment on this in a while), while they would approach the asymptotic state more slowly. However, the indications of these two cases seem to be consistent with the claim about the stability of linearly stable distributions, as we mentioned in Section 2.4, that monotonically decreasing functions of the energy (in a frame where the plasma is at rest) are stable.

From these results, we have very strong indications about the asymptotic state of the system in this case. Thanks to the symmetry of the equilibrium distribution and of the perturbation, electrons with both $v \sim v_\phi$ and $v \sim -v_\phi$ resonate with the wave, so that two travelling waves of equal amplitude and opposite phase velocity are excited; these two travelling waves do not overlap in the phase space, where we see the vortices described above. When averaging over $v$, however, the two waves are

superposed and the result is a standing wave, as we have observed for the electric field. Asymptotically in time, the electric field is seen to perform steady-state oscillations at the frequency given by the linear dispersion relation (within our numerical accuracy), while the space averaged distribution has a minimum at exactly the phase velocity of the wave (both at $v > 0$ and at $v < 0$). Note that, because of the conservation of the total energy in the system, $< f >$ cannot tend asymptotically towards a time-independent curve (as apparently suggested in [20]) while the electric field amplitude (and therefore the electric energy) is oscillating in the way described above; $< f >$ will continue to oscillate in the resonant region, the oscillations being very small (not seen in our graphics) but undamped.

The recursion time (see Sect. 4.2) for this case is $T_R \approx 380$. Nothing strange seems to happen at that time, no pathological behaviour is seen in the electric field amplitude or in the averaged distribution. Note that, on the contrary, in the simulation with $\epsilon = 0.01$ the electric field amplitude clearly exhibits an anomaly at $t \approx T_R$. This is due to the fact that, in the presence of a weaker electric field, the free-streaming contribution to the solution remains relevant for longer times. In the case $\epsilon = 0.1$ we have repeated the simulation using $M = 512$ and have observed no change in the electric field amplitude and in the averaged distribution. Obviously, having obtained the same results with a finer grid in velocity space, the results for the electric field and the averaged distribution are correct and, for some reason, unaffected by the recursion problem. A rigorous explanation for this fact is still lacking; other authors have come to the conclusion that the filamentation process stops at some time and the fine structure created in the region of the vortices is smoothed out by nonlinear effects. In our opinion, since there is no dissipative mechanism in this system, there is no reason to expect a smoothing. We rather tend to believe that, as the filamentation

becomes finer and finer, its contribution to the averaged quantities becomes less and less important; therefore, it is necessary to retain all the details of the distribution only until the contribution of the fine structure to the averaged quantities is relevant.

It has been claimed [20-21] that the asymptotic state for this system is a BGK equilibrium. As we have seen in Section 2.5, BGK equilibria are travelling waves which, due to the nonlinearity of the equations, cannot be superposed, while the asymptotic behaviour of the electric field is that of a standing wave and not that of a travelling wave. Therefore, this asymptotic state can rather be viewed as a superposition of two solutions of the BGK equations but not as a BGK equilibrium itself. Moreover, for each of the two travelling waves to be asymptotically a BGK solution, the vortices that have formed in phase space should not rotate, which clearly doesn't happen if the filamentation process continues indefinitely. Therefore, we conclude that the asymptotic state approached by the system when a maxwellian equilibrium is perturbed with a reflection symmetric perturbation is not that of a BGK equilibrium.

If the more general expression (5.1.3) is considered for the initial distribution, we have from Poisson's law:

$$\begin{aligned}\frac{\partial E}{\partial x} &= 1 - \int f_0(v)[1 + \tilde{\epsilon}(v)\cos kx] \\ &= -\left[\int f_0(v)\tilde{\epsilon}(v)\right]\cos kx\end{aligned}$$

giving

$$E(x,0) = -\frac{1}{k}\left[\int f_0(v)\tilde{\epsilon}(v)\right]\sin kx$$

which shows that the amplitude of the electric field is proportional to the overlap integral of the perturbation $\tilde{\epsilon}(v)$ with the equilibrium distribution. Therefore, if $\tilde{\epsilon}(v)$ is chosen to be significantly different from zero only on the tail of the equilibrium

maxwellian, the amplitude of the electric field at $t = 0$ will be very small, with the unpleasant consequence that recursion effects will be felt very soon, making a study of such case far into the nonlinear regime very expensive. As an example, figs. 5.7a and 5.7b show the amplitude of the fundamental mode of the electric field as a function of time, for the same equilibrium maxwellian as in fig.1a, and with

$$\tilde{\epsilon}(v) = e^{-(v-V_0)^2},$$

with $V_0 = 4.5$ and $M = 256$ and $M = 512$ respectively. The recursion time is $T_R \approx 383$ and $T_R \approx 766$ respectively. Note the initial increase in the electric field amplitude, due to the transients that appear in the linear solution, followed by an impressively regular Landau damping phase at exactly the damping rate given by the Landau dispersion relation (the least damped mode), with oscillations at the linear frequency. Note that, by doubling the recurrence time, nonlinear effects did not appear at all. Using O'Neal's scaling for the trapping time, $\tau \sim \sqrt{\epsilon}$, since for $\epsilon = 0.1$ we have $\tau \approx 22$ and taking $\epsilon \approx 4.5 \times 10^{-5}$ (the amplitude of the electric field when it reaches its maximum before Landau damping occurs), we have for this case $\tau \approx \sqrt{22/45 \times 10^{-6}} \approx 700$ before the mode starts growing. In order to study this case, a grid with at least 5000 points in the velocity variable would have to be used.

Being forced to perturb with functions that are significantly non zero on the bulk of the maxwellian equilibrium distribution, we have chosen

$$\tilde{\epsilon}(v) = \frac{1}{(v - V_0)^2 + v_t^2},$$

with $V_0 = 1$ and $v_t = 0.5$. The results are shown in figs. 5.8 ($|E_1|$). 5.9a-h (level curves of $f$ at selected times), 5.10a-f (space averaged distribution at positive and negative velocities) and 5.11a-f (electric field at selected times). As in the case of a symmetric perturbation, two travelling waves, with $\pm v_\phi \equiv \omega_r/k$ have been excited

at $t = 0$. However, while in the previous case the symmetry of the perturbation forced the amplitudes of these two waves to be the same, so that a standing wave could result from their superposition, now their amplitudes are different, so we have a travelling wave with modulated amplitude. The space averaged distribution settles to a curve with minimi at $\pm v_\phi$, but the sizes of the small bumps at $v < 0$ and $v > 0$ are different. The electric field remains approximately sinusoidal during the whole simulation, and clearly behaves like a travelling wave whose amplitude varies in time in the way shown in fig. 5.8. Again, vortices appear in phase space, but the number of trapped electrons in each of them is different.

Again, the numerical results indicate that the asymptotic state can be described as a superposition of two solutions of the BGK equations (this time with different amplitudes), but it is not a BGK equilibrium by itself.

### 5.3 Linearly unstable distributions.

While O'Neil's theory provides a good description of the nonlinear evolution of a perturbation to a maxwellian equilibrium under certain circumstances, there is no satisfactory theoretical description of the behaviour of the solution following saturation for linearly unstable distributions. Most theoretical investigations are devoted to calculating the amplitude of the unstable field mode at saturation, or the amplitude of the oscillations in the asymptotic state. Moreover, most of these models apply only to weakly unstable modes, since they use expansions about the (linearly) neutrally stable state. The discrepancies among different theories are serious and we shall address this problem numerically in Sect. 5.4.

While linearly stable and unstable equilibria behave in a qualitatively different way during the early evolution of the system, strong similarities are observed – in

several cases – in the nonlinear regime and in the asymptotic state; in particular, the damping of the amplitude oscillations and the steady-state oscillations at the linear frequency in the asymptotic state are common to the maxwellian, the symmetric bump-on-tail and the two-stream distributions (although, as we shall see, the linear frequency is zero in this latter case). The amplitude of the asymptotic oscillations, however, while it is related to the strength of the perturbation in the stable case, it rather depends on the saturation amplitude in case of instability.

### 5.3.1 Symmetric bump-on-tail distribution.

A symmetric bump-on-tail distribution

$$f_0(v) = \frac{n_p}{\sqrt{2\pi}} e^{-\frac{v^2}{2}} + \frac{n_b}{\sqrt{2\pi}} [e^{-\frac{1}{2}(\frac{(v-V_0)}{v_t})^2} + e^{-\frac{1}{2}(\frac{(v+V_0)}{v_t})^2}] \qquad (5.3.1)$$

is predicted to be unstable by linear theory when the wave number of the perturbation lies in a certain range. In (5.3.1), $n_p$ is the plasma density, $n_b$ the beam density, $V_0$ the beam drift velocity and $v_t$ its thermal spread. Note that, because of the normalization condition $\int f_0 = 1$, we must have $n_p + 2v_t n_b = 1$. This distribution has never been subject of numerical investigation with the splitting scheme; some numerical results have been obtained by Klimas [38] using the Fourier-Fourier algorithm, but the simulations were not carried far enough in time for the system to be close to its asymptotic state. Our results are the first to appear in this case. With $n_p = 0.9$, $n_b = 0.1$, $v_t = 0.5$, $V_0 = 4.5$ and $k = 0.3$ the symmetric bump-on-tail is unstable, the linear dispersion relation giving $\omega_r = 1.05$ and $\gamma = 0.148$, with a phase velocity $v_\phi = 3.5$, well within the rising portion of the distribution. Initially, we perturbed according to (5.1.1) with $\epsilon = 0.04$ and $m = 3$. Figs 5.12a-d show the amplitudes $|E_1|$, $|E_2|$ and $|E_3|$ and the electric energy $W$ as functions of time. Figs. 5.15a-f show the electric field at selected times. The system evolves according to linear theory ($\omega_r \approx 1.04$ and $\gamma \approx 0.14$ from our simulation) until saturation occurs, than the

behaviour is very similar to the one observed in the case of a maxwellian equilibrium, with damped amplitude oscillations. In figs. 5.13a-l the level curves of the distribution function are shown at selected times. Again, vortices have formed in phase space, with the same qualitative features as in the maxwellian case. The vortices move parallel to the x-axis, in opposite directions, their speed being equal to the phase velocity of the wave. Note how the structure of the vortices becomes smoother and smoother as time proceeds. Figs. 5.14a-l show the space averaged distribution, which coincides with the original bump-on-tail equilibrium at $t = 0$, then undergoes modifications and settles to a shape with the minimum at the phase velocity of the wave; note that the initial bump has been greatly reduced, since most of the kinetic energy of the resonant electrons has been pumped into the potential energy of the instability.

The numerical results seem to indicate an asymptotic state with the same qualitative features seen for the maxwellian. The electric field performs steady state oscillations and behaves like a standing wave, indicating that this asymptotic state is a superposition of two solutions of the BGK equations but not a BGK equilibrium by itself.

As we have seen, choosing a smaller value for $\epsilon$ has a significant influence on the nonlinear evolution of a perturbation to a maxwellian equilibrium; this is not so in the case of an unstable distribution. Fig. 5.16 shows the amplitude of the fundamental mode of the electric field when $\epsilon = 0.004$. Saturation occurs somewhat later, but the saturation amplitude is exactly the same as for the case with $\epsilon = 0.04$ and the same is true for the frequency of the amplitude oscillations that follow saturation, which is seen to depend upon the saturation amplitude. This fact gives an indication about stability of linearly unstable distributions, suggesting that, at least in the present case, linear instability implies instability.

While the choice of a non symmetric perturbation (in velocity) led to travelling waves in the maxwellian case, the behaviour looks different for the symmetric bump-on-tail. The results when perturbing with

$$\tilde{\epsilon}(v) = e^{-(v-V_0)^2}$$

with $V_0 = 4.5$ are shown in figs. 5.17 (amplitude of the fundamental mode of the electric field), 5.18a-l (level curves of $f$), 5.19a-l ($< f >$ at positive velocities), 5.20a-f ($< f >$ at negative velocities) and 5.21a-l (electric field). During the whole linear evolution of the system (until $t \approx 40$) the electric field behaves like a travelling wave, with a phase velocity $v_E$ which decreases in time ($v_E \approx 5.5$ at $t = 0$ and $v_E \approx 4$ at $t = 25$, as it appears from figs. 5.21a-d) and turns rapidly into a standing wave at saturation. Two travelling waves, at $\pm v_\phi = \pm \omega_r / k$ have been initially excited with different amplitudes (because of the asymmetry in the perturbation). Due to the symmetry of the equilibrium distribution, they both become unstable, they saturate with the same amplitude and at the same time and then superpose to yield a standing wave. Note, from the level curves in phase space, how the two vortices which have formed at $\pm v_\phi$ appear to have the same size after saturation, while during the linear evolution of the system (at $t = 25$ and $t = 26$) the modifications in $f(x, v, t)$ at $v < 0$ are negligible. The same information is given by the plots of the space averaged distribution; the initial bump is washed away much more slowly at negative velocities, but the shape of $< f >$ looks, asymptotically, roughly the same for $v > 0$ and for $v < 0$. The considerations about the asymptotic state are identical to those for the case of a symmetric perturbation.

Finally (in figs. 5.30a-l), we report the level curves of the distribution function again for the case of the symmetric perturbation but with $M = 512$ instead of 256. It is quite clear that the smoothing of the structure in the vortices proceeds in the

same way; if this is a purely numerical effect, a much smaller grid would have to be used in order to detect it. The problem remains wide open.

### 5.3.2 One sided bump-on-tail distribution.

Numerical results for the one sided bump-on-tail equilibrium distribution

$$f_0(v) = \frac{n_p}{\sqrt{2\pi}} e^{-\frac{v^2}{2}} + \frac{n_b}{\sqrt{2\pi}} e^{-\frac{1}{2}(\frac{v-V_0}{v_t})^2}$$

when perturbing according to (5.1.1) have been obtained by Shoucri [21] with the splitting scheme algorithm. He used $n_p = 0.9$, $n_b = 0.2$, $v_t = 0.5$, $V_0 = 4.5$, $k = 0.3$, $m = 3$ and $\epsilon = 0.04$. Unfortunately, this simulation couldn't be carried far enough in time because, as shown in [39-40], nonlinear wave-wave interaction becomes important after $t \sim 200$ due to the growing sidebands, which disrupt the trapped particles oscillations in the fundamental mode. The problem can be avoided by perturbing with $m = 1$ instead of $m = 3$, and the evolution of the system can be followed for longer times. Our results are shown in figs. 5.22a-d (fundamental mode and first two harmonics of the electric fieldand electric field energy), 5.23a-h (level curves at selected times), 5.24a-l (space averaged distribution) and 5.25a-l (electric field). The fundamental mode of the electric field remains dominant during the whole simulation, so $E(x,t)$ is approximately sinusoidal for all times. The mode grows initially with a growth rate $\gamma \approx 0.19$, then saturates and performs the damped amplitude oscillations that we have already seen in investigating the previous distributions. The oscillations at the rapid time scale, however, appear to be of a very different nature than those seen in the other cases. The electric field amplitude doesn't go to zero, but oscillates slightly about some mean value. Moreover, looking at the behaviour of the electric field, we see that, now, the nodes do not remain fixed but do propagate, so $E(x,t)$ behaves like a travelling wave, as was to be expected since $f_0(v)$ is not symmetric in this case. Because of this asymmetry in the equilibrium distribution, only one

unstable travelling wave is excited in this case; as a consequence, we wouldn't expect to see the oscillations on the fast time scale in $|E_1|$, since the term $e^{ikx+i\omega_r t}$ is absent in the linear solution for $E_1$. The oscillations seen in the numerical results are due to the beating between the unstable mode and the least damped mode, which happens to be at $\omega_r \approx -1.1$. Then the observed frequency should be $\omega_r \approx 2.1$; from our numerical results we have $\omega_r \approx 2.09$, in excellent agreement. Note that these small oscillations persist throughout the whole simulation and that there is no indication that they might die out asymptotically (as it is clear from the graph of $W$ as well).

In phase space, we observe that only one vortex is formed, located at positive velocities, centered at $v_\phi = \omega_r/k$ and travelling parallel to the space axis at the phase velocity of the wave. In the space averaged distribution,the size of the initial bump has decreased, as the energy of the resonant electrons has been transformed into the electric energy of the instability. As the system evolves towards its asymptotic state, the shape of $< f >$ is qualitatively the same as the one we have seen in the previous cases, with the minimum performing small attenuated oscillations about a value close to the wave phase velocity. The numerical results, however, leave in this case the uncertainty of whether the minimum settles asymptotically exactly at the phase velocity of the unstable mode or at a slightly shifted position, maybe related to the beating frequency mentioned above.

Although the system is seen to approach the asymptotic state more slowly in this case, the numerical results indicate that the electric field amplitude will perform steady-state oscillations, with the electric field behaving like a travelling wave. Since travelling waves rather than standing waves dominate the nonlinear behaviour of this system, there is enough motivation to look for BGK equilibria in the asymptotic state. In the case of a BGK equilibrium, as we have seen in Sect. 2.5, the electric field must

have the form $E(x,t) = E(x - Vt)$ for some real $V$. Therefore, for the electric energy we must have

$$\begin{aligned} W(t) &= \int_0^L [E(x,t)]^2 \, dx \\ &= \int_0^L [E(x - Vt)]^2 \, dx \\ &= \int_{-Vt}^{-Vt+L} [E(y)]^2 \, dy \end{aligned}$$

which is independent of time thanks to the periodicity of $E(x,t)$. Since the small oscillations on the fast time scale do not seem to disappear asymptotically, as we have already observed, the system does not approach a BGK equilibrium. In this respect, even on the basis of the same numerical results, our interpretation of the asymptotic state is in contradiction with the conclusions drawn in [21].

### 5.3.3 Two-stream distribution.

When solving the linear dispersion relation for the two-stream equilibrium distribution

$$f_0(v) = \frac{1}{2\pi} v^2 e^{-\frac{v^2}{2}}$$

with $k = 0.5$, one finds $\omega_r = 0$ and $\gamma \approx 0.26$. With $v_\phi = \omega_r / k = 0$ one expects no oscillations at the plasma frequency but, since the mode grows unstable, electron trapping should occur until saturation, with subsequent oscillations at the trapping frequency. If these slow oscillations are damped, the electric field (and therefore the potential) should approach asymptotically a time independent spatially periodic structure which could be a candidate for a BGK equilibrium. That BGK equilibria are the asymptotic states of the system when starting from a two-stream equilibrium distribution has been speculated for many years and, more recently, numerical evidence has been supplied in support of this idea (see [41] and references cited therein).

Our results, shown in figs. 5.26a-d (fundamental mode and first two harmonics of

the electric field and electric field energy), 5.27a-h (level curves), 5.28a-f (space averaged distribution) and 5.29a-f (electric field), are fully consistent with those obtained by Ghizzo et al. [41]. The electric field remains, again, approximately sinusoidal during the whole simulation, settling asymptotically to a time independent curve. In phase space, only one vortex has formed, which appears not to move at all when the system is approaching the asymptotic state. Note, again, how the fine structure which has formed in the vortex gets smoothened as time proceeds. Note also that the vortex, which appears to be centered at the origin for quite long time, has slightly moved later on and its center seems to settle, asymptotically, to a point nearby the origin on the space axis; at the same time, the nodes of the electric field have moved as well and, asymptotically, place themselves slightly off the boundary points $x = 0$ and $x = L$. Since the symmtery property illustrated in Sect. 2.2 is respected by the initial data for this case, and therefore $E(0,t) = E(L,t) = 0$ has to remain true for all $t$, we regard this displacement (which can be observed in [41] as well) as a purely numerical effect which, however, does not seem to affect significantly the conclusions that can be drawn from the results.

For this distribution, the asymptotic state seems to have all the required properties for being a BGK equilibrium. The only question which remains open is about the filamentation process which, in principle, should stop if a BGK equilibrium has to be approached.

### 5.4 The saturation amplitude for weakly unstable modes.

As we know, some spatially homogeneous equilibrium distributions are unstable against perturbations having wave number lying in a certain range. When one of these linearly unstable modes is excited, it grows according to linear theory and then it

saturates with some amplitude $\Gamma$ (the saturation amplitude), which in turn determines the frequency of the amplitude oscillations that follow saturation. Several theoretical models have been developed in order to calculate the saturation amplitude in terms of the relevant parameters of the problem, all of them giving different answers.

In order to outline the starting points and the predictions of these models, let us consider the (Case-Van Kampen) linear dispersion relation in its dimensional form:

$$\Lambda(\nu) \equiv 1 - \frac{\omega_p^2}{k^2} \int \frac{\partial f_0/\partial v}{v - \nu} = 0$$

where all the parameters have been previously defined. Suppose that $\Lambda(\nu)$ has only one zero, say $\nu_0$, for $k = k_0$ and not for any other $k$. Moreover, let $n = n_0$ be the value of the density for which $\nu_0$ is real, i.e. the plasma is linearly stable. As the density is increased to $n = n_0(1 + \Delta)$, with $\Delta \ll 1$, the eigenvalue moves off axis and the mode $k = k_0$ becomes linearly unstable. Simon and Rosenbluth [13] and Burnap, Miklavcic, Willis and Zweifel [12] calculated the saturation amplitude $\Gamma$ as function of $\Delta$ using perturbation techniques. The two results agree in that the functional dependence of $\Gamma$ on $\Delta$ is $\Gamma(\Delta) \sim \Delta^{1/2}$ but the coefficients are different. As shown by Larsen, Burnap and Zweifel [42], the growth rate scales linearly with $\Delta$, when $\Delta$ is small, so we also have $\Gamma \sim \gamma^{1/2}$. In an earlier paper [11], O'Neil, Winfrey and Malmberg proposed a simplified model that describes the nonlinear interaction of a low density electron beam with a cold one-dimensional plasma. They adopted a single-wave model and developed a set of scaled equations for the beam electrons and the time evolution of the wave, including the background plasma only as a dielectric. The scaled equations are written in terms of universal variables, so they need to be solved only once. Their numerical result indicates that saturation occurs when $\omega_t \equiv \sqrt{e\Gamma k/m} = \sqrt{1.6}\gamma$, where $\gamma$ is the growth rate. Thus, the saturation amplitude scales as $\gamma^2$. In terms of $\Delta$, we then have $\Gamma \sim \Delta^2$ (for small $\Delta$). Note that the scaling $\Gamma \sim \gamma$ found by O'Neil

is independent of the numerical solution of his scaled equations, but it is rather a consequence of the fact that the ratio $\omega_t/\gamma$ can be expressed uniquely in terms of his universal variables. Since the validity of his model mainly relies on the single-wave approximation, we expect the scaling $\Gamma \sim \gamma^2$ to be valid in a finite system where, due to the discrete nature of the spectrum, it is easy to prepare the initial conditions so that a single mode remains dominant at all times. Note, also, that the scaling found by Simon et al. and Burnap et al. is expected to be valid only for weakly unstable modes, since their expansion parameter, $\Delta$, must be small. No such assumption is made in O'Neil's model; on the contrary, his scaling is supposed to be valid in a wide range of initial conditions and, therefore, growth rates. For example, in the cases that we have studied in Sect. 5.3 for the symmetric and one sided bump-on-tail, $\Delta = 1.07$ and $\Delta = 1.59$ respectively, so those instabilities are not in the regime where the expansions of Simon et al. and Burnap et al. are valid. Finally, the analyses of Simon et al. and Burnap et al. are asymptotic in nature, so what they calculate is rather the amplitude of the asymptotic oscillations $\Gamma_\infty$ than the saturation amplitude. It is possible, in principle, that the instability apparently saturates with some amplitude $\Gamma$ and then it rises again, more slowly, to saturate much later with a (second) saturation amplitude which scales as $\Delta^{1/2}$. Alternatively, if we believe (as we have done so far) that the saturation amplitude and the asymptotic amplitude are of the same order of magnitude, the discrepancy remains. More recently [14], J.D. Crawford has proposed a model that makes use of bifurcation theory methods and came to a third independent calculation of the saturation amplitude. Although collisions are included in his theory via the Krook collision model [1], his result agrees with the Simon and Rosenbluth scaling.

So far, two numerical investigations have been devoted to solving the discrepancy.

In the first one, Denavit [23] considered a plasma with cold immobile ions and an electron population with a large cold component and a smaller component having a bump-on-tail distribution. The simulations were carried out with two different algorithms, the leap frog [18] and the long-time-scale algorithm [43], both devised by Denavit himself and none of which can be claimed to solve the Vlasov-Poisson system exactly. The leap frog algorithm is basically a particle simulation model in which the distribution of the particles in phase space is reconstructed every $N_{rec}$ time steps: as shown in the simulations presented in the original paper [18], the results, although qualitatively correct for short times, are very sensitive to $N_{rec}$ and to the type of averaging operations used for the reconstruction. The long-time-scale algorithm assumes and uses the knowledge of the trajectories of the particles on the short time scale characterized by the inverse plasma frequency and actually performs the integration over times of the order of the slow scale characterized by the inverse trapping frequency. Therefore, while for the leap frog scheme the time step has to be much smaller than the inverse plasma frequency, only time steps much smaller than the inverse trapping frequency need to be taken with the long-time-scale algorithm and the numerical integration proceeds much faster. Several weakly unstable cases were followed until saturation using these two schemes; the values for $\Delta$ ranged between $3.15 \times 10^{-4}$ and 0.367 giving growth rates between $1.605 \times 10^{-4}$ and $2.4 \times 10^{-2}$. The results of the two algorithms agree for $\Delta$ not too small ($\Delta > 0.1$) but show some discrepancy (mainly in the growth rates) as $\Delta$ is getting smaller; in any case, they seem to indicate that both $\gamma$ and the trapping frequency at saturation $\sqrt{e\Gamma k/m}$, behave linearly with $\Delta$ in the range of $\Delta$'s there considered, thus confirming O'Neil's $\Delta^2$ scaling rather than the $\Delta^{1/2}$ of Simon et al. However, the discrepancy is not completely solved by Denavit's numerical calculations. For the case $\Delta = 0.13$ (with $\gamma \approx 0.01$), as shown in the paper, the amplitude of the electric field keeps increasing,

after this first apparent saturation, at a much slower rate, allowing for a (second) saturation at some later time. This very long simulation was apparently performed with the long-time-scale algorithm only; the leap frog scheme does not allow very long simulations, due to the appearance of numerical instabilities (there interpreted as beaming instabilities). Whether this increase of the electric field amplitude following saturation is a numerical artifact or a true feature of the physical solution of (VP) for this case is still an open question.

More recently, Simon, Radin and Short [24] carried out a few simulations following the behaviour of the solution for much longer times than Denavit did, using again the leap frog algorithm. They observed the onset of the beaming instability, attributing the cause of it to the formation of ripples in the space averaged distribution near $v = 0$. In a second run, they were able to control the onset of these large oscillations in the electric field amplitude (shifting it much later in time) by warming the cold background electron component; this allowed them to follow the behaviour of the electric field amplitude for a much longet time, until it actually reached a value very close to the asymptotic prediction of Simon et al., at which time the large oscillations of the beaming instability set up. Ripples on the space averaged distribution had appeared much earlier, rising legitimate doubts on the reliability of the results. In a third run, they eliminated the background component, leaving only the bump-on-tail equilibrium distribution, but the beaming instability (and the ripples on the space averaged distribution) showed up shortly after saturation, making any conclusion impossible to be drawn. In these three simulations, although $\Delta$ was kept small, they claimed that the conditions for the time asymptotic estimate of Simon et al. to be valid were not met; not only $\Delta \ll 1$ is required, but also $q \ll 1$, where

$$q \equiv 24 \times \Delta \times \frac{v_t^6 v_l^4}{\bar{\nu}^6 v_b^2 (v_d^2 - \bar{\nu}^2)}$$

with $v_b$ the thermal spread of the bump, $v_d$ its peak velocity, $v_t$ the thermal spread of the main maxwellian component, $v_l \equiv \omega_r/k$ the linear phase velocity and $\bar{v}$ the real eigenvalue corresponding to the stable case (i.e. $\Delta = 0$). In their last simulation they arranged the parameters so that $\Delta \ll 1$ and $q \ll 1$ were both satisfied, succeeding in this way in producing a simulation free from the large oscillations in the electric field amplitude, although the ripples in the space averaged distribution developed again. In this case, the time evolution of the electric field could be followed for much longer time, but the asymptotic limit that the field seems to approach is still 20 times below the value predicted by Simon et al.

Given the wide range of uncertainty left by the above mentioned simulations, mainly because of the numerical approaches used, the need is felt for attacking the problem with the more accurate splitting scheme algorithm. First, we check the scaling of the saturation amplitude $\Gamma$ with the parameter $\Delta$, carrying out the calculation for both the symmetric and the one sided bump-on-tail distributions; by continuing the calculation for a few trapping periods, we also check the dependence of $\omega_A$ (the frequency of the amplitude oscillations) with $\Delta$. Subsequently, we produce two simulations carried out far enough after saturation which confirm the increase in the amplitude of the electric field. Again, we would like to emphasize that the indications given by the splitting scheme are not totally exempt from uncertainty, especially because of the smoothing of the phase space structure that still needs to be understood. However, the results about the saturation amplitude are certainly correct and the results of longer simulations have much more credibility than those obtained with other algorithms.

In addressing the problem with our code based on the splitting scheme algorithm, which uses the dimensionless formulation of (VP), we are not free to vary the density,

but the only parameter that we have at our disposal, and that we have to relate to the fractional density $\Delta$, is the wave number $k$. What the relationship between $\Delta$ and $k$ is, is readily found by noting that, as $n \rightarrow n(1+\Delta)$ we have $\omega_p \rightarrow \omega_p\sqrt{1+\Delta}$ and $\lambda_D \rightarrow \lambda_D\sqrt{1+\Delta}$. Therefore, if $k_0$ is the wave number corresponding to the stable case, we have to choose

$$k(\Delta) = \frac{k_0}{\sqrt{1+\Delta}} \tag{5.4.1}$$

for our simulations.

As anticipated above, we first check the functional relationship of $\gamma$, $\Gamma$ and $\omega_A$ with $\Delta$, both for the symmetric and the one sided bump-on-tail distributions. We use the same parameters as in Sect. 5.3.1 and 5.3.2, i.e. $V_0 = 4.5$, $v_t = 0.5$, $n_p = 0.9$ and $n_b = 0.1$ for the symmetric and $n_b = 0.2$ for the one sided bump-on-tail. Using Nyquist diagrams [1] and the expressions given in Sect. 3.4, we find $k_0 = 0.4314$ for the symmetric and $k_0 = 0.4824$ for the one sided bump-on-tail. Then, increasing $\Delta$ and calculating $k$ from (5.4.1), we solve the linear dispersion relation to obtain $\gamma$. In table 5.1a and 5.1b $\Delta$ and the corresponding values for $k$ and $\gamma$ are shown in the first three columns, while fig. 5.31 shows $\gamma$ as a function of $\Delta$, for the symmetric and the one sided bump-on-tail. The linear relationship between $\gamma$ and $\Delta$ for small $\Delta$ is clearly confirmed. In reporting the results for $\Gamma$ and $\omega_A$ we shall express them in terms of $\gamma$ instead of $\Delta$.

For each of the values of $\Delta$ listed in tables 5.1a and 5.1b we performed a simulation with our code, following the evolution of the unstable mode until it saturates, so that $\Gamma$ could be read directly from the output. For a few simulations with the one sided bump-on-tail and some more with the symmetric one, we have followed the unstable mode for a few trapping periods after saturation, allowing for the calculation of $\omega_A$. The last three columns of tables 5.1a and 5.1b show $\omega_A$ in those cases where

we followed the evolution for longer times, the saturation amplitude $\Gamma(\Delta)$ and the quantity $\Gamma(\Delta) - \Gamma(\Delta = 0)$. In figs. 5.32 and 5.33 $\omega_A(\gamma)$ and $\Gamma(\gamma) - \Gamma(\gamma = 0)$ are shown for the symmetric and the one sided case. Clearly, as $\gamma \to 0$, or $\Delta \to 0$, the $\Gamma \sim \Delta^2$ scaling of O'Neil is confirmed, so our results are consistent with Denavit's. The results for $\omega_A$ are in excellent agreement with O'Neil's model, as can be seen from fig. 5.32, where the straight lines corresponding to $\omega_A = \sqrt{1.6}\gamma$ for the one sided and $\omega_A = 1.64\gamma$ for the symmetric bump-on-tail have been drawn for comparison.

In all the simulations that we have performed the observed growth rate was very close to the value given by the linear dispersion relation; we always used this latter to express the functional dependence of $\Gamma$ and $\omega_A$ upon $\gamma$.

As mentioned earlier, the analysis of Simon et al. and Burnap et al. is asymptotic in nature, so what it calculates is actually the amplitude of the asymptotic oscillations. That the usually observed saturation might be only apparent has been suggested by the numerical simulations performed with Denavit's code. Unfortunately, the complete answer to the question implies many long and expensive computer runs that we are unable to produce at the moment, leaving room for future work. However, a moderately long run is enough to understand if the saturation is only apparent or not. Here, we produce two simulations, one for the one sided and one for the symmetric bump-on-tail distribution. For the case with $\Delta = 0.07$ we followed the time evolution of the instability long after the first apparent saturation which occurs in both cases at $t \approx 100$; our simulation for the one sided case runs until $t = 5000$ and the one for the symmetric case until $t = 3000$. The amplitude of the fundamental mode of the electric field is shown in figs. 5.34a-e for the one sided and in figs. 5.35a-c for the symmetric case, this time in linear rather than logarithmic scale. The electric field energy for the symmetric bump-on-tail from $t = 2000$ to $t = 3000$ is shown in

Fig. 5.35d. It is clear that the saturation of the fundamental mode at $t \approx 100$ is only apparent in the one sided case. The rate of increase of $|E_1|$ appears to be very slow and the (second) saturation has to occur much later. In the symmetric case, the saturation of the fundamental mode at $t \approx 100$ seems to be real, the amplitude is not seen to increase any longer. However, from Fig. 5.35d, it is clear that the electric energy does increase after the saturation of the fundamental mode, indicating that the contribution of some other mode must have become important, although not dominant since the oscillations appear to have the same frequency for $|E_1|$ and $W$. When this simulation was performed, we looked only at the first two harmonics, which do not show any sign of increase at long times;some higher mode must bear the responsibility for this phenomenon. Perhaps, a reason for this could rely on the fact that O'Neil considers an electric field with only one Fourier component; on the other hand, the effect of the continuous spectrum in the linear solution (see 3.3.9) is neglected – invoking Landau damping – in the approaches of Simon et al. and of Burnap et al., while it is present in O'Neil's model, though heuristic it might be.

In the simulation for the one-sided bump-on-tail we did not observe, as Simon et al. did in [24], the formation of ripples in the space averaged distribution near $v = 0$; this makes the extension to much longer runs very promising.

A final comment is in order at this point. This apparent saturation of the amplitude should not sound alarming for the conclusions that we drew in the previous sections with regard to the asymptotic states for similar distributions. In all of the cases, for which we described the asymptotic state as being characterized by an electric field amplitude performing steady-state oscillations, switching from the usual logarithmic to the linear scale did not change the result, i.e. there was no evident increase in the electric field amplitude after saturation. For some of the runs that

we have presented here up to final times $\sim$ 200 or $\sim$ 400 we prolonged the simulation until $t = 1000$ and, again, we observed steady-state oscillations in the electric field amplitude. Those cases, of course, could not be classified as weakly unstable. This problem opens the interesting question of why the electric field amplitude keeps increasing in some cases while in others it doesn't.

### 5.5 Comment on linear theory and asymptotic states.

It is rather remarkable how linear theory, which can adequately describe the early evolution of the system but has to be abandoned during the nonlinear evolution, can at least be partially restored in the description of the asymptotic state, in which we observe an electric field performing steady-state oscillations at the linear frequency and the space averaged distribution settling with a minimum at the phase velocity of the wave. In the course of the nonlinear evolution of the system, in correspondence to the alternating phases of damping and growth of the electric field amplitude, the minimum of the space averaged distribution oscillates about the wave phase velocity, $v_\phi$, so that at some times $v_\phi$ lies in the rising portion of the distribution and in the falling portion at some other times. Although an attempt to apply linear theory to these intermediate times would fail, since the position of $v_\phi$ relative to the minimum and the instantaneous damping (or growth) rate are incompatible with the linear description, in all cases that we checked, using the numerical method outlined in Sect. 3.4.1, the system always tends to a state which can be understood in terms of the eigenvalue of the space averaged distribution. On one hand, this observation makes us more confident in the reliability of the numerical indications about the asymptotic state and, on the other, we are strongly tempted to draw the conclusion that linear theory might have a more profound validity than it is usually assumed.

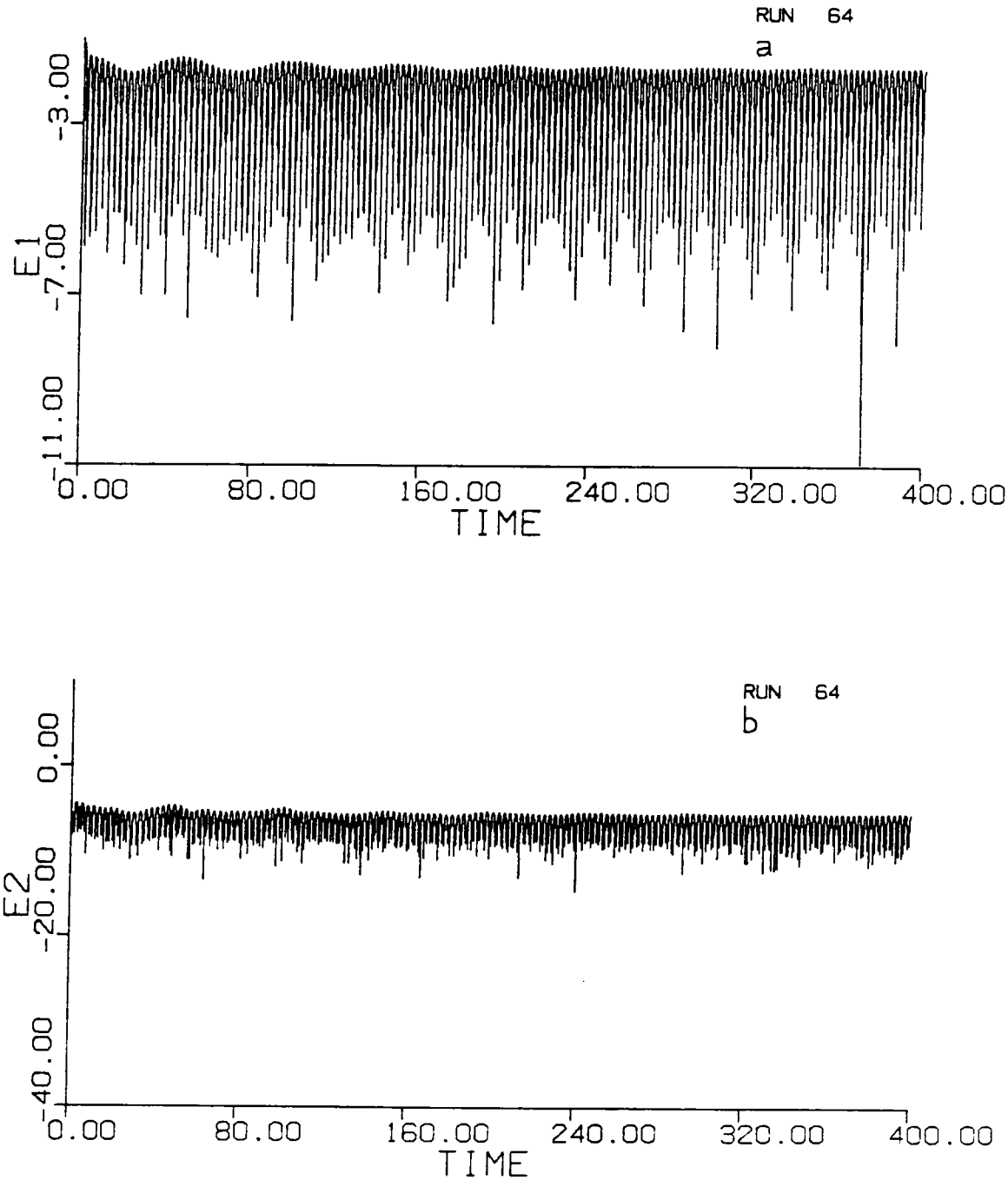


**Fig. 5.1** $|E_1|$ **(a) and** $|E_2|$ **(b) for the maxwellian case with** $\epsilon = 0.1$ **and** $m = 1$.

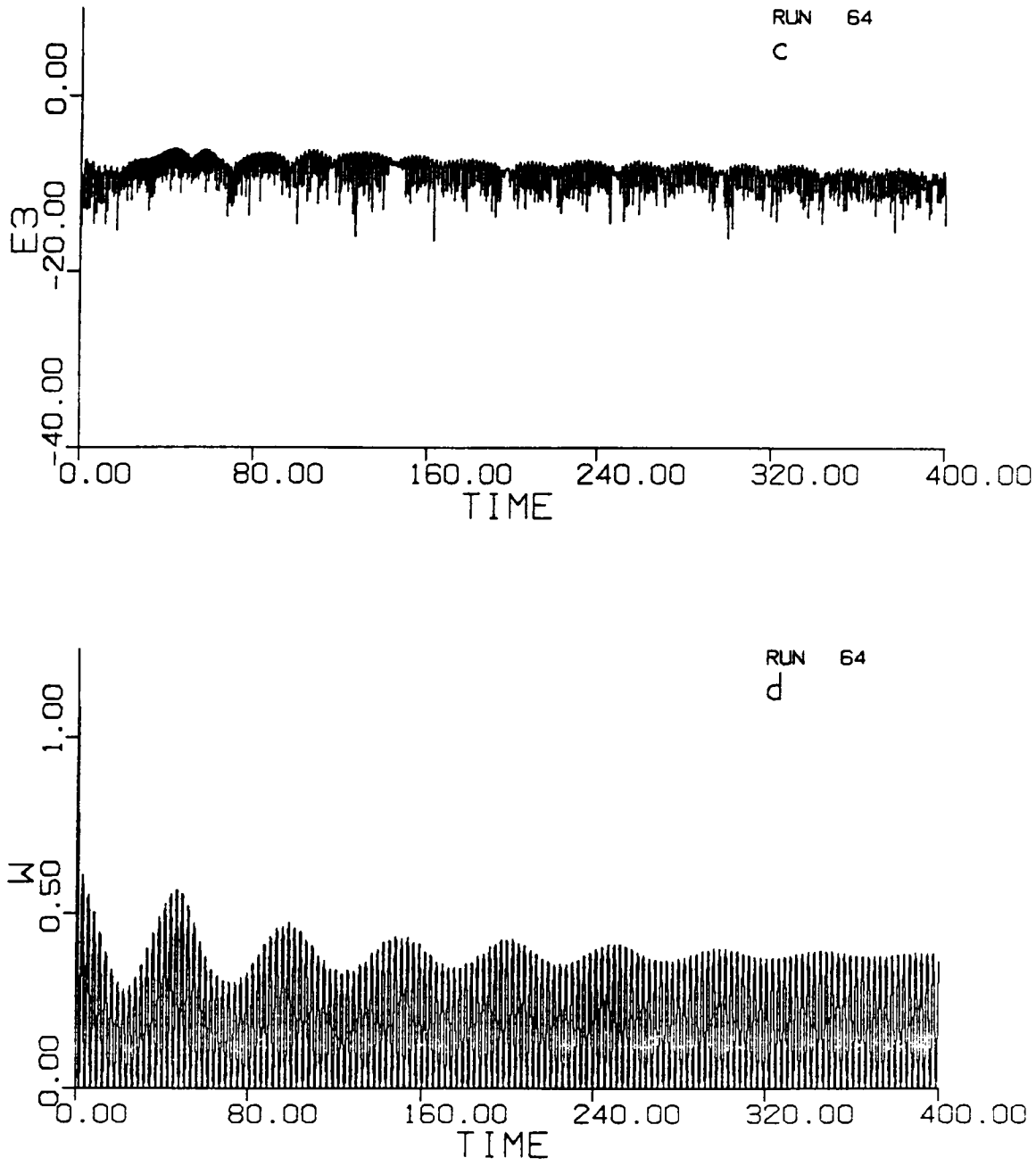


**Fig. 5.1** $|E_3|$ **(c)** and $W$ **(d)** for the maxwellian case with $\epsilon = 0.1$ and $m = 1$.

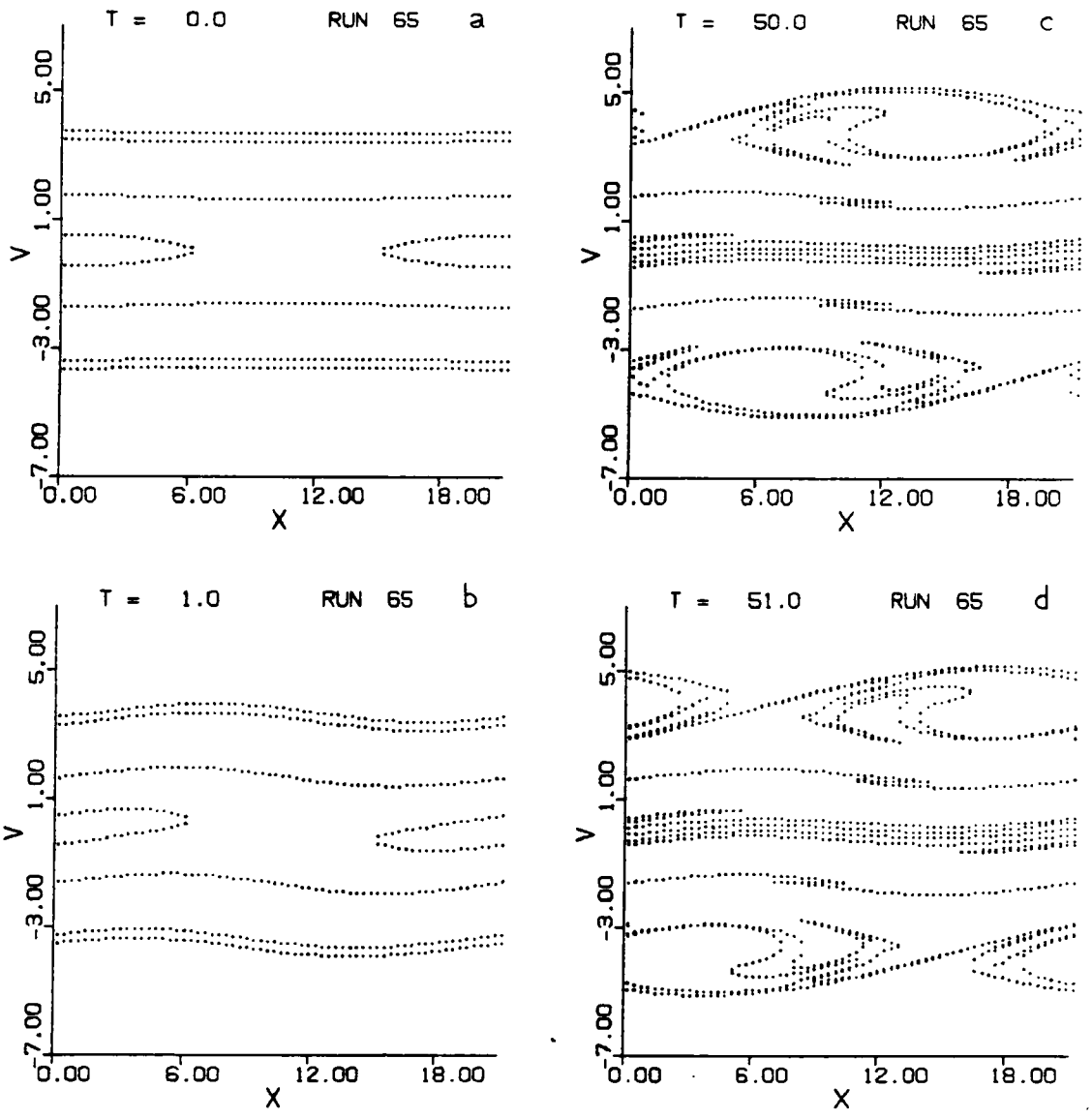


Fig. 5.2 (a)-(d) Level curves for the same case as in Fig. 5.1.

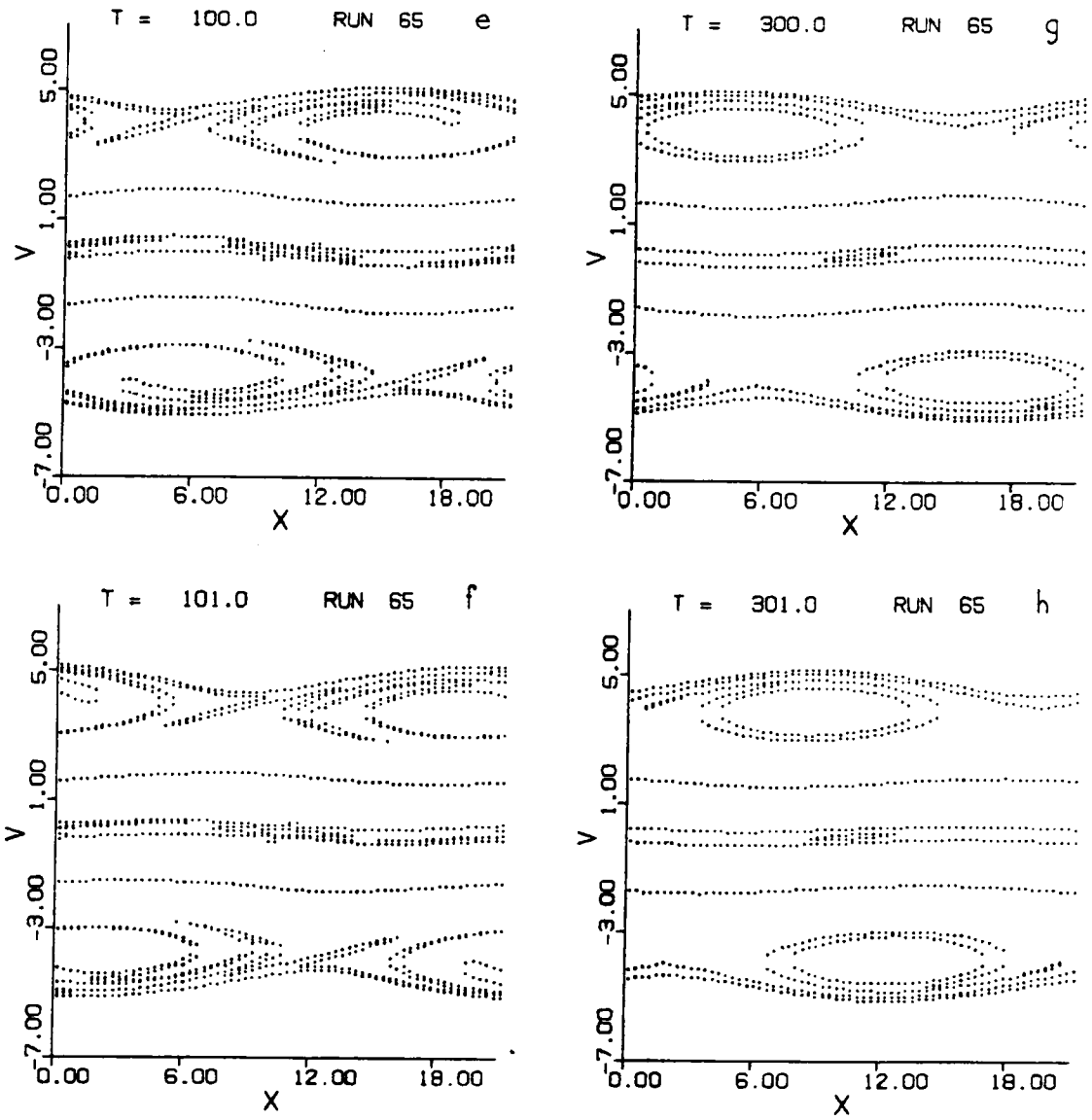


Fig. 5.2 (e)-(h) Level curves for the same case as in Fig. 5.1.

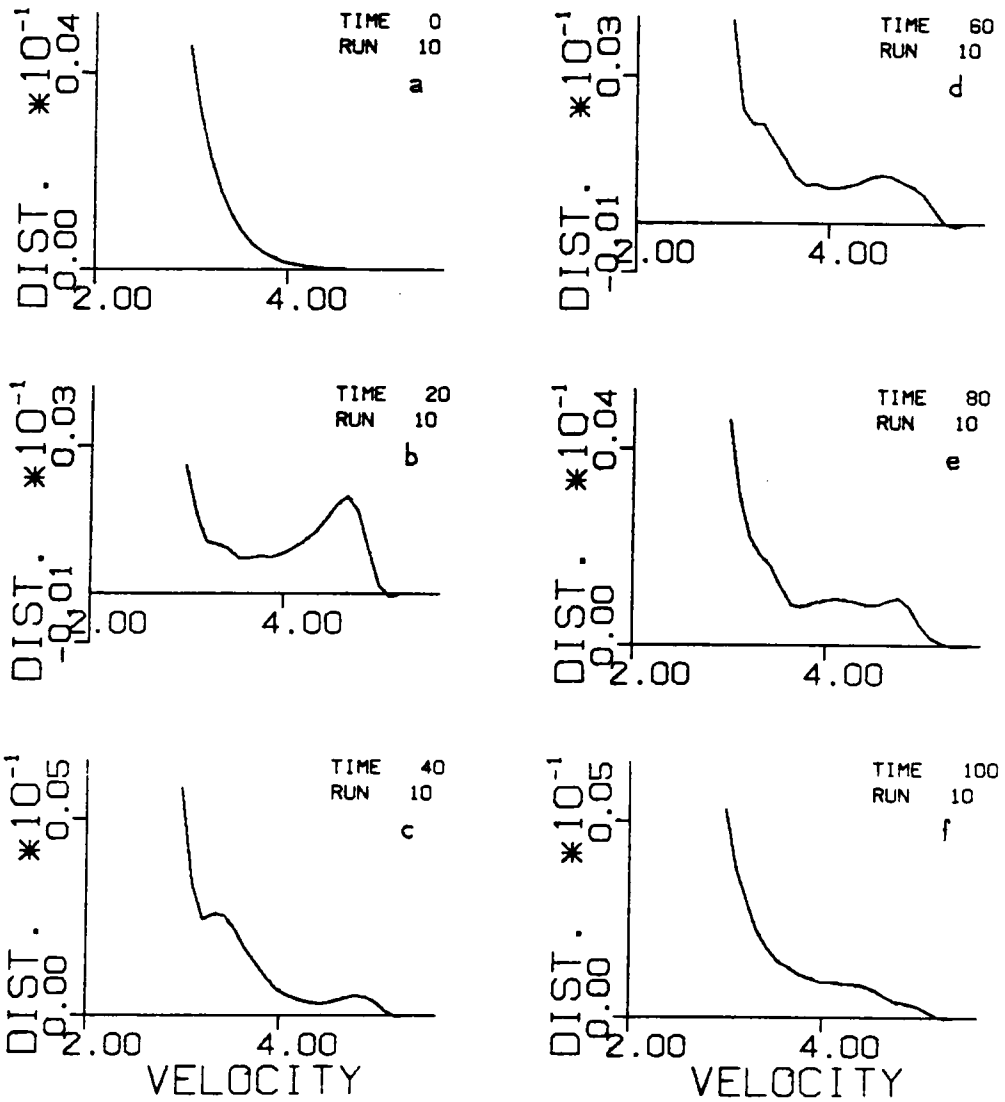


**Fig. 5.3 (a)-(f)** Space averaged distribution for the same case as in Fig. 5.1.

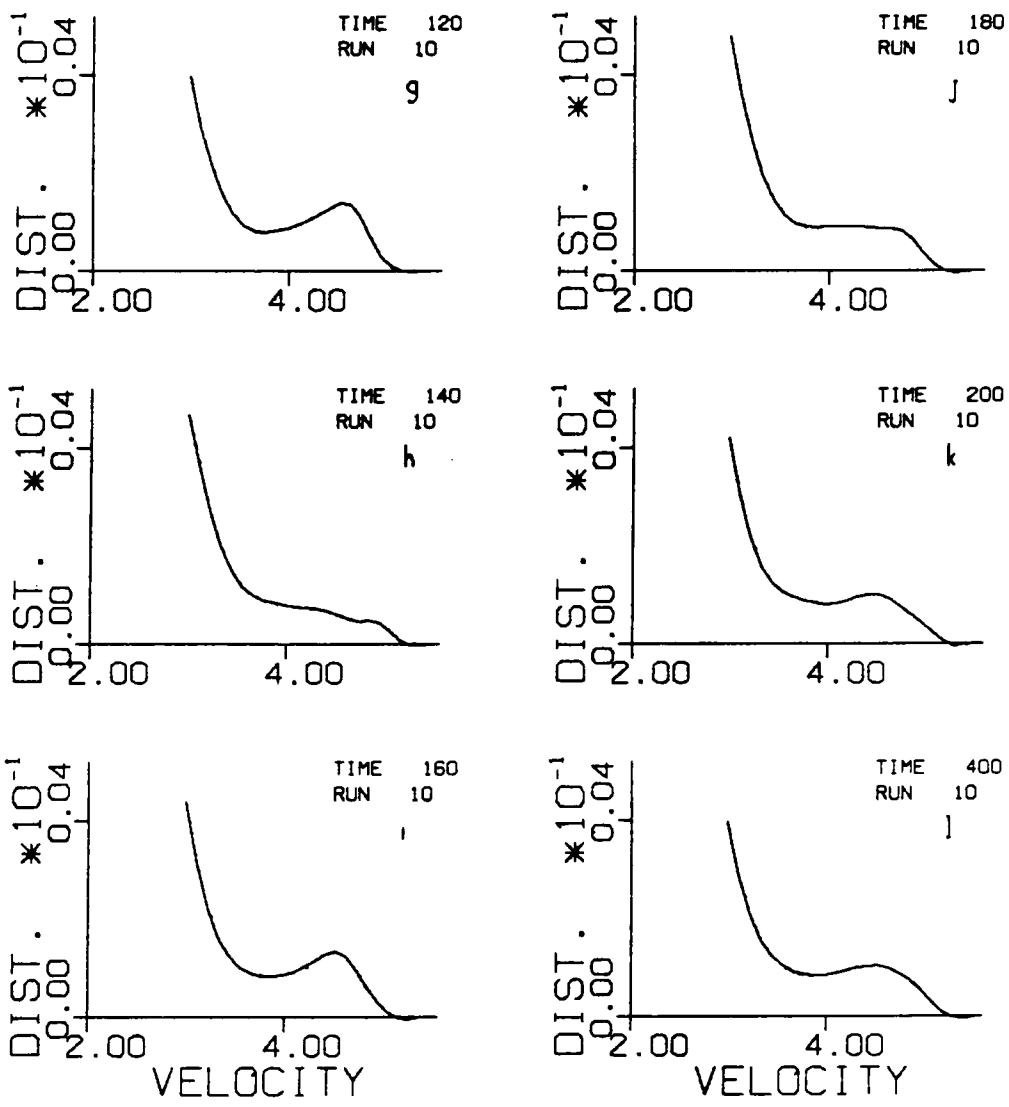


Fig. 5.3 (g)-(l) Space averaged distribution for the same case as in Fig. 5.1.

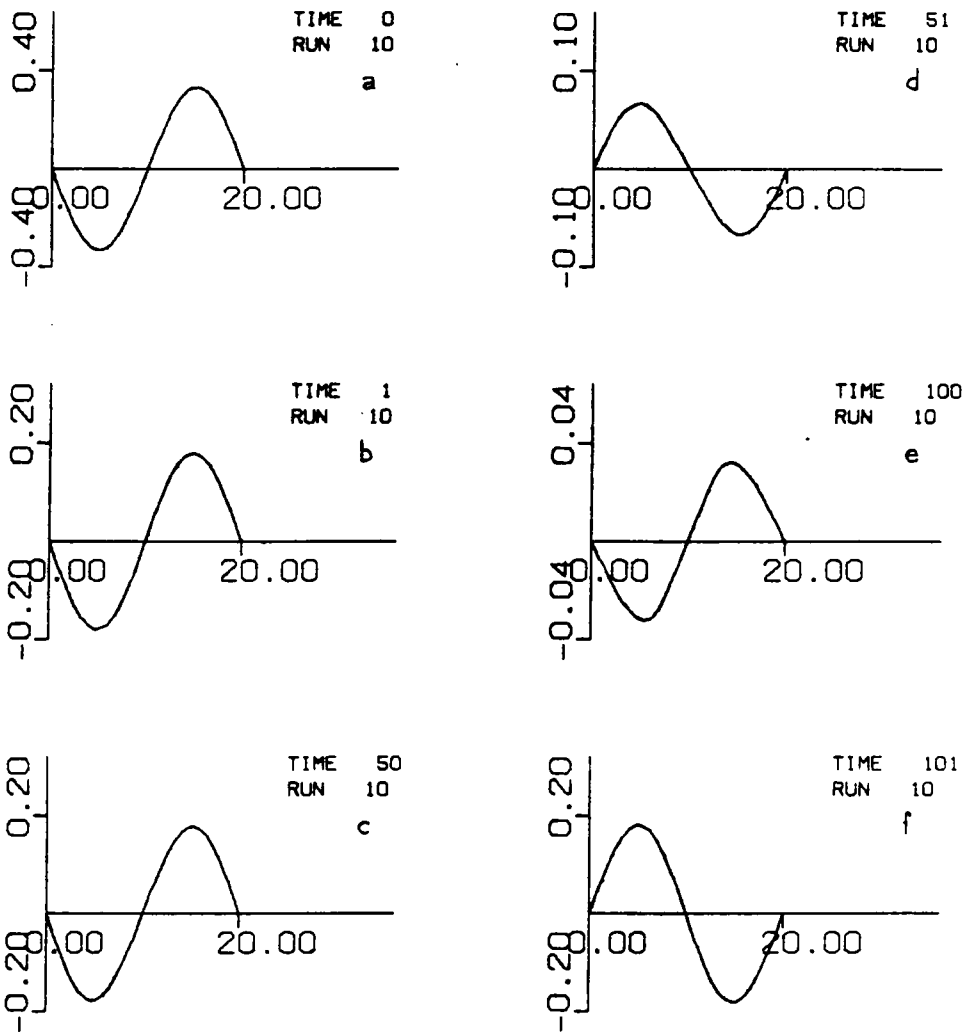


Fig. 5.4 (a)-(f) Electric field for the same case as in Fig. 5.1.

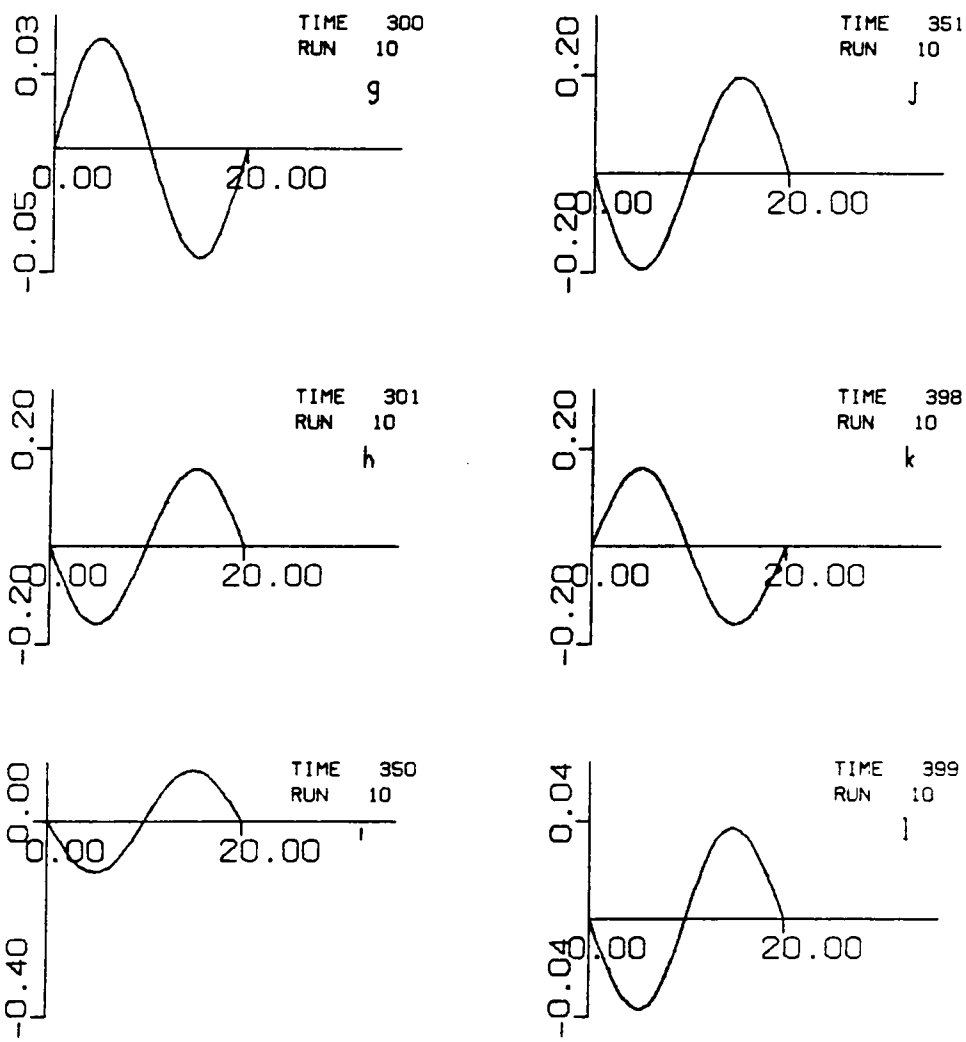


Fig. 5.4 (g)-(l) Electric field for the same case as in Fig. 5.1.

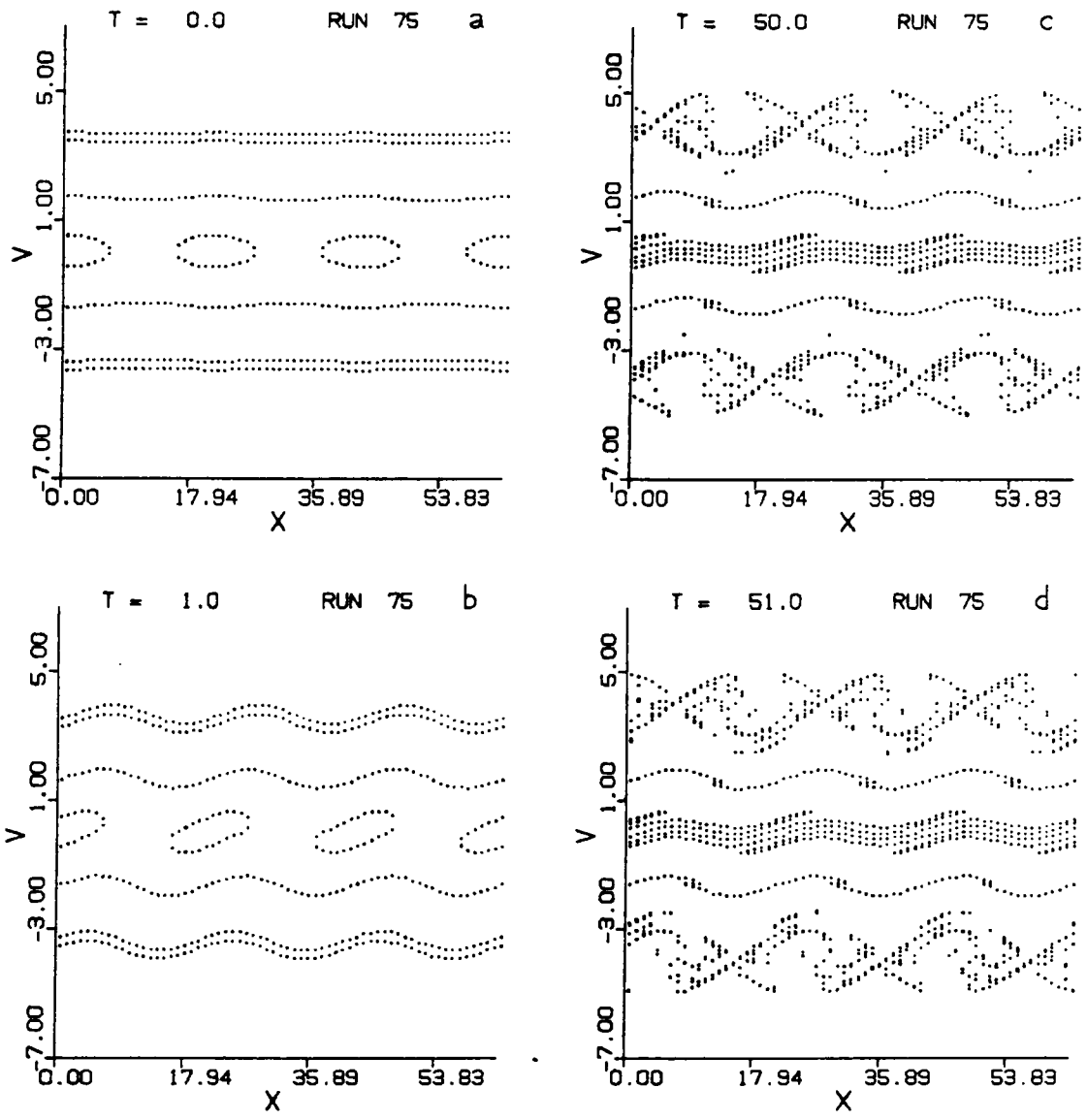


Fig. 5.5 (a)-(d) Level curves for the maxwellian case with $\epsilon = 0.1$ and $m = 3$.

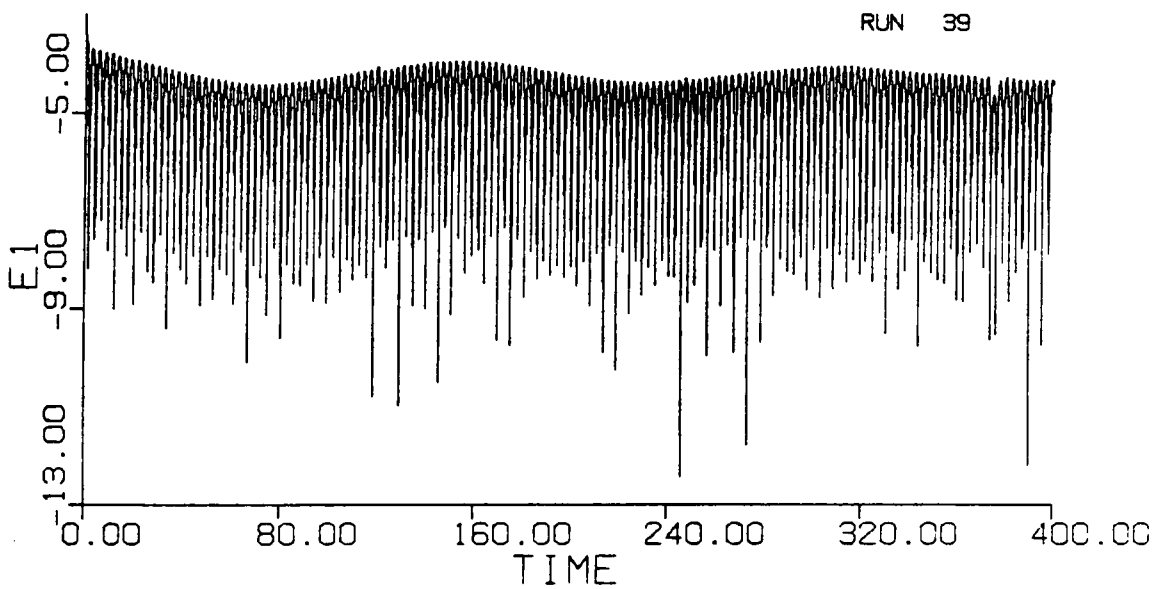


**Fig. 5.6** $|E_1|$ for the maxwellian case with $\epsilon = 0.01$ and $m = 1$.

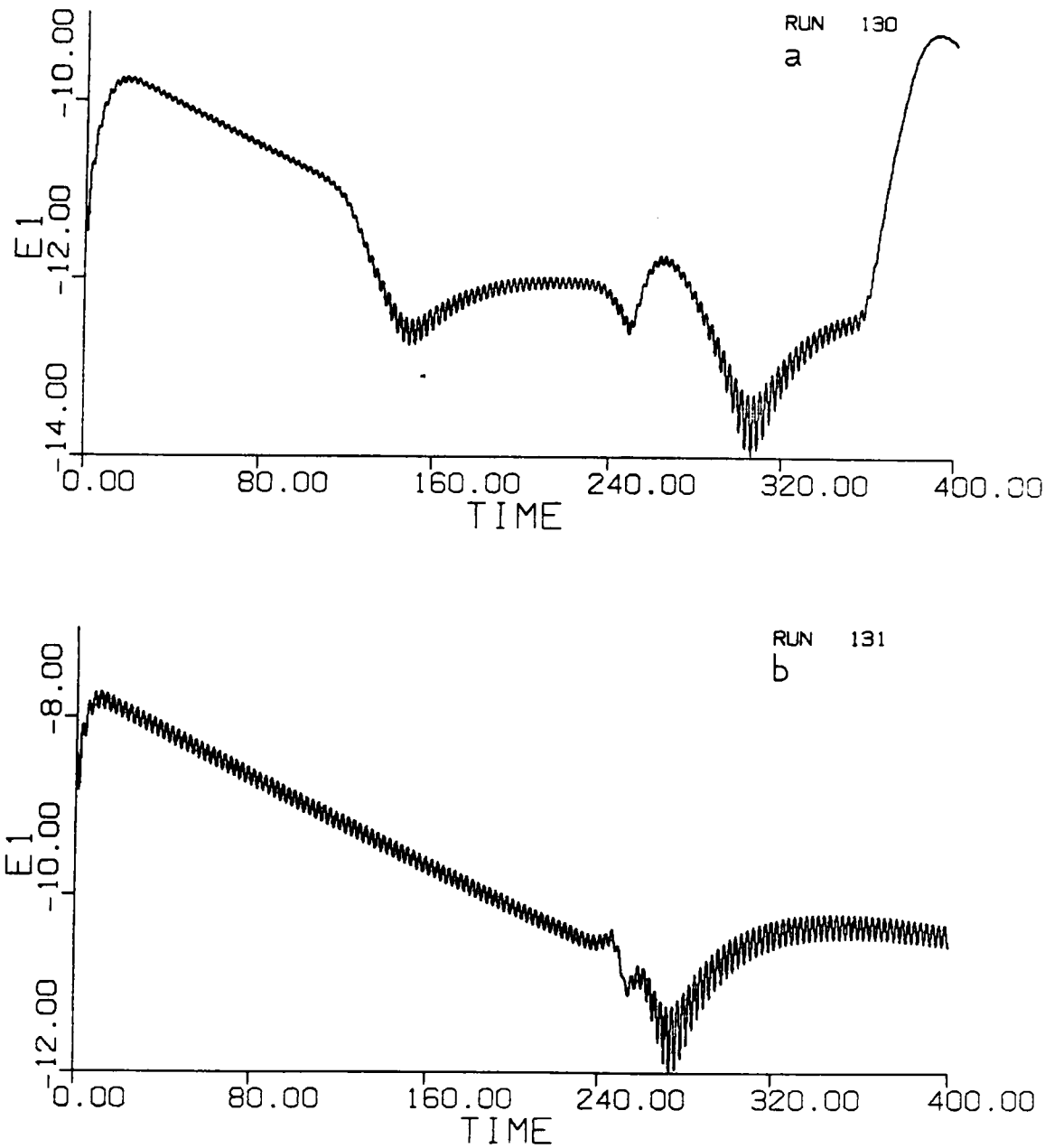


Fig. 5.7 $|E_1|$ for the maxwellian case with $\tilde{\epsilon}(v) = e^{-(v-V_0)^2}$, $V_0 = 4.5$ and $NV = 256$ (a) and $NV = 512$ (b).

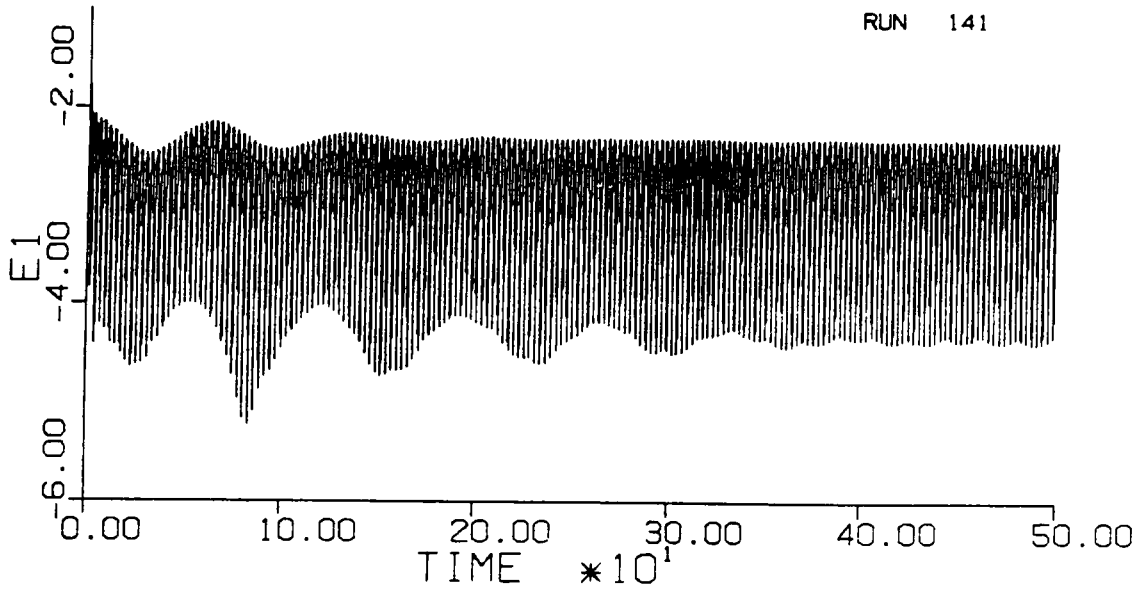


**Fig. 5.8** $|E_1|$ for the maxwellian case with $\tilde{\epsilon}(v) = \frac{1}{(v-V_0)^2+v_t^2}$, $V_0 = 1$, $v_t = 0.5$.

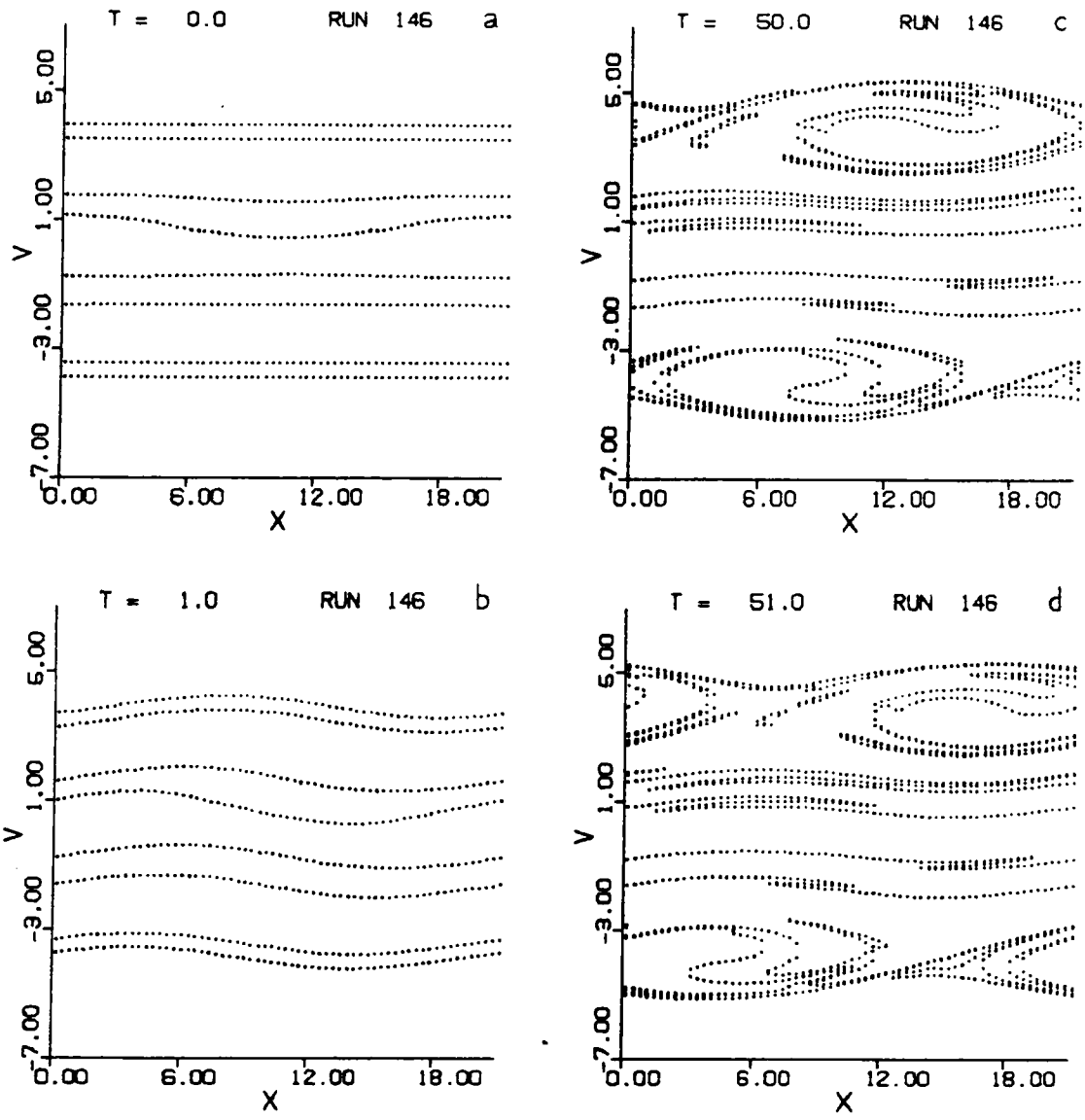


Fig. 5.9 (a)-(d) Level curves for the same case as in Fig. 5.8.

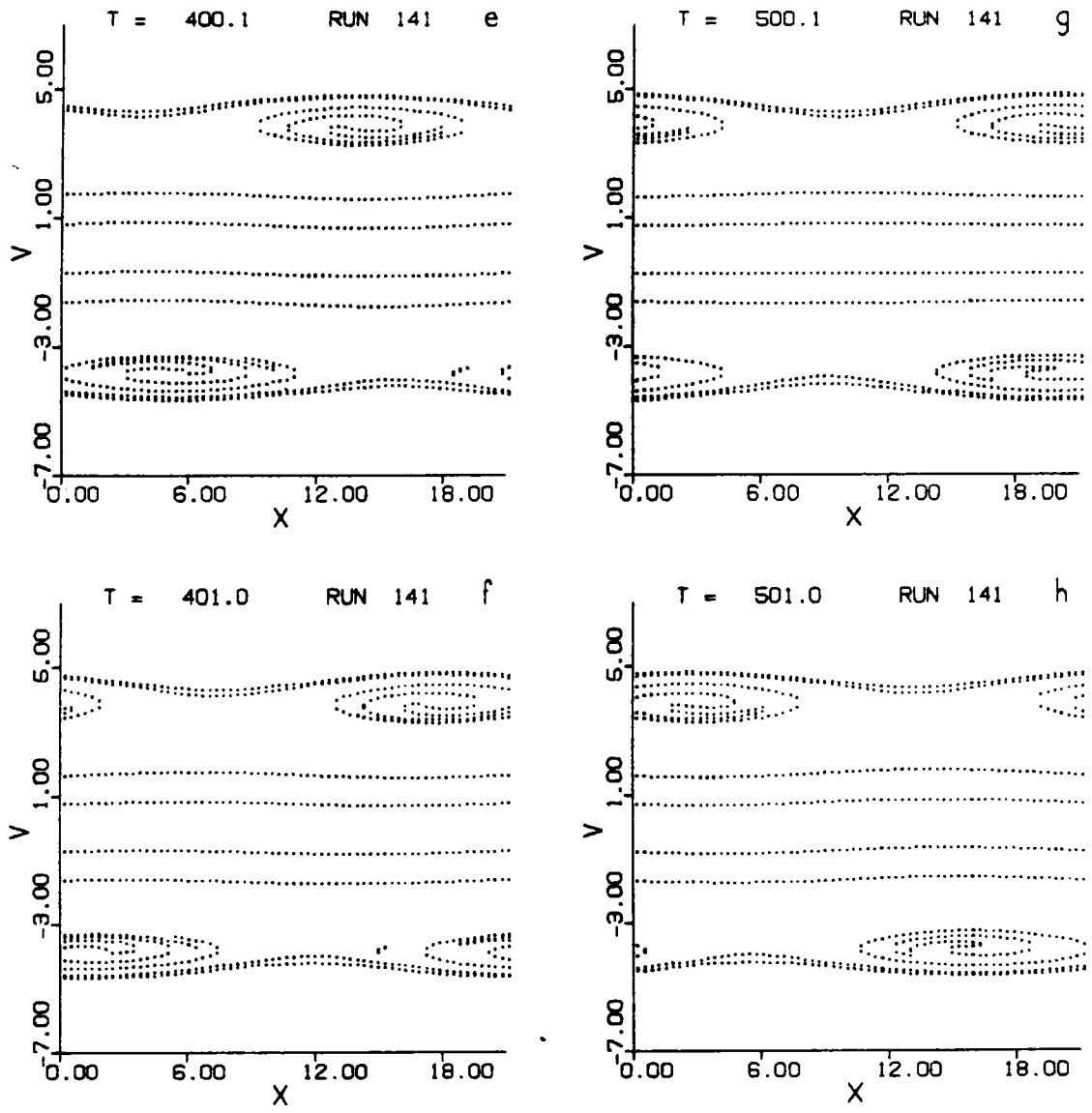


Fig. 5.9 (e)-(h) Level curves for the same case as in Fig. 5.8.

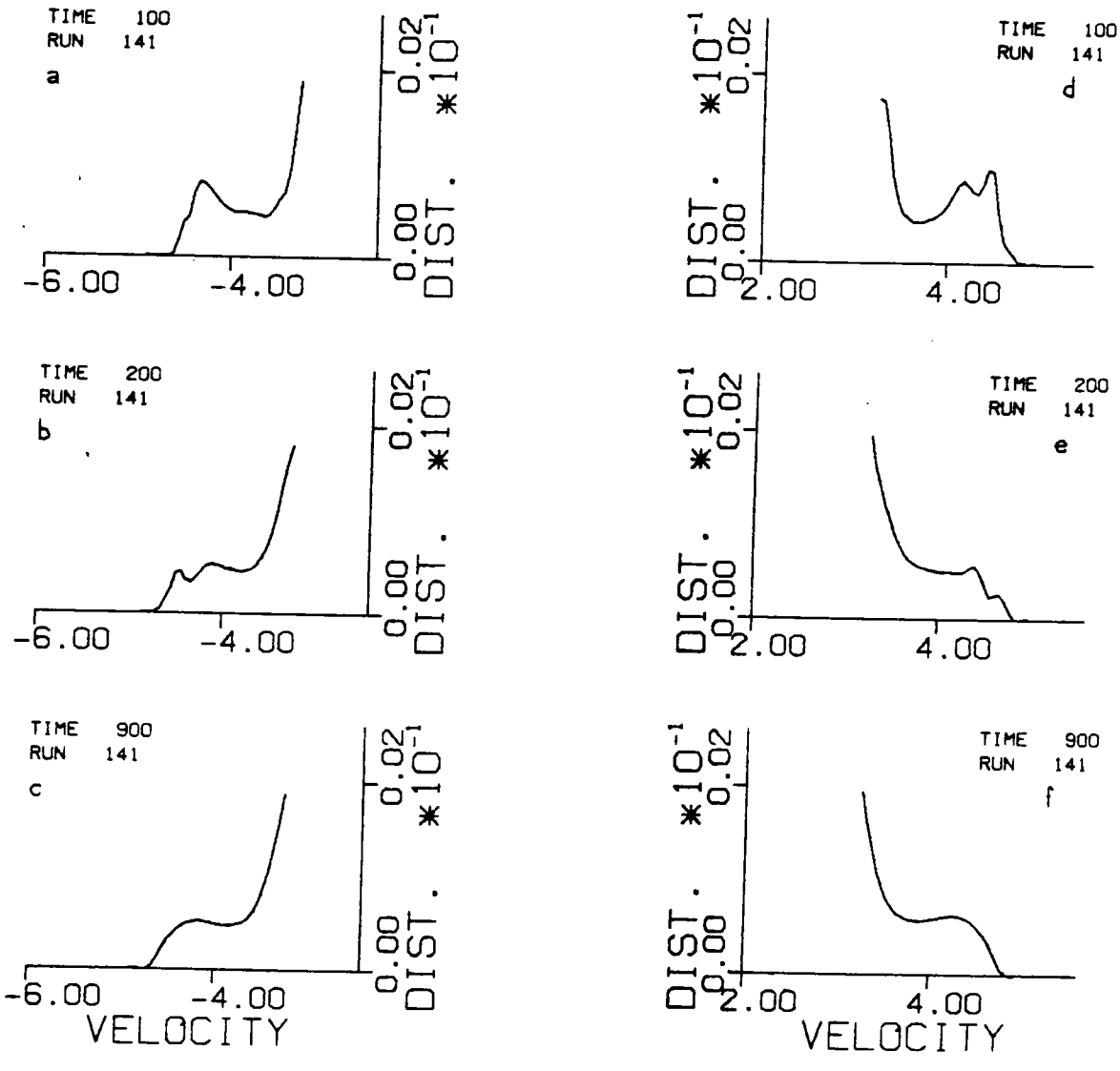


**Fig. 5.10 (a)-(f)** Space averaged distribution for the same case as in Fig. 5.8.

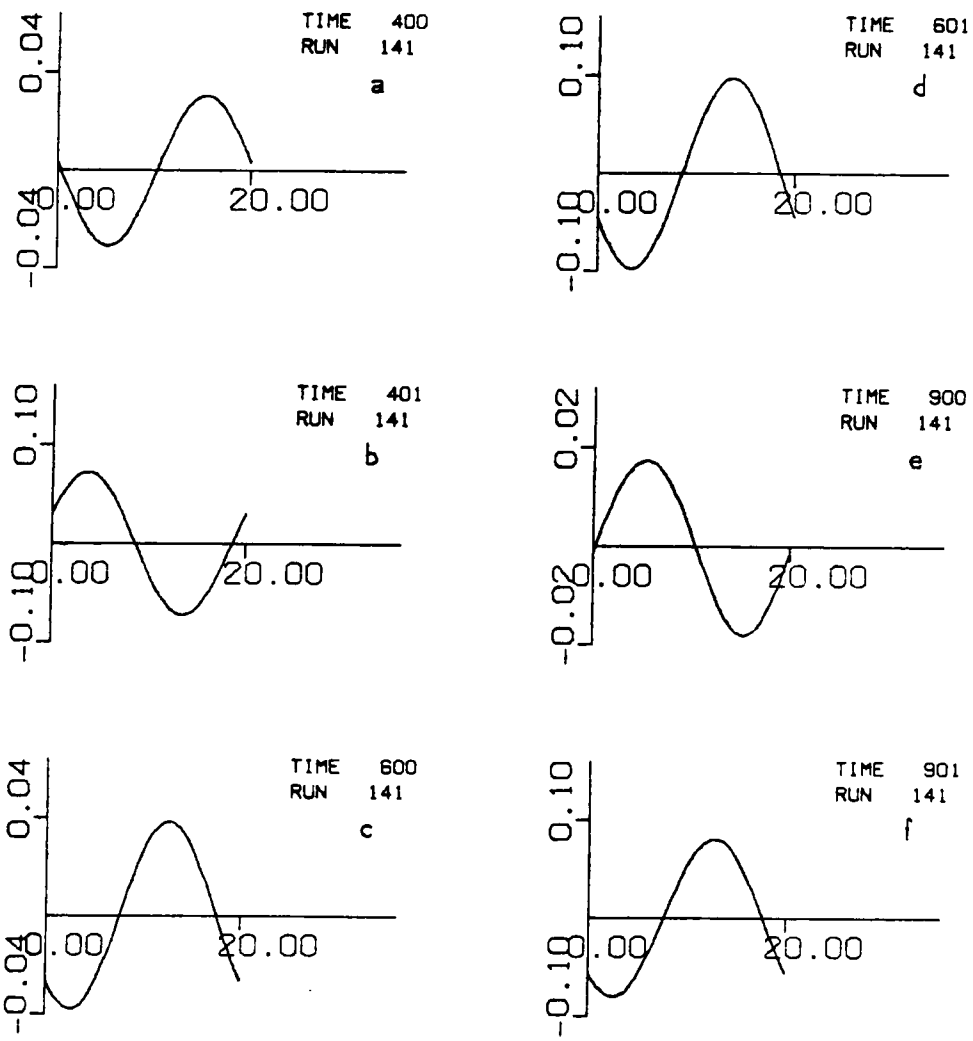


Fig. 5.11 (a)-(f) Electric field for the same case as in Fig. 5.8.

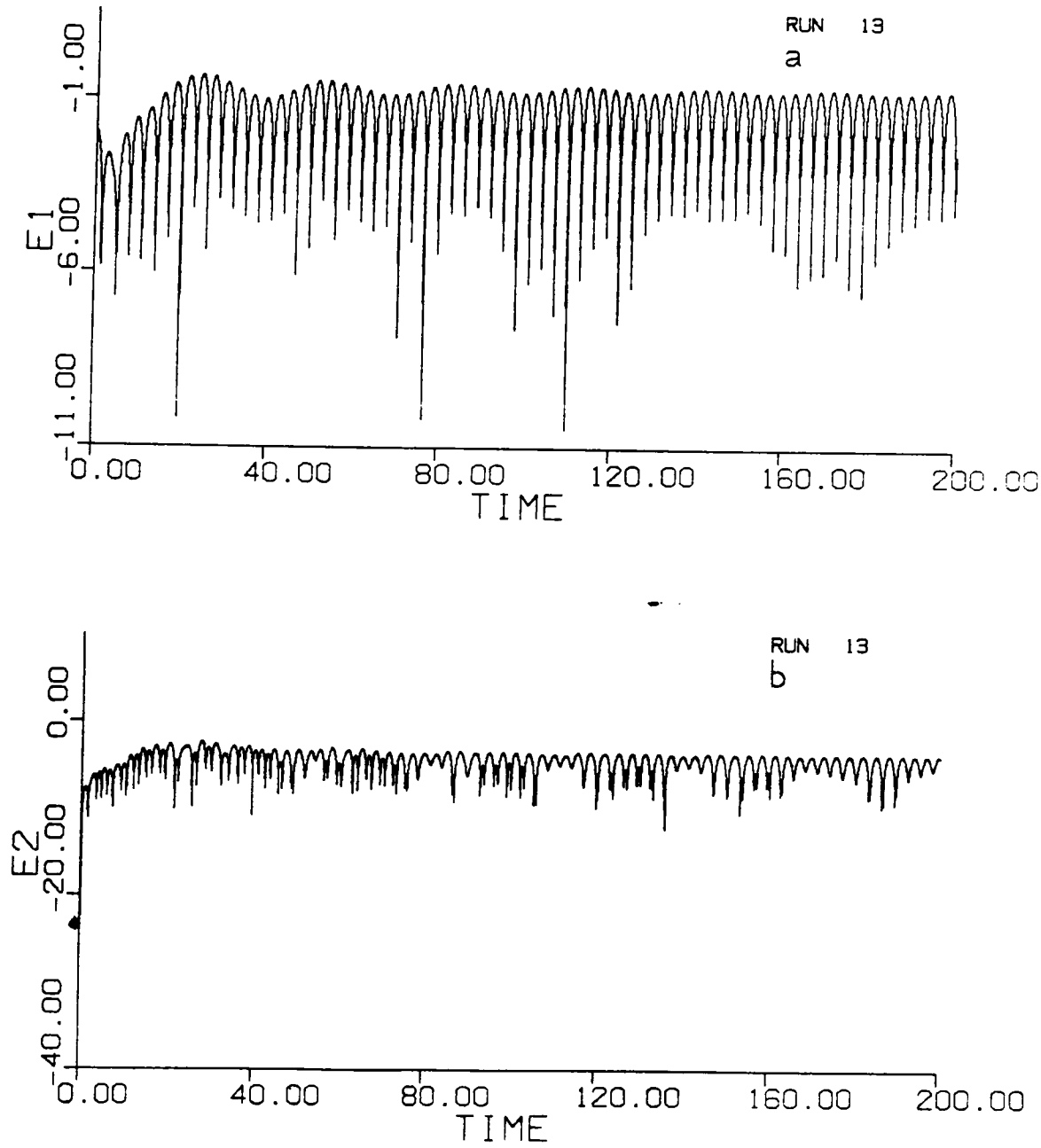


**Fig. 5.12** $|E_1|$ (a) and $|E_2|$ (b) for the symmetric bump-on-tail case with $\epsilon = 0.04$ and $m = 3$.

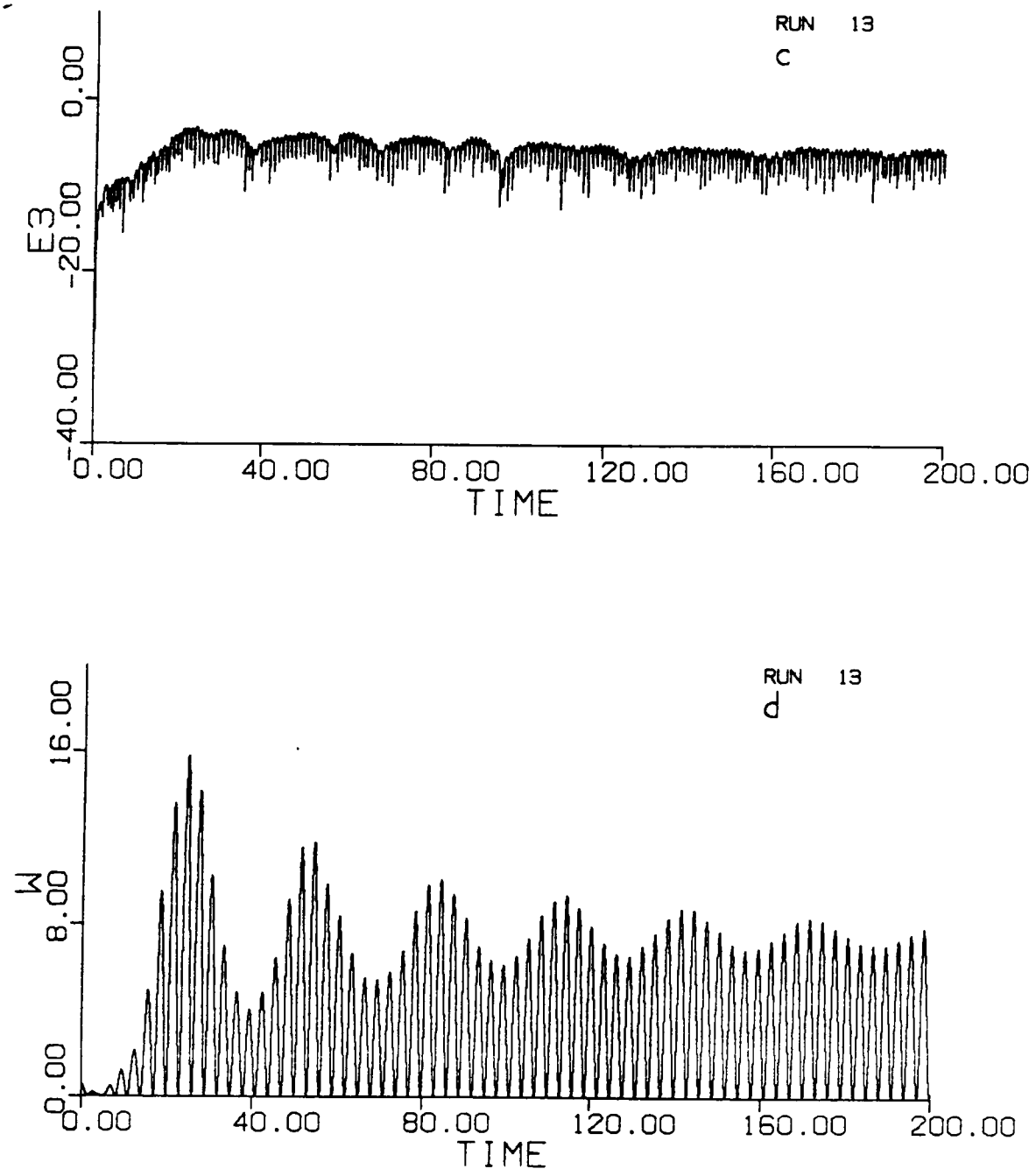


**Fig. 5.12** $|E_3|$ **(c)** and $W$ **(d)** for symmetric bump-on-tail case with $\epsilon = 0.04$ and $m = 3$.

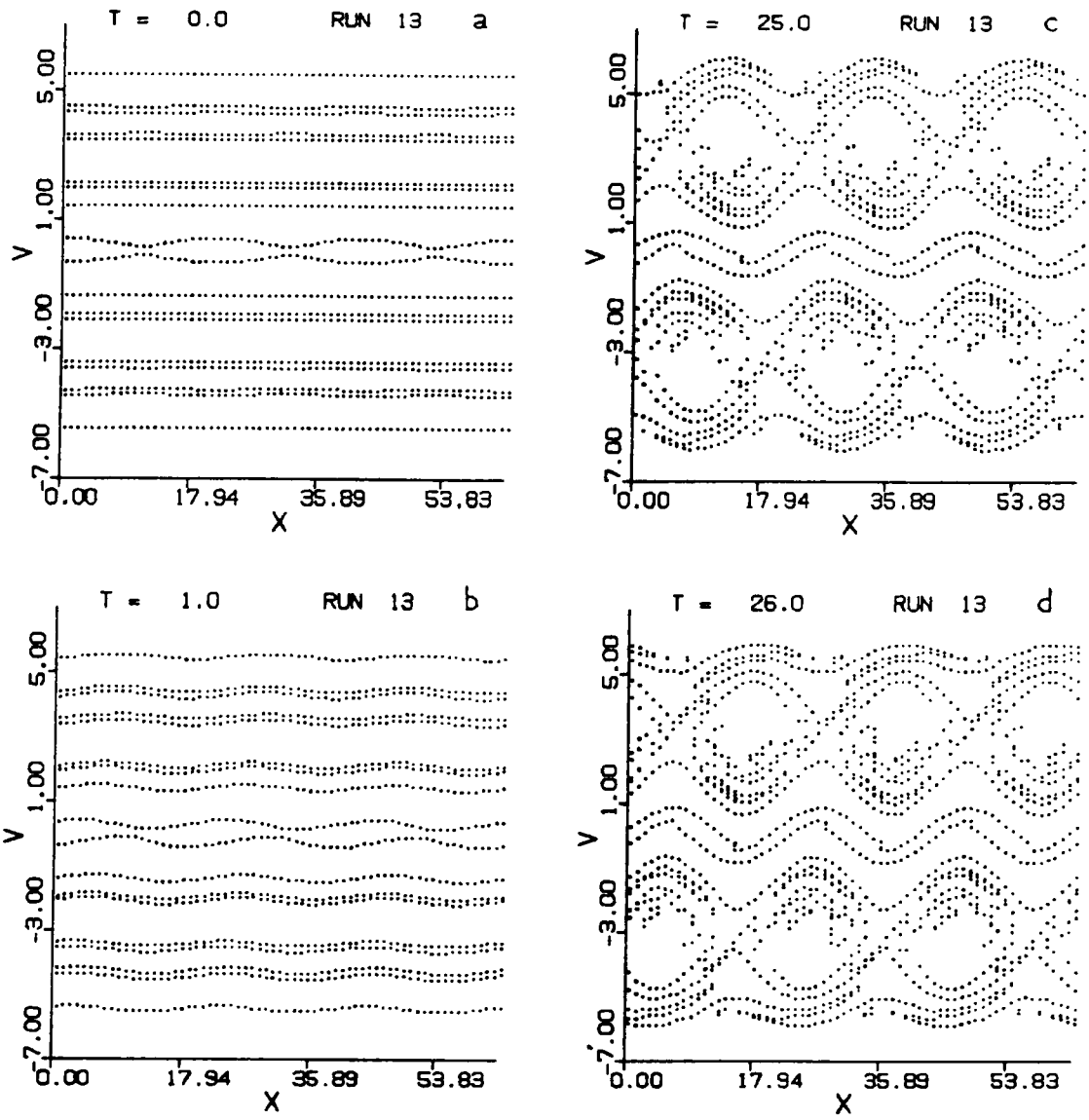


Fig. 5.13 (a)-(d) Level curves for the same case as in Fig. 5.12.

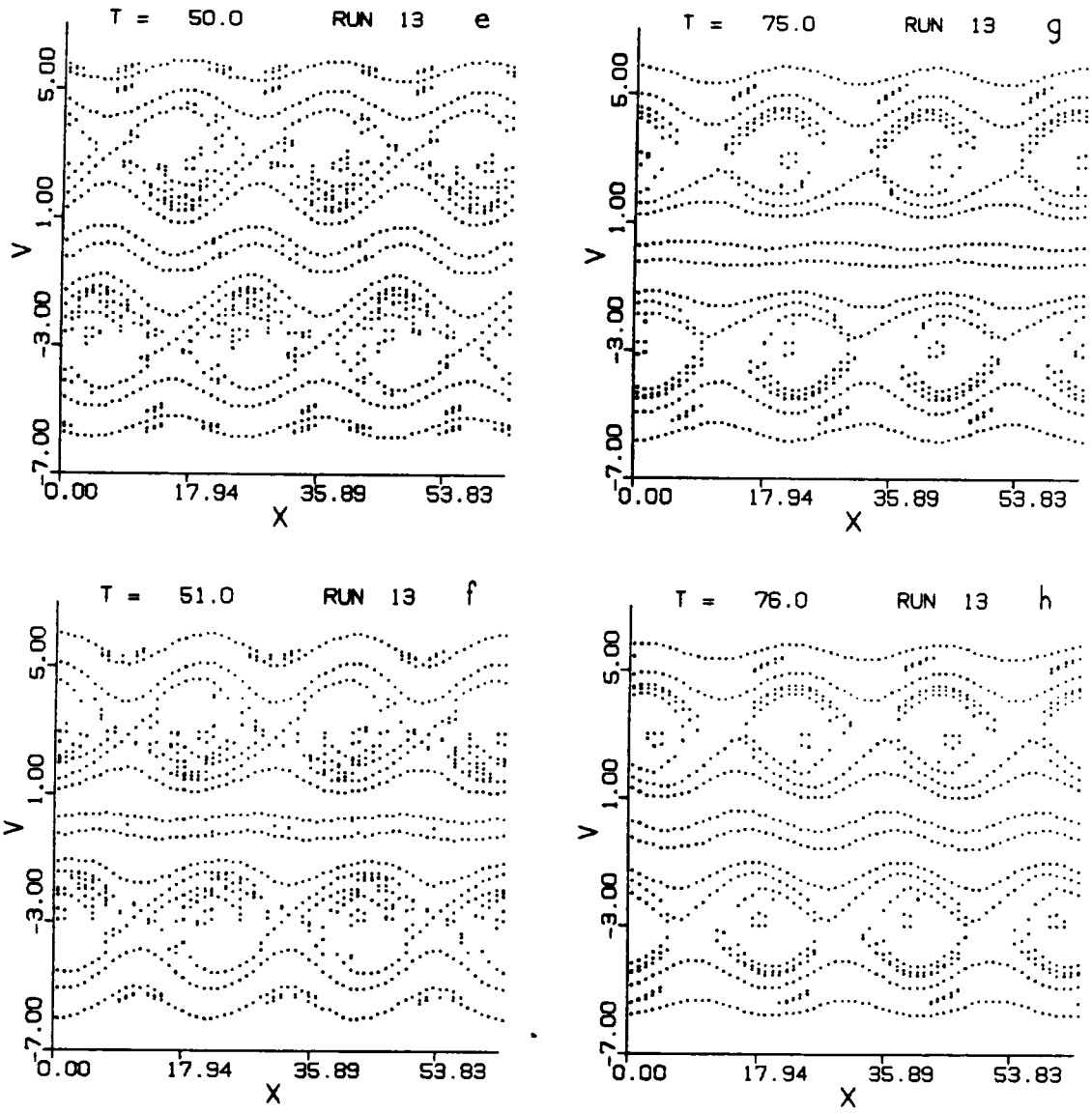


Fig. 5.13 (e)-(h) Level curves for the same case as in Fig. 5.12.

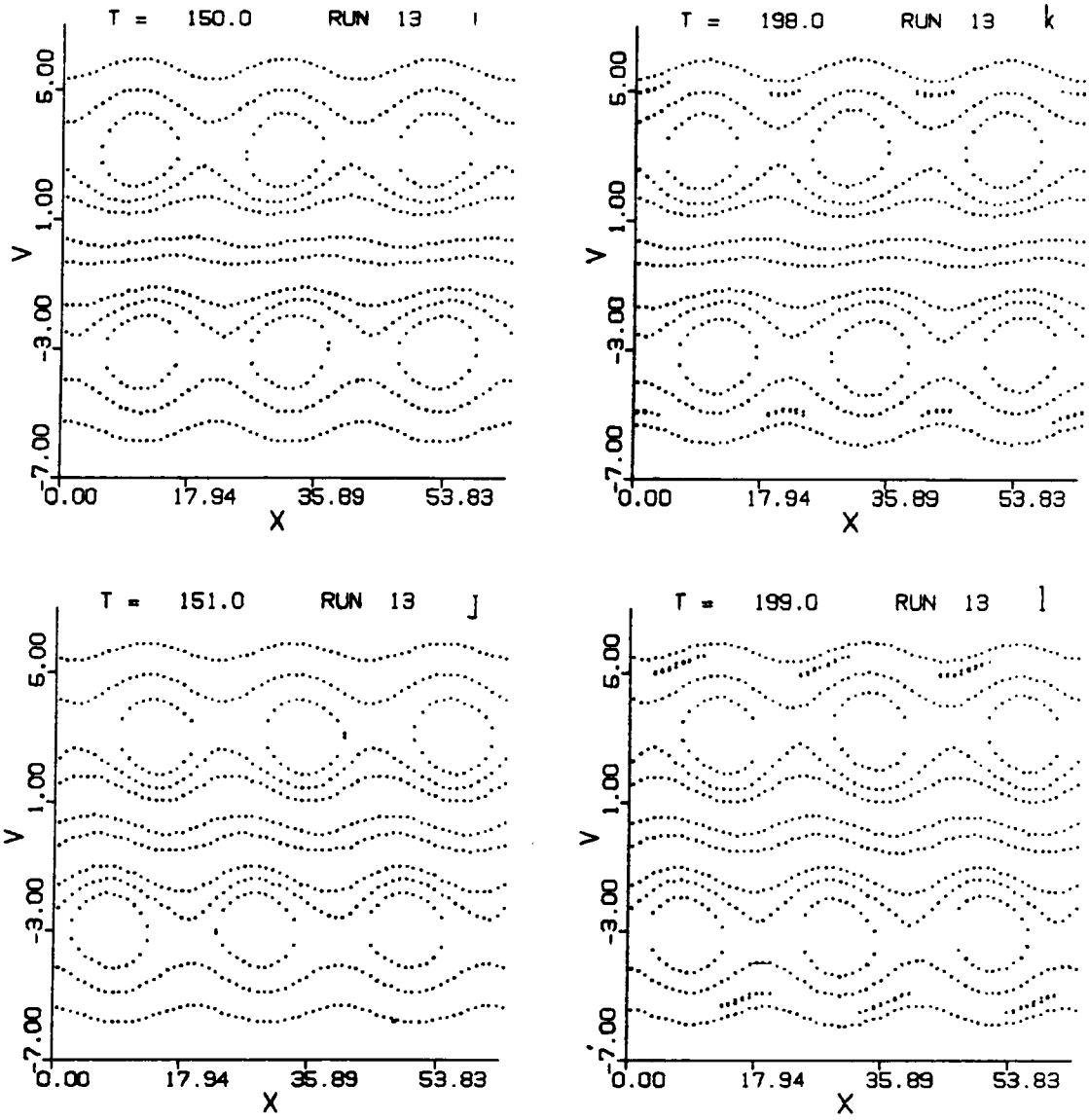


Fig. 5.13 (i)-(l) Level curves for the same case as in Fig. 5.12.

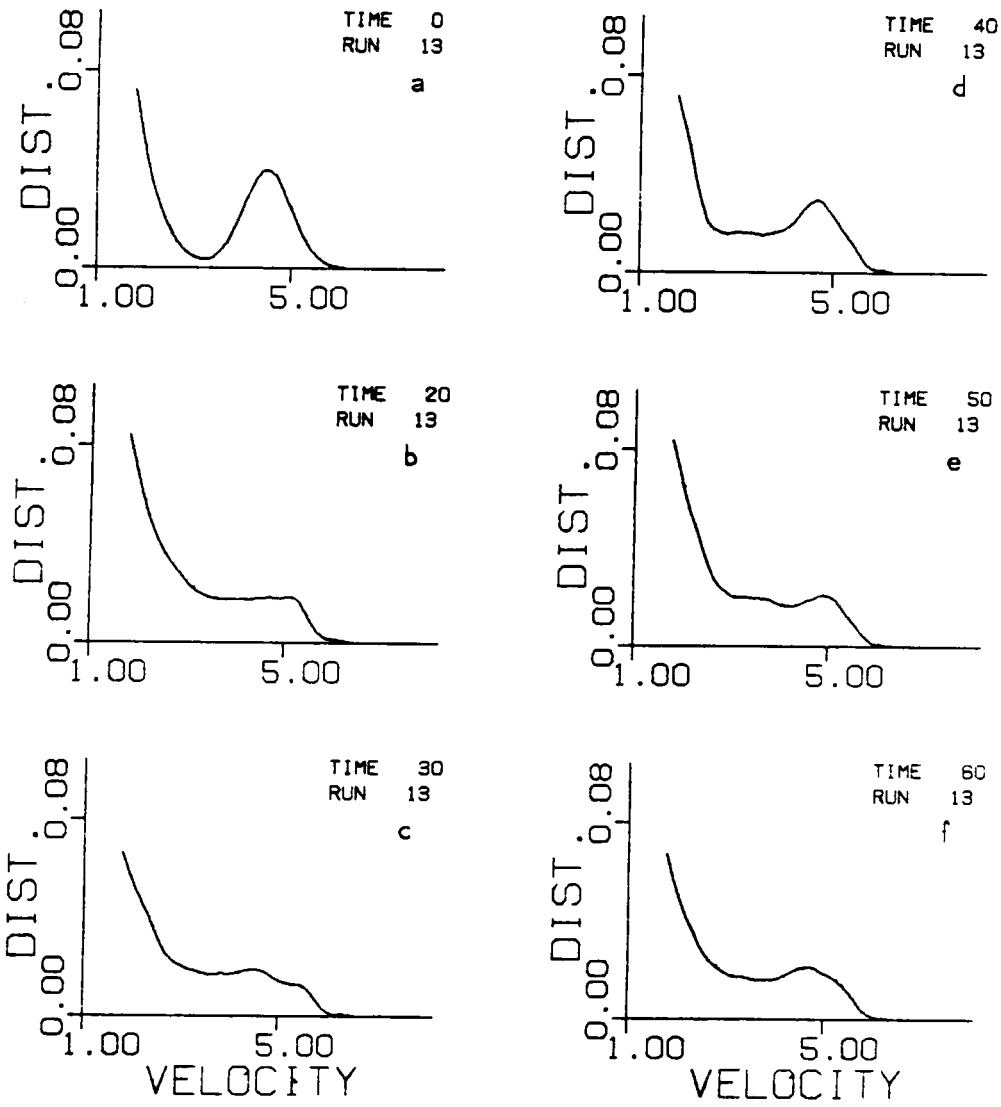


**Fig. 5.14 (a)-(f)** Space averaged distribution for the same case as in Fig. 5.12.

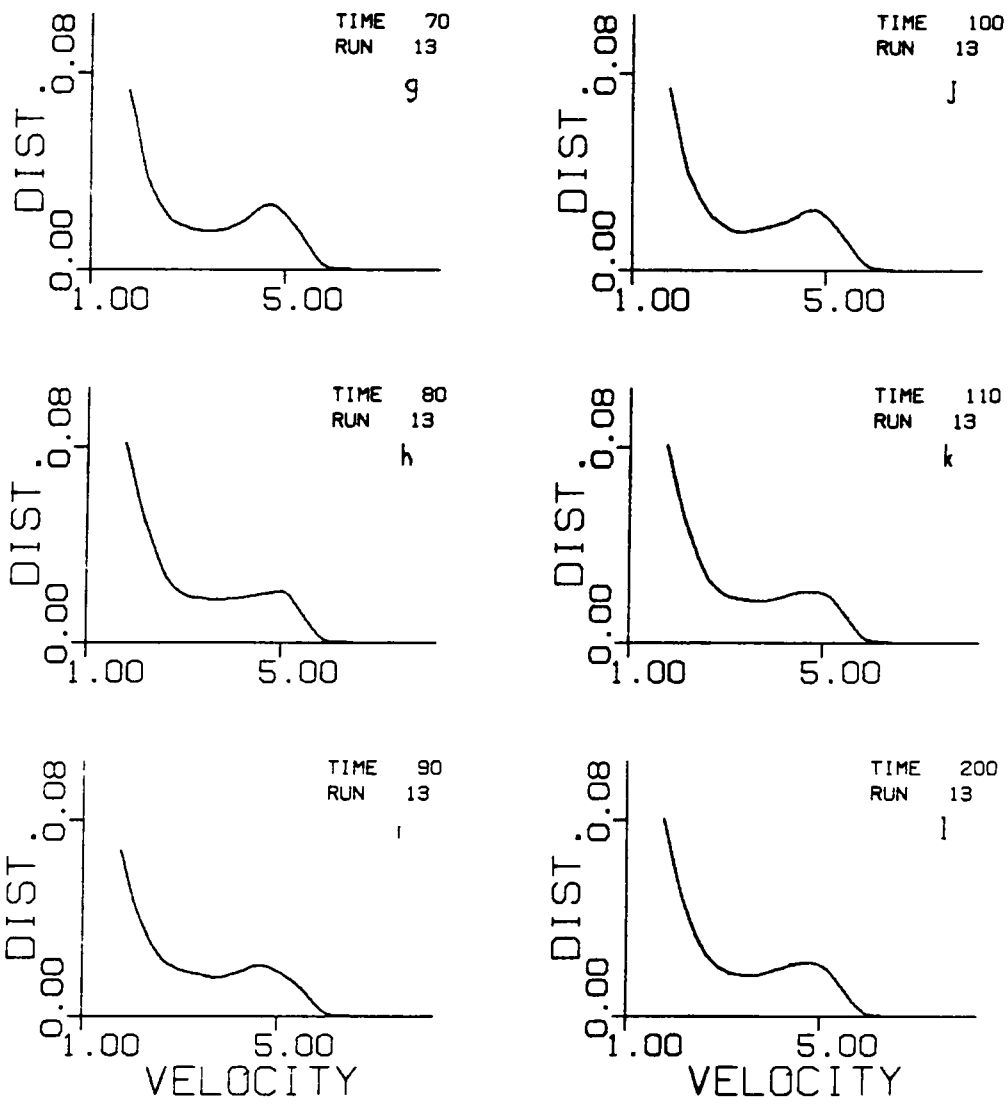


**Fig. 5.14 (g)-(l)** Space averaged distribution for the same case as in Fig. 5.12.

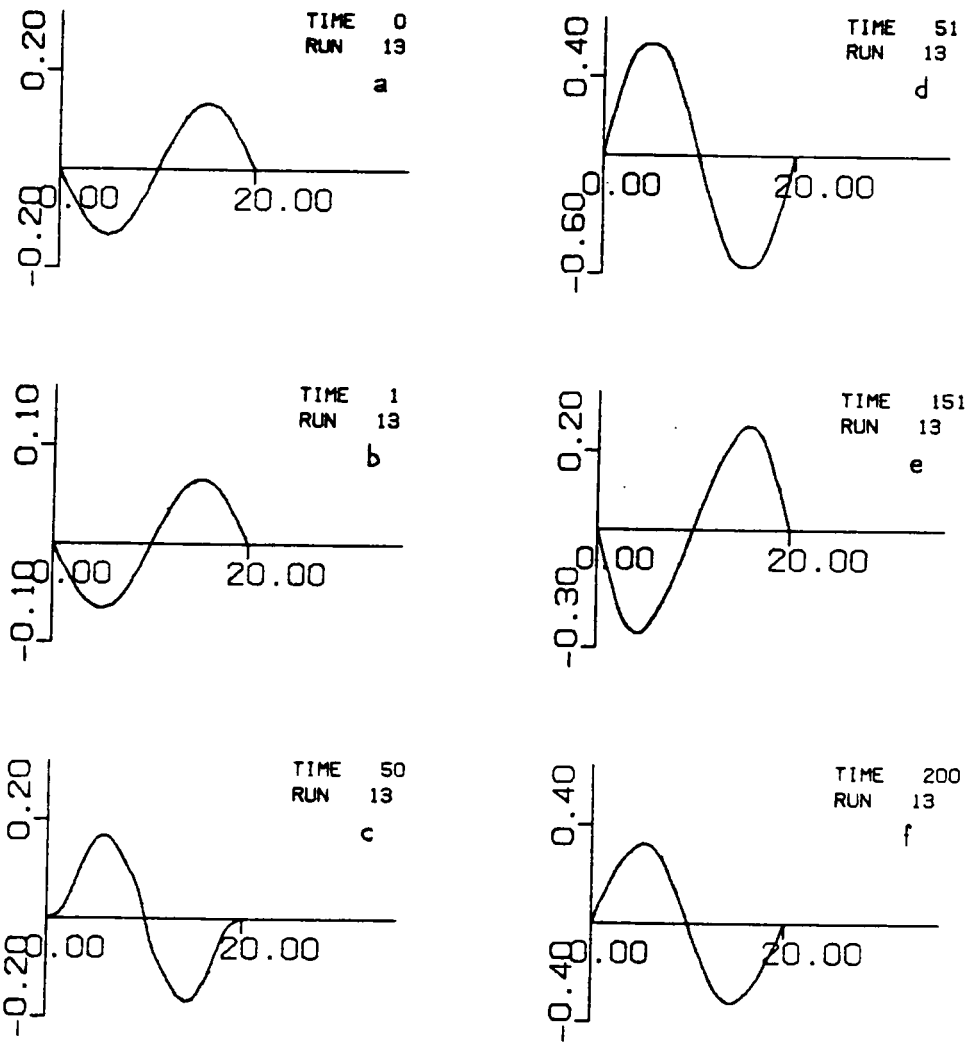


Fig. 5.15 (a)-(f) Electric field for the same case as in Fig. 5.12.

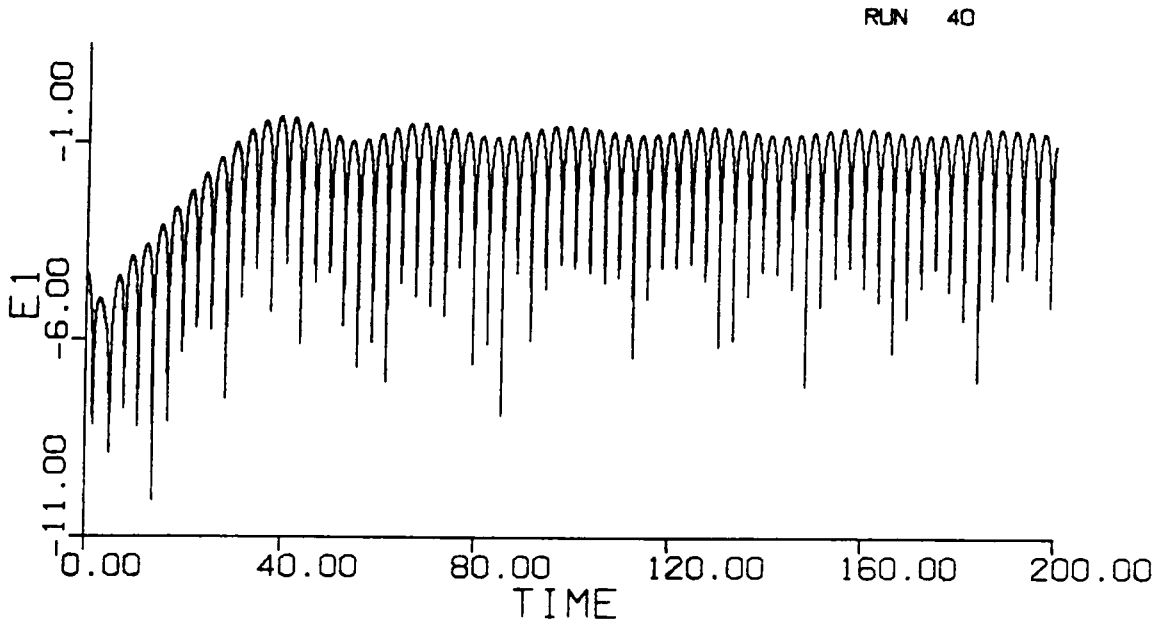


Fig. 5.16 $|E_1|$ for the symmetric bump-on-tail case with $\epsilon = 0.004$.

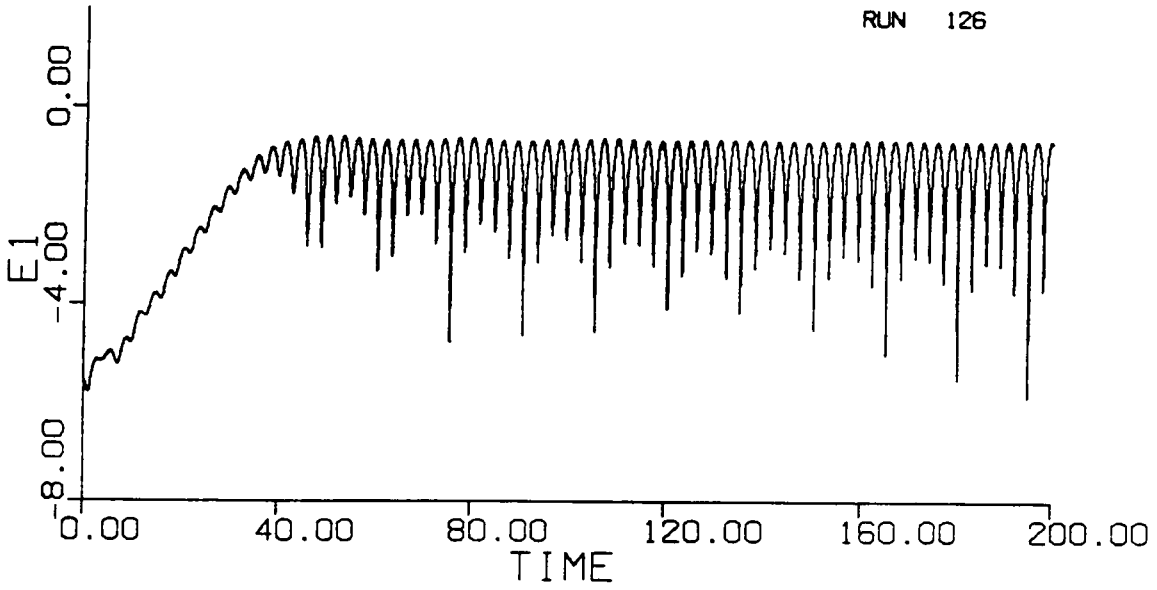


**Fig. 5.17** $|E_1|$ for the symmetric bump-on-tail case with $\tilde{\epsilon}(v) = e^{-(v-V_0)^2}$, $V_0 = 4.5$.

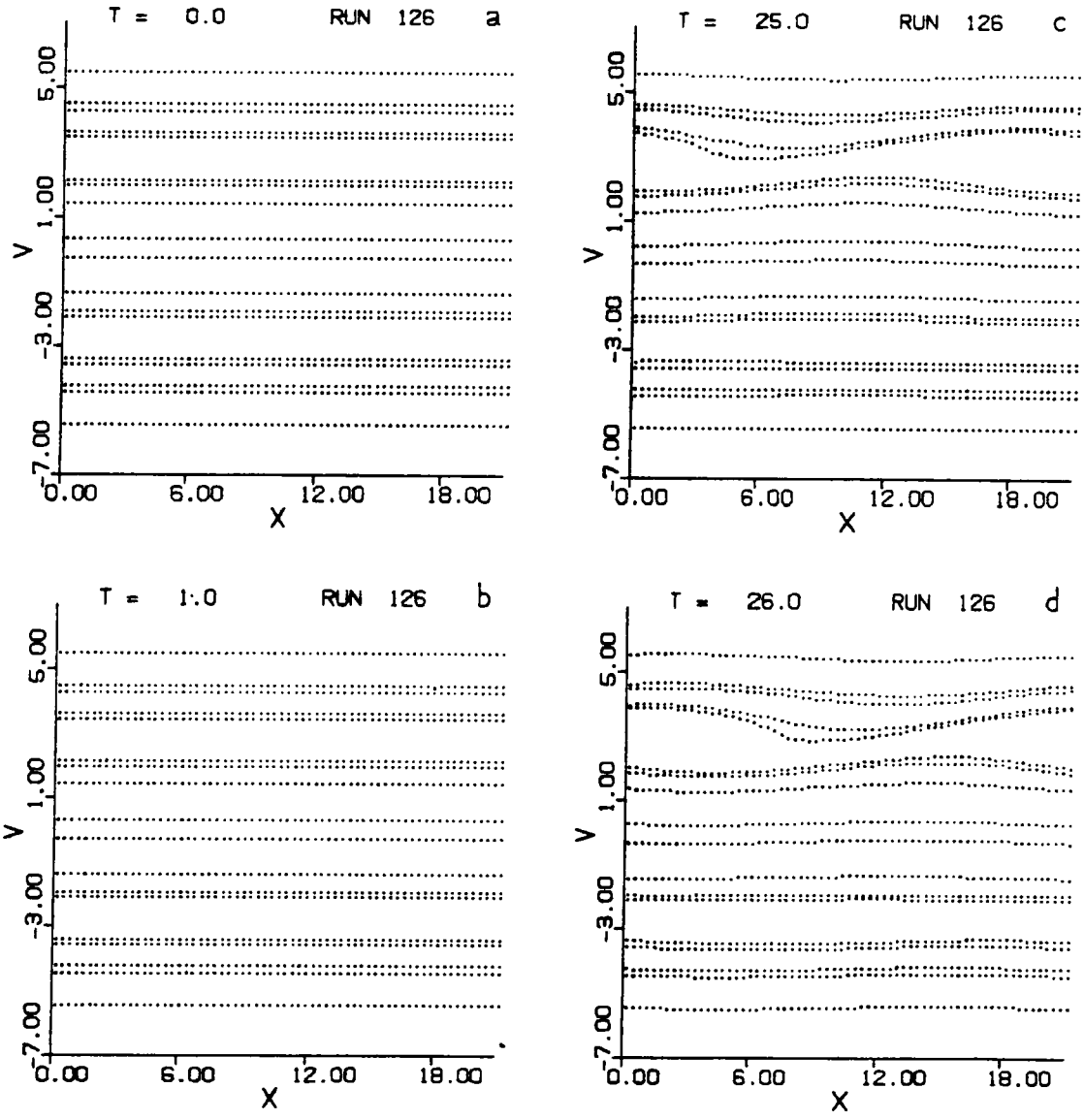


Fig. 5.18 (a)-(d) Level curves for the same case as in Fig. 5.17.

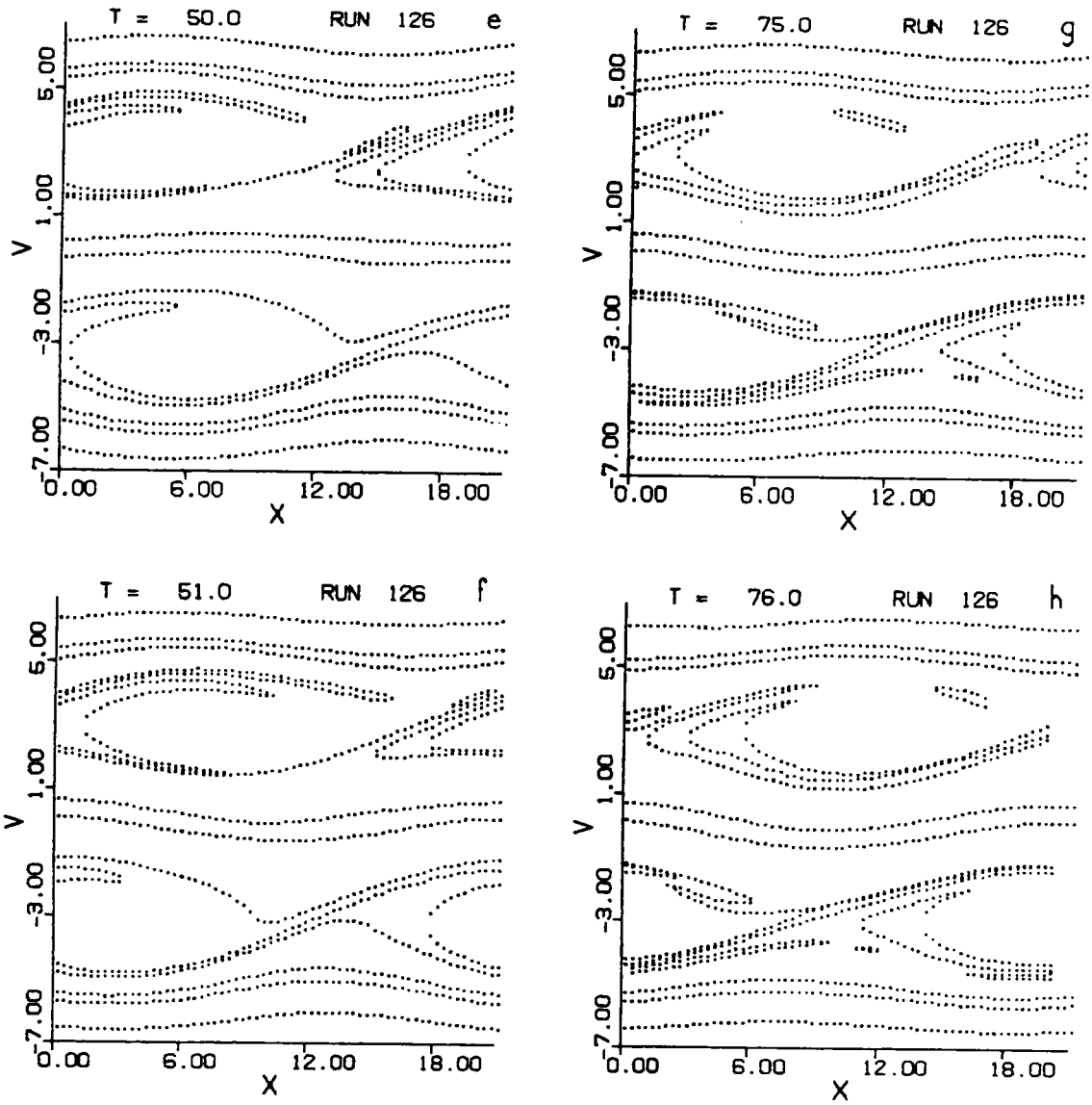


Fig. 5.18 (e)-(h) Level curves for the same case as in Fig. 5.17.

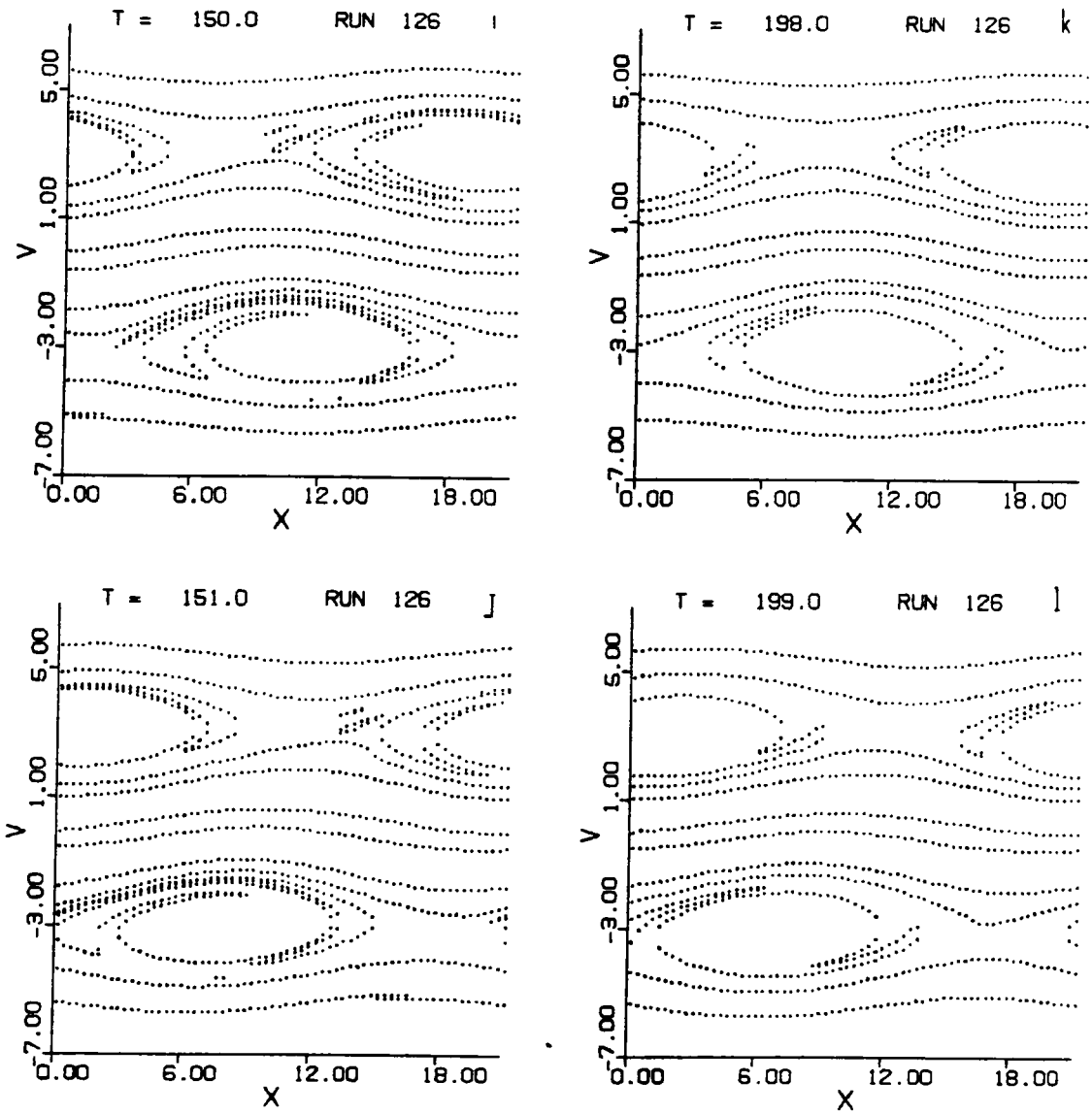


Fig. 5.18 (i)-(l) Level curves for the same case as in Fig. 5.17.

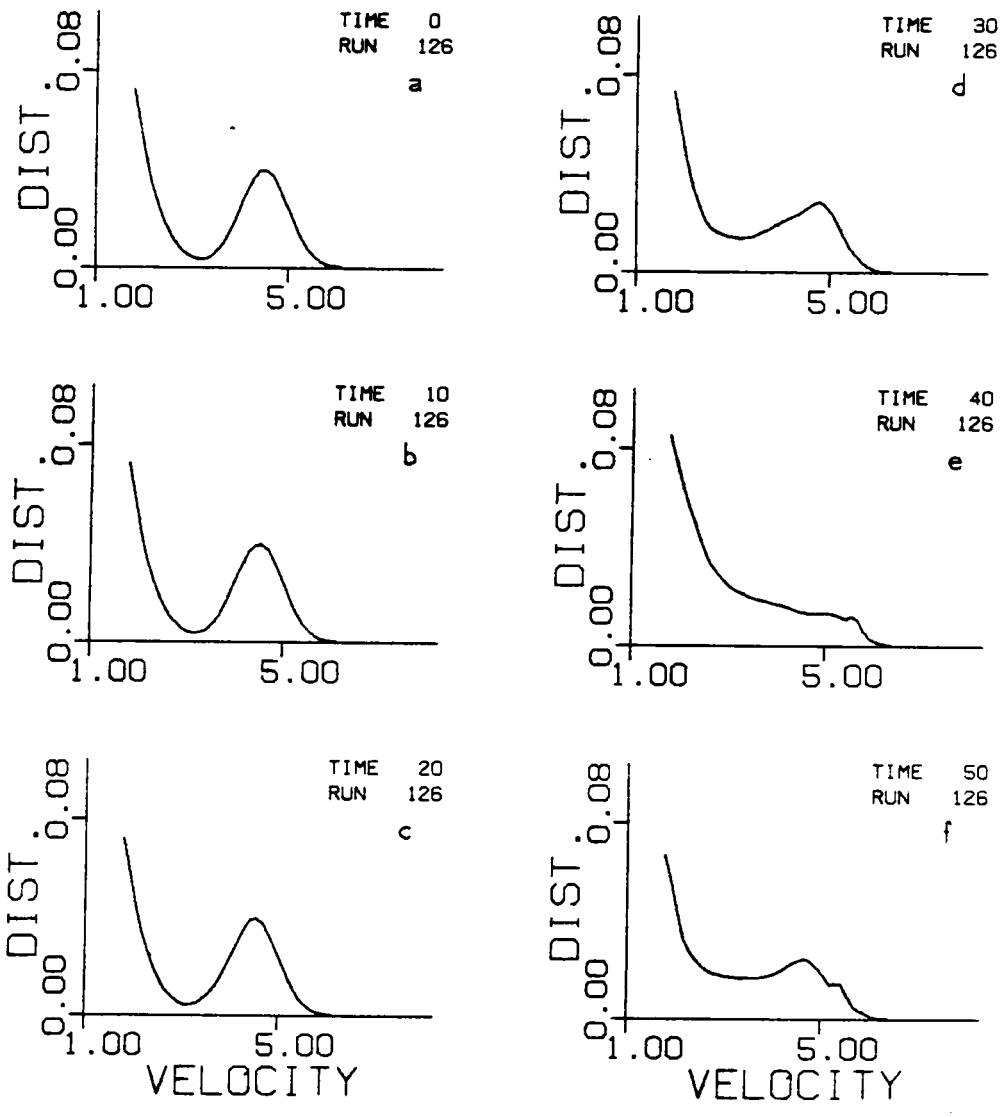


**Fig. 5.19 (a)-(f)** Space averaged distribution for $v > 0$ for the same case as in Fig. 5.17.

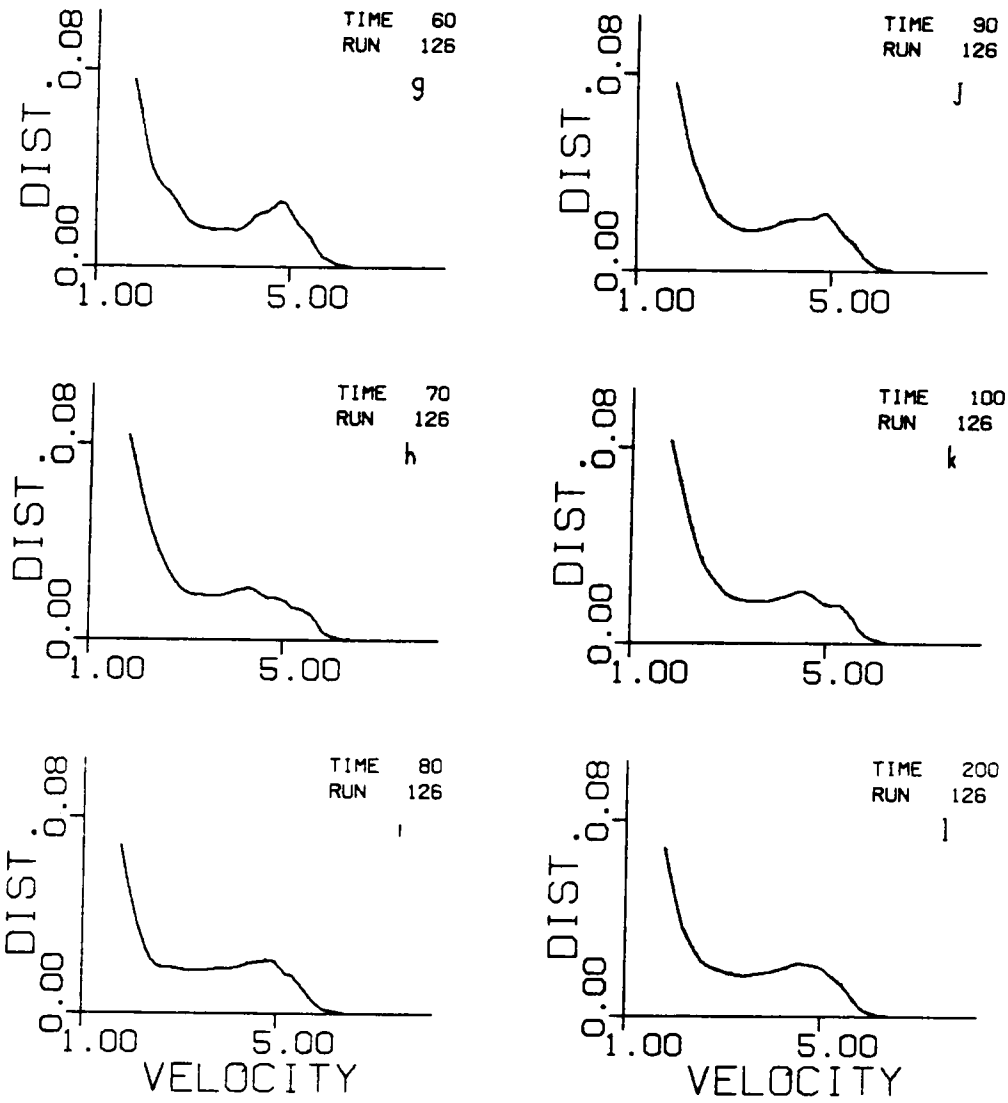


Fig. 5.19 (g)-(l) Space averaged distribution for $v > 0$ for the same case as in Fig. 5.17.

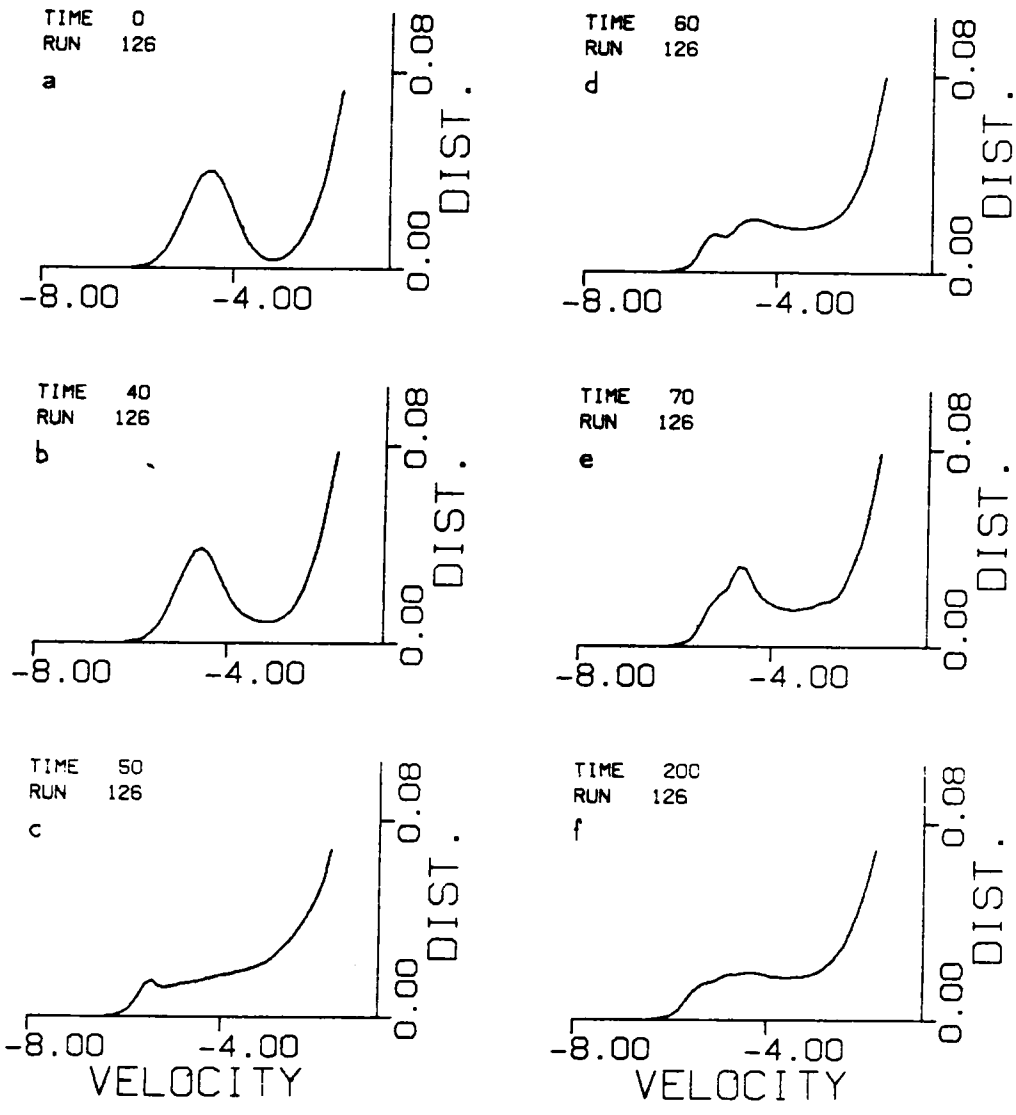


**Fig. 5.20 (a)-(f)** Space averaged distribution for $v < 0$ for the same case as in Fig. 5.17.

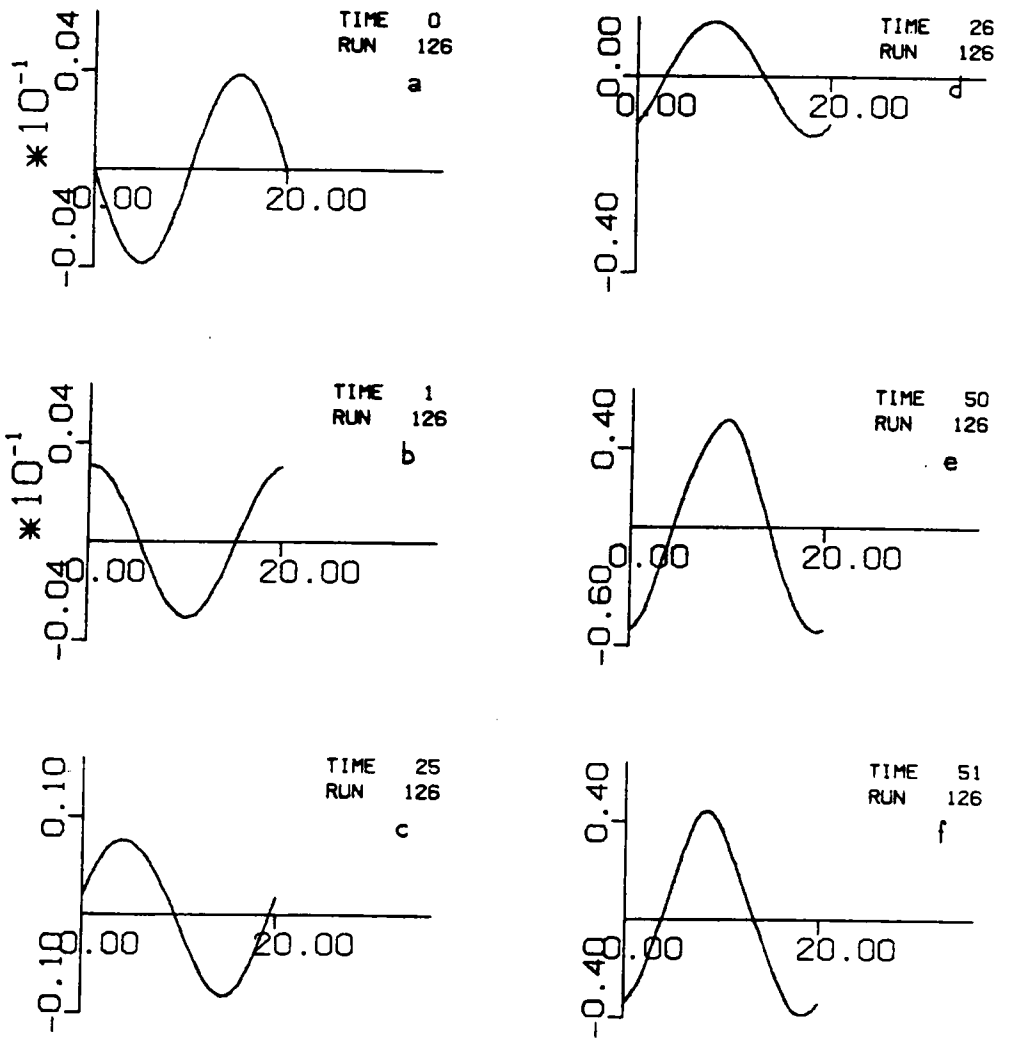


Fig. 5.21 (a)-(f) Electric field for the same case as in Fig. 5.17.

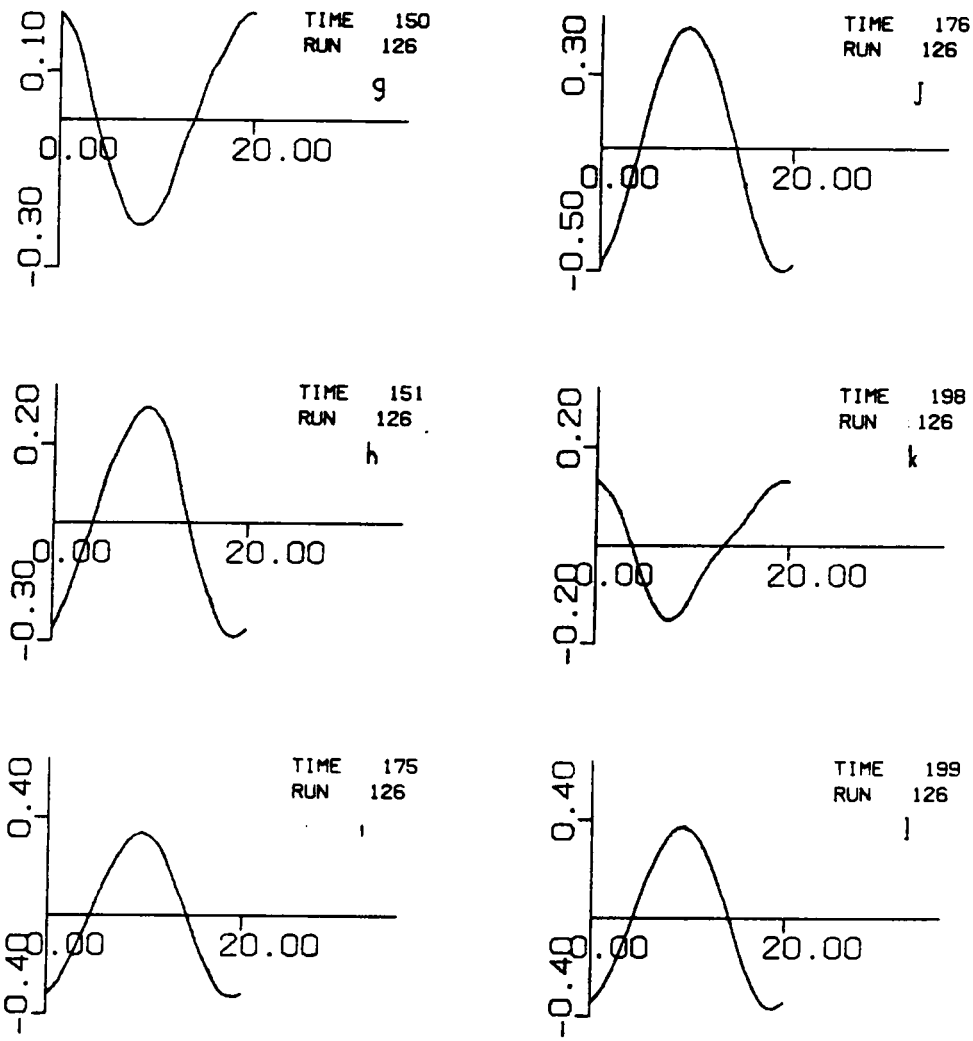


Fig. 5.21 (g)-(l) Electric field for the same case as in Fig. 5.17.

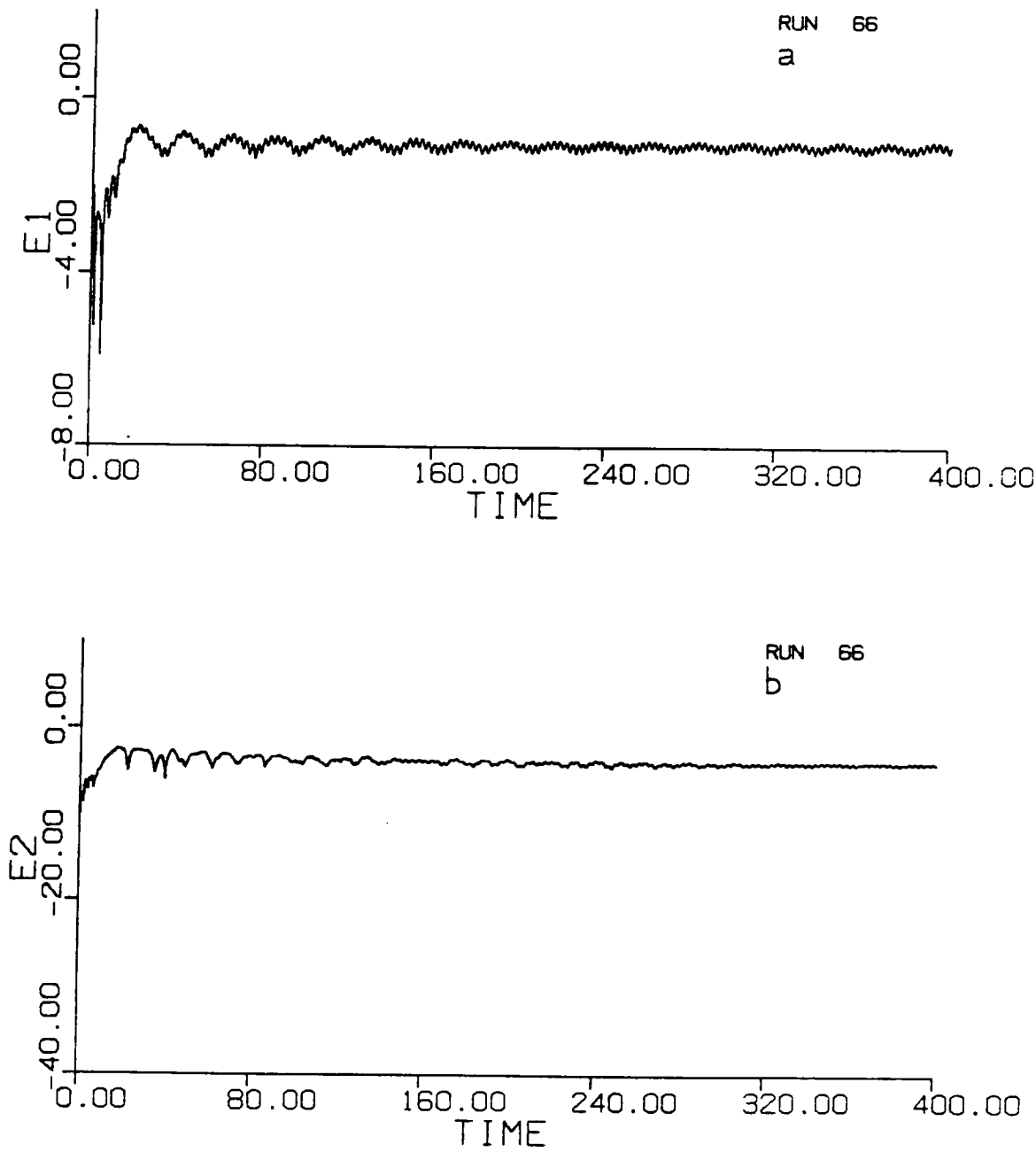


Fig. 5.22 $|E_1|$ (a) and $|E_2|$ (b) for the one sided bump-on-tail case.

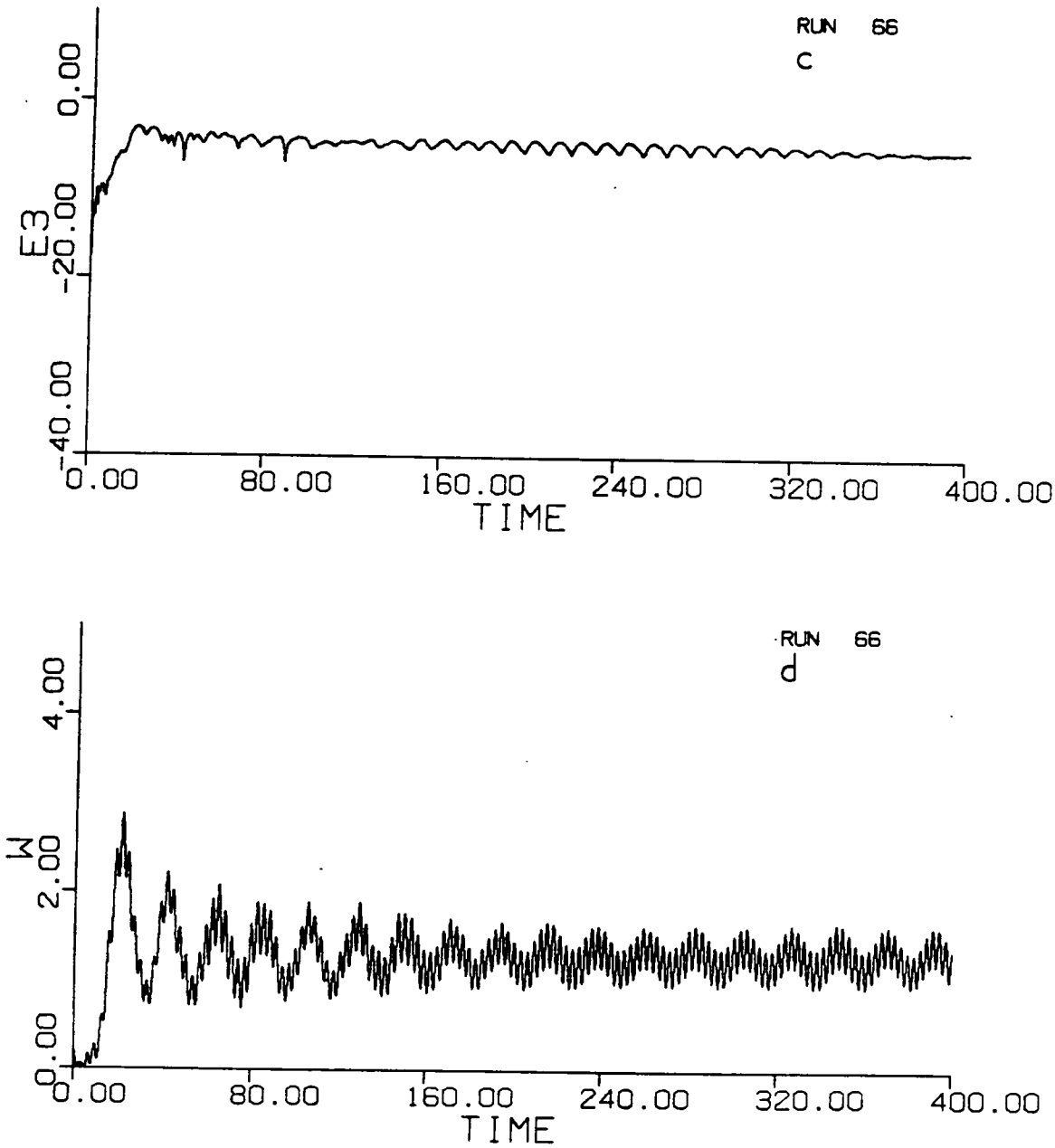


Fig. 5.22 $|E_3|$ (c) and $W$ (d) for the one sided bump-on-tail case.

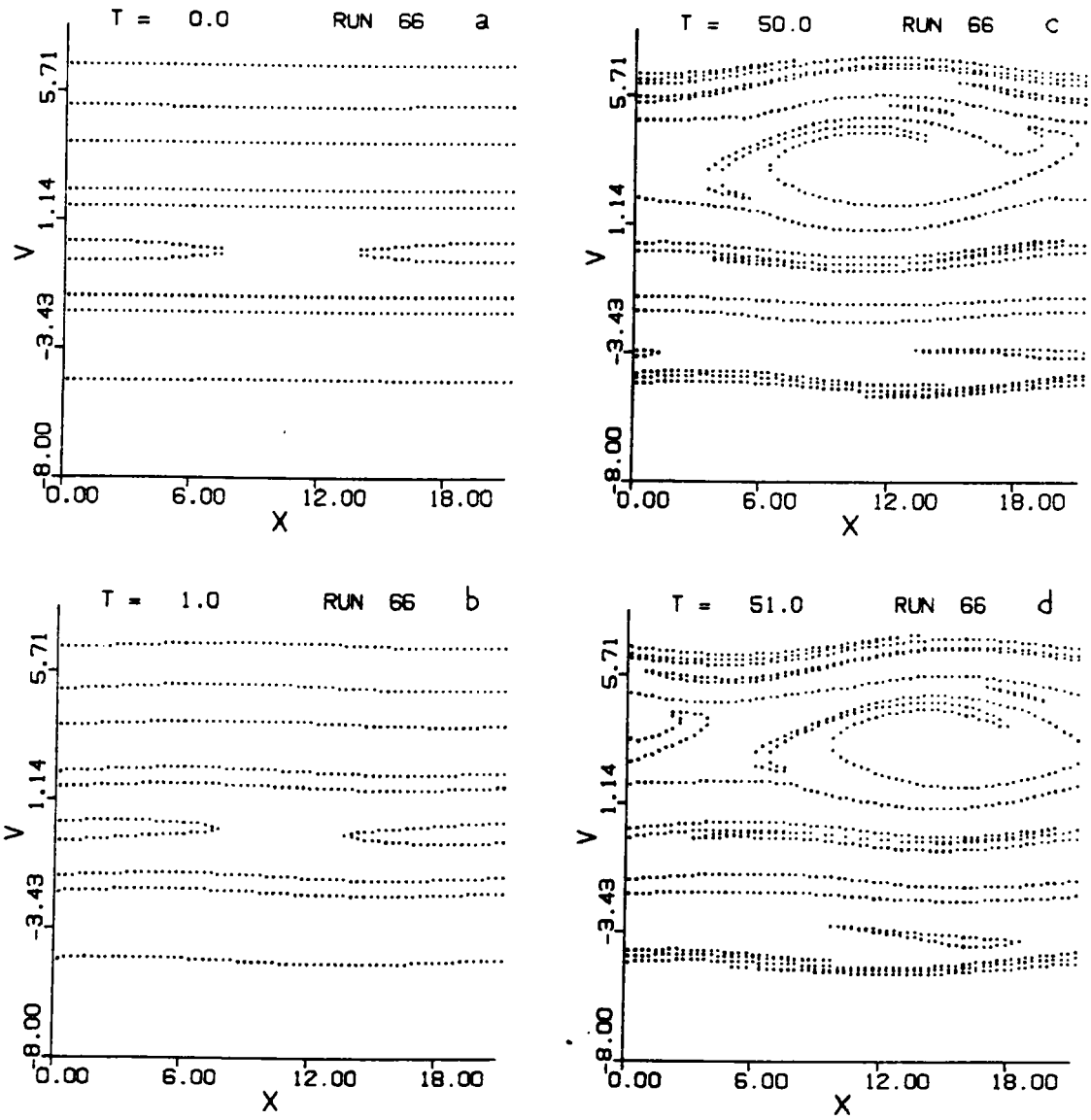


Fig. 5.23 (a)-(d) Level curves for the same case as in Fig. 5.22.

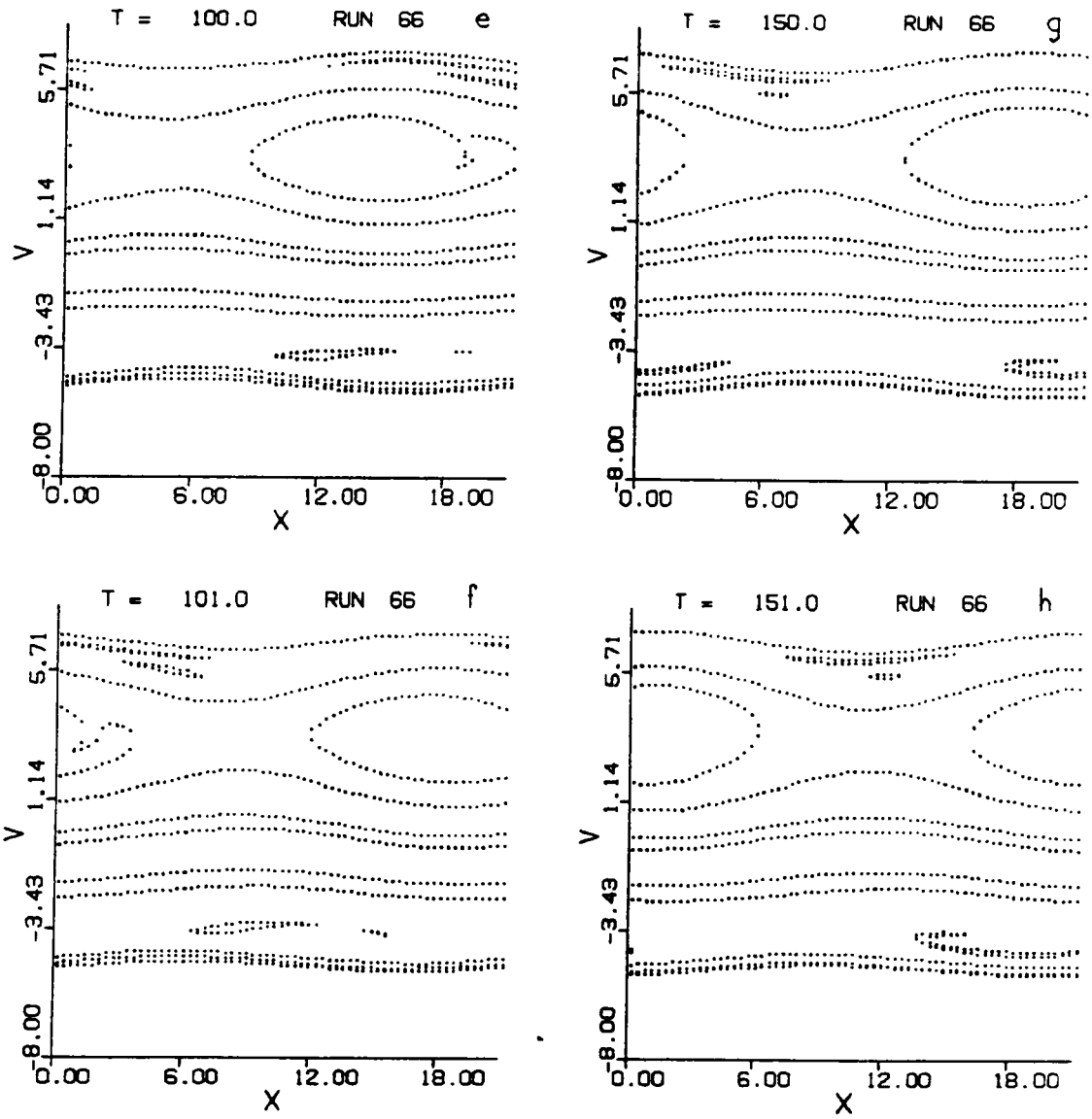


**Fig. 5.23 (e)-(h)** Level curves for the same case as in Fig. 5.22.

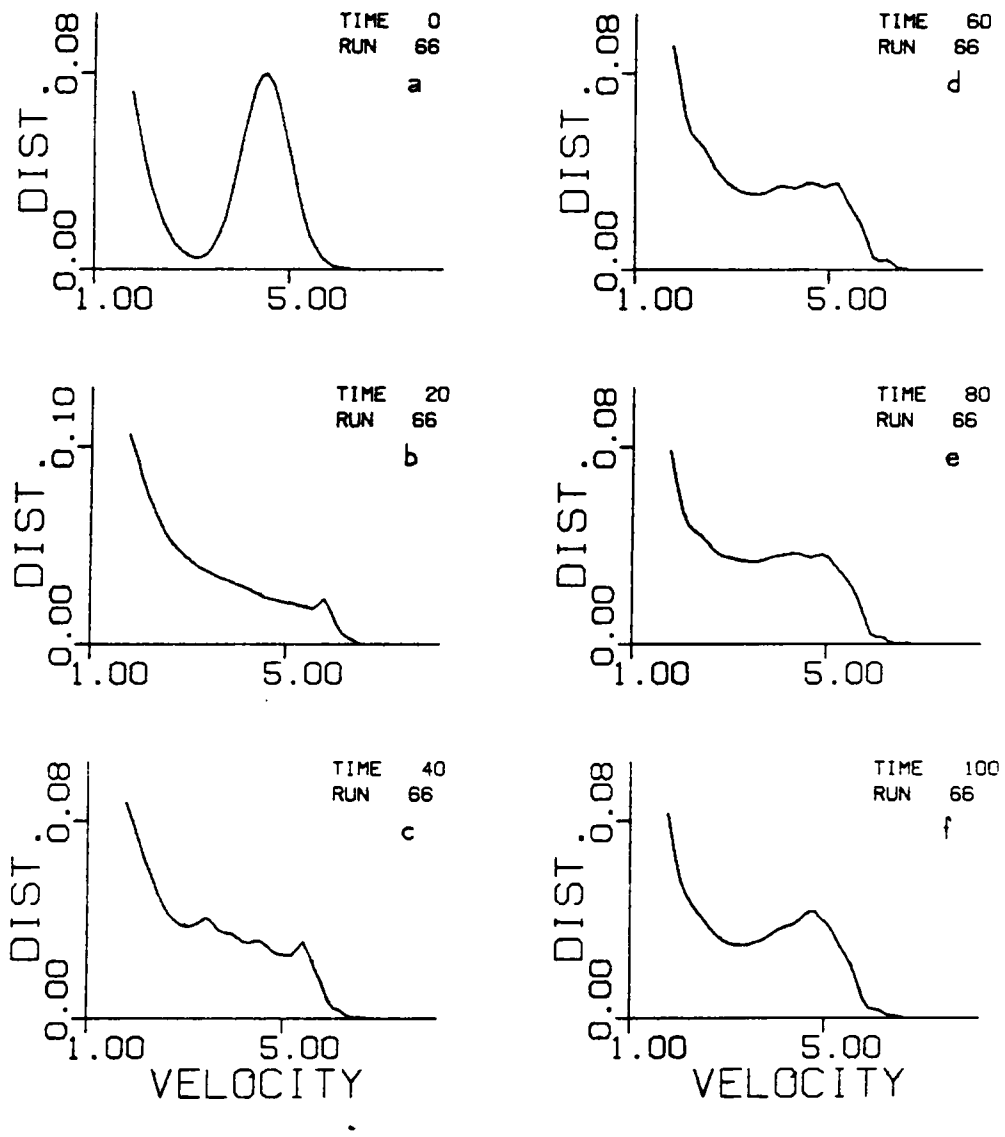


**Fig. 5.24 (a)-(f)** Space averaged distribution for the same case as in Fig. 5.22.

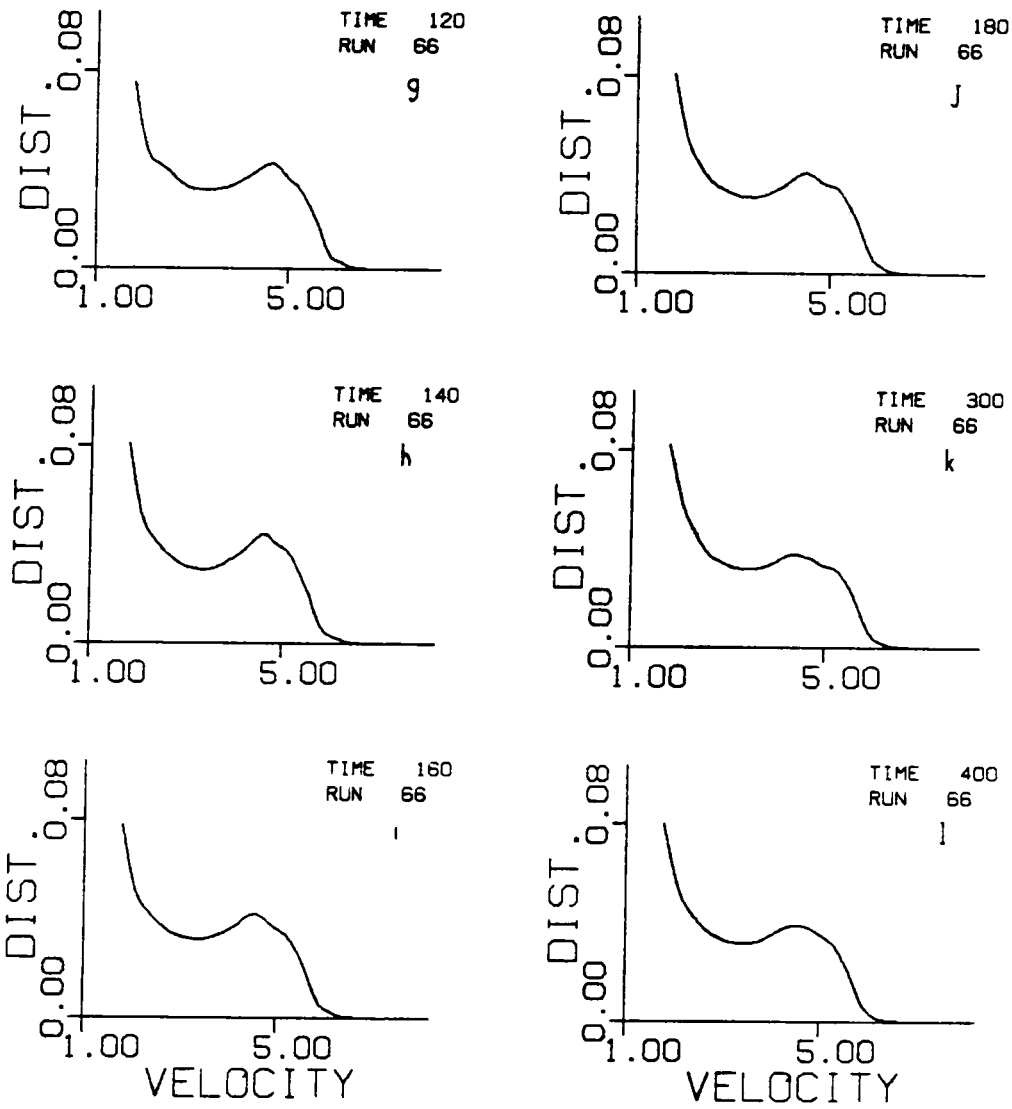


Fig. 5.24 (g)-(l) Space averaged distribution for the same case as in Fig. 5.22.

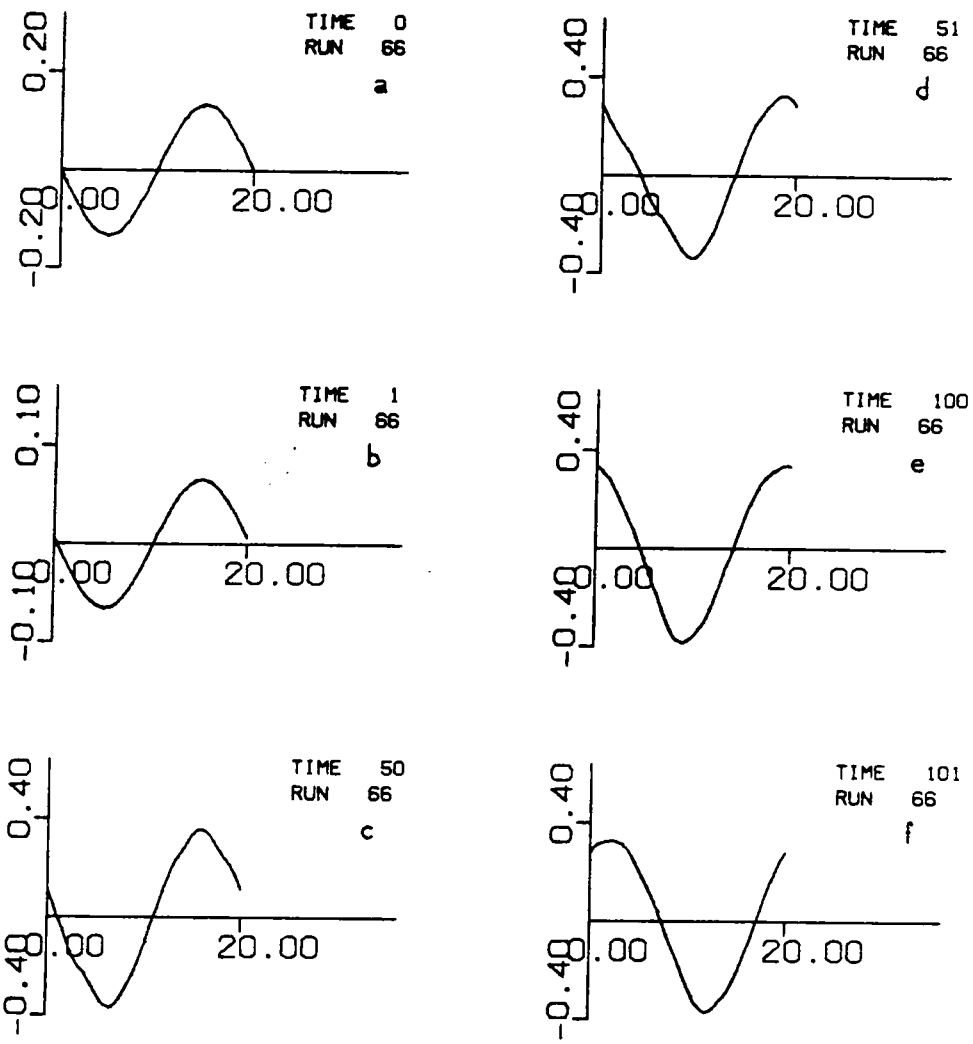


Fig. 5.25 (a)-(f) Electric field for the same case as in Fig. 5.22.

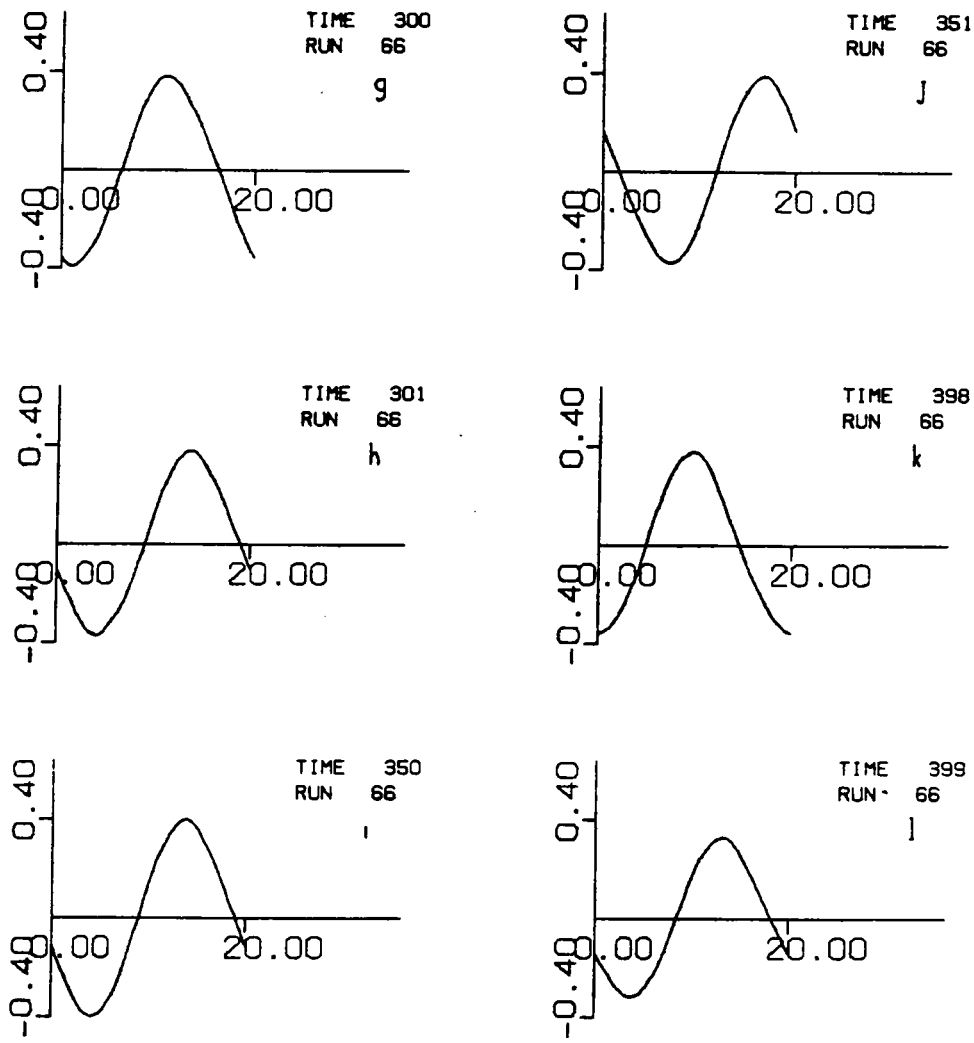


Fig. 5.25 (g)-(l) Electric field for the same case as in Fig. 5.22.

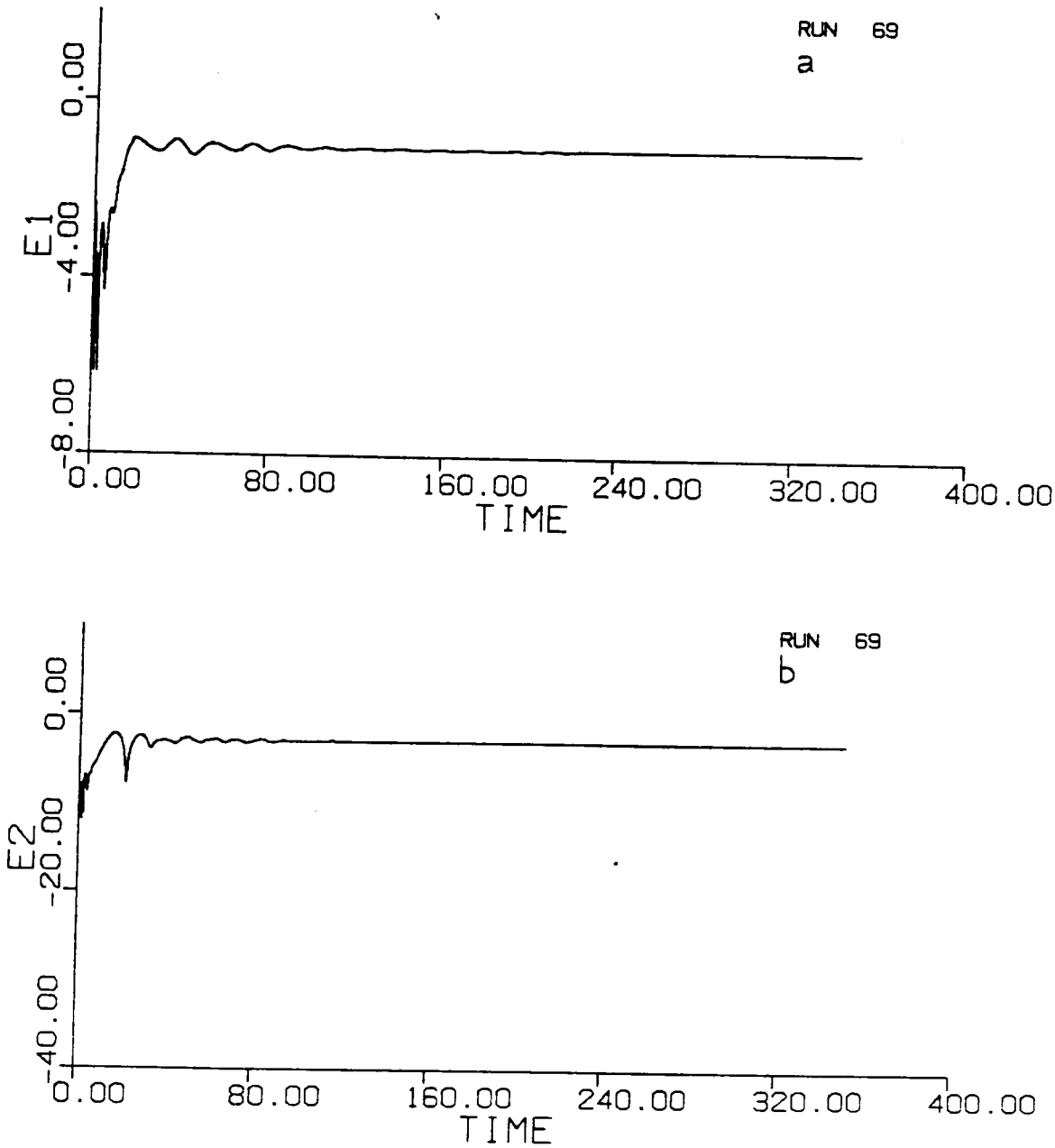


**Fig. 5.26** $|E_1|$ **(a)** and $|E_2|$ **(b)** for the two-stream case.

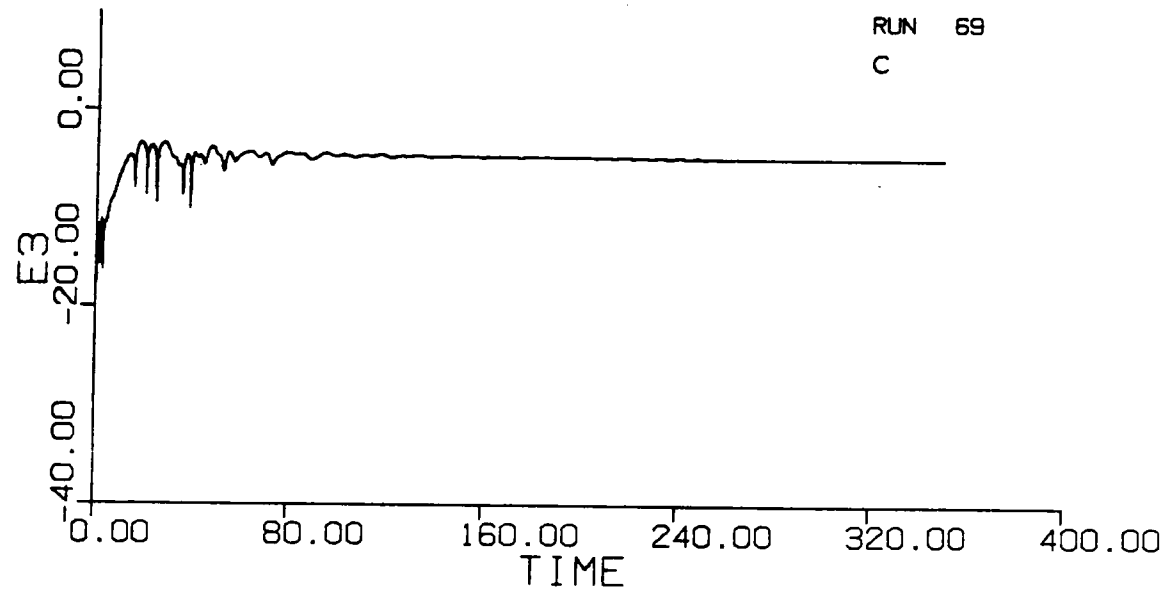


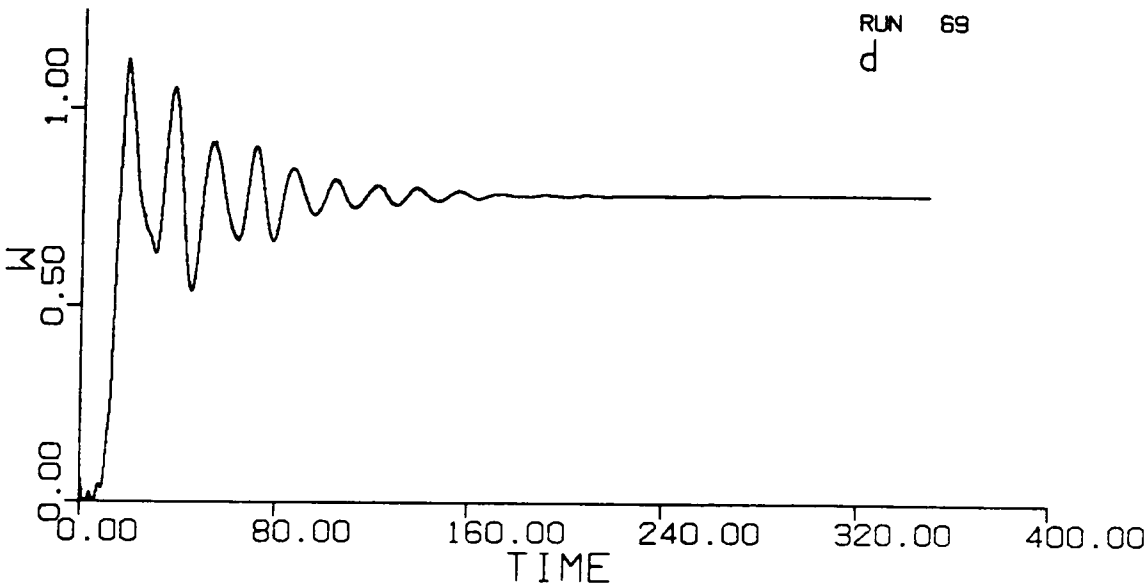


**Fig. 5.26** $|E_3|$ **(c)** and $W|$ **(d)** for the two-stream case.

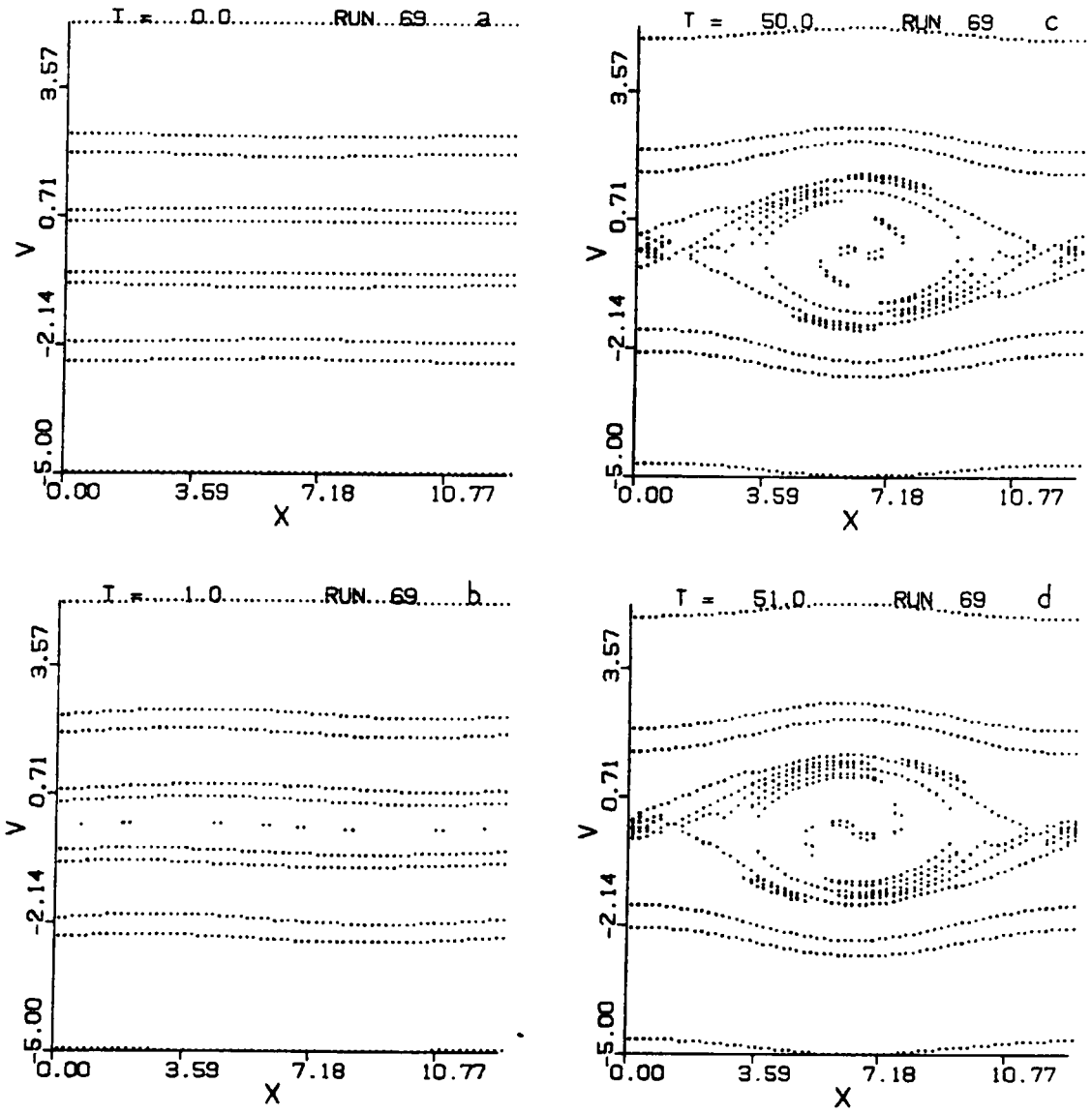


Fig. 5.27 (a)-(d) Level curves for the two-stream case.

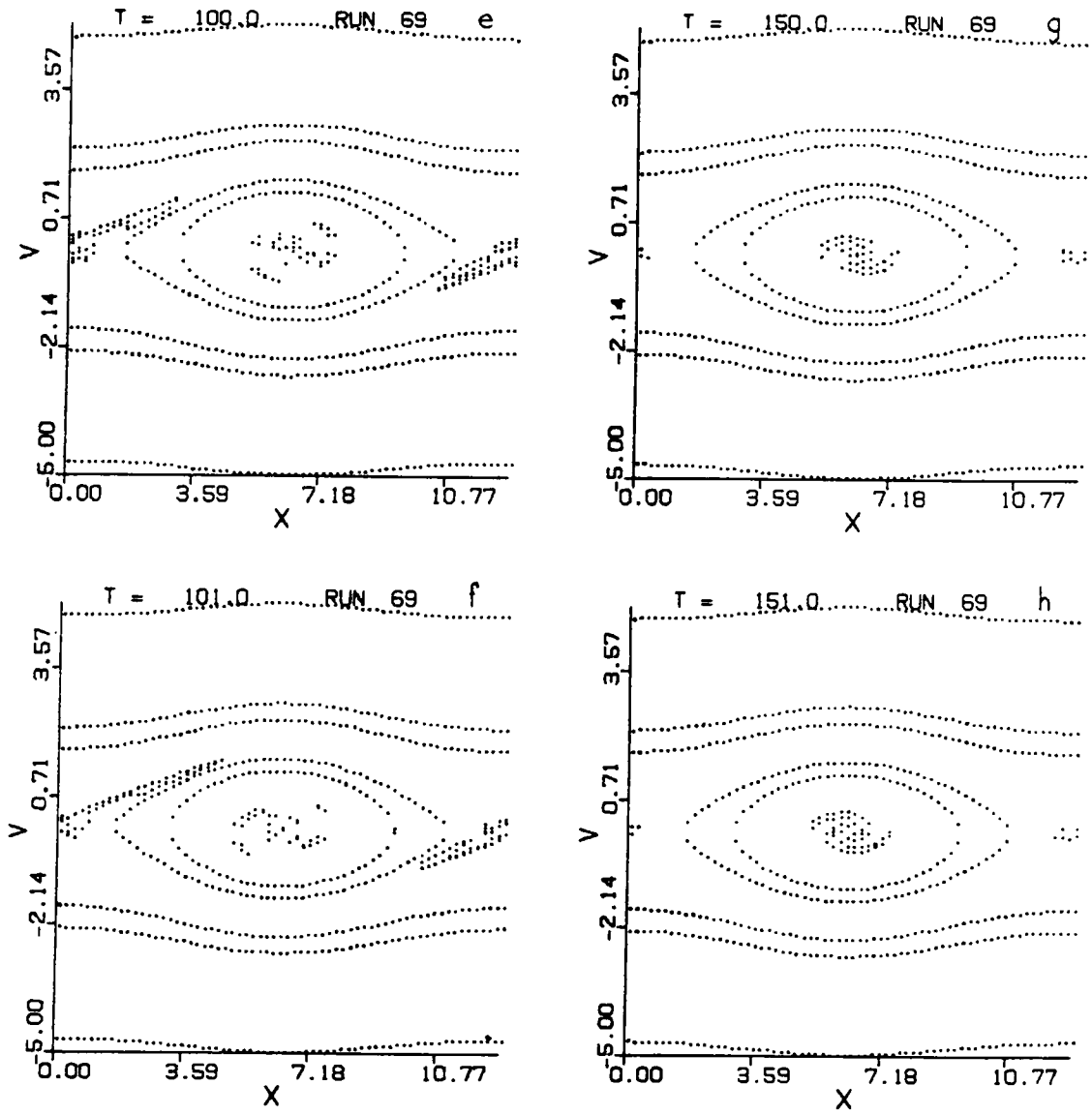


Fig. 5.27 (e)-(h) Level curves for the two-stream case.

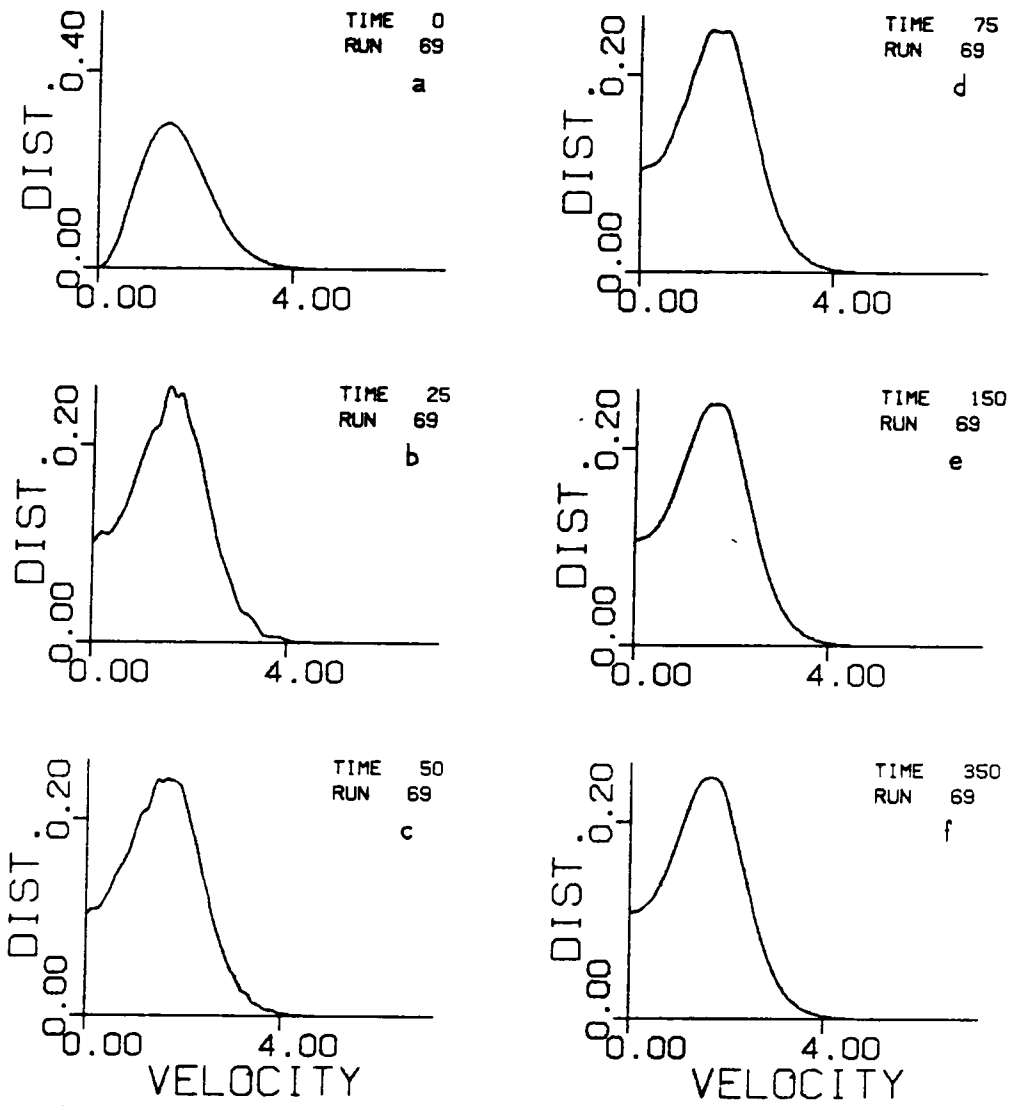


**Fig. 5.28 (a)-(f)** Space averaged distribution for the two-stream case.

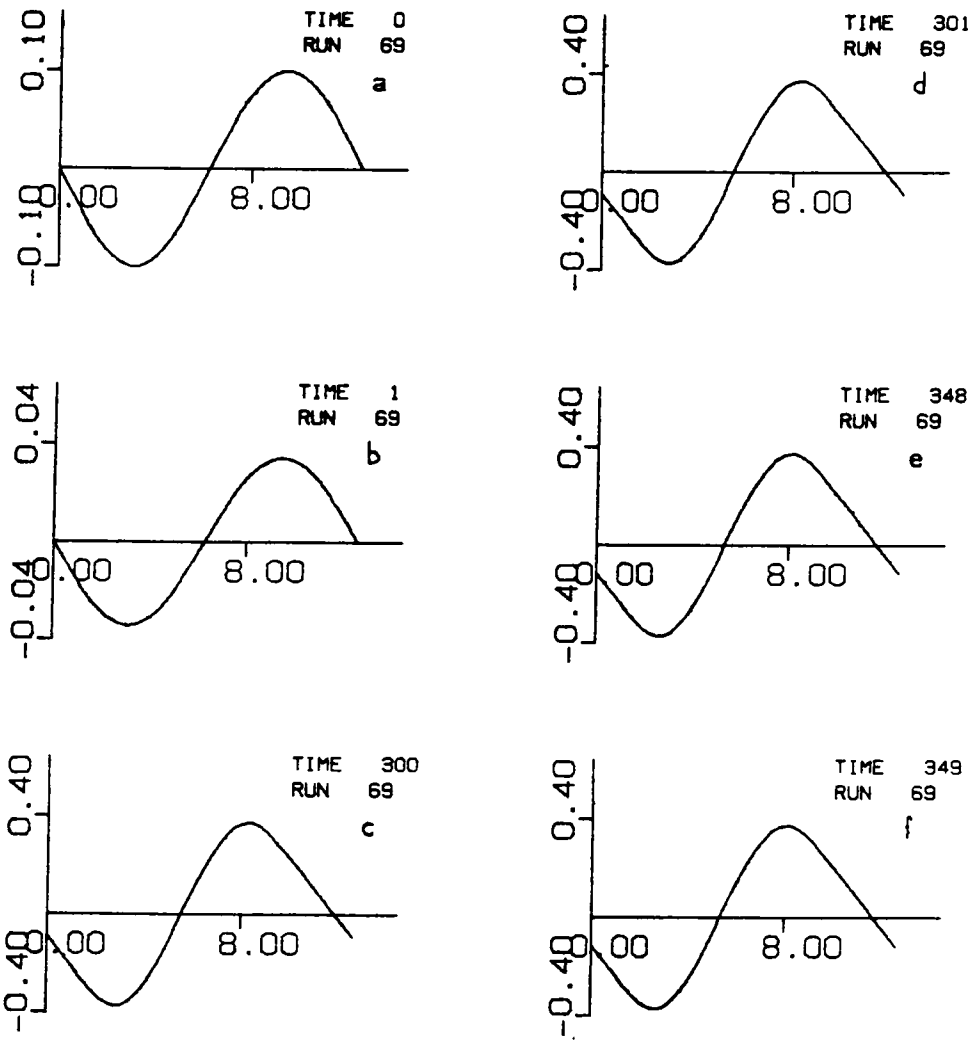


Fig. 5.29 (a)-(f) Electric field for the two-stream case.

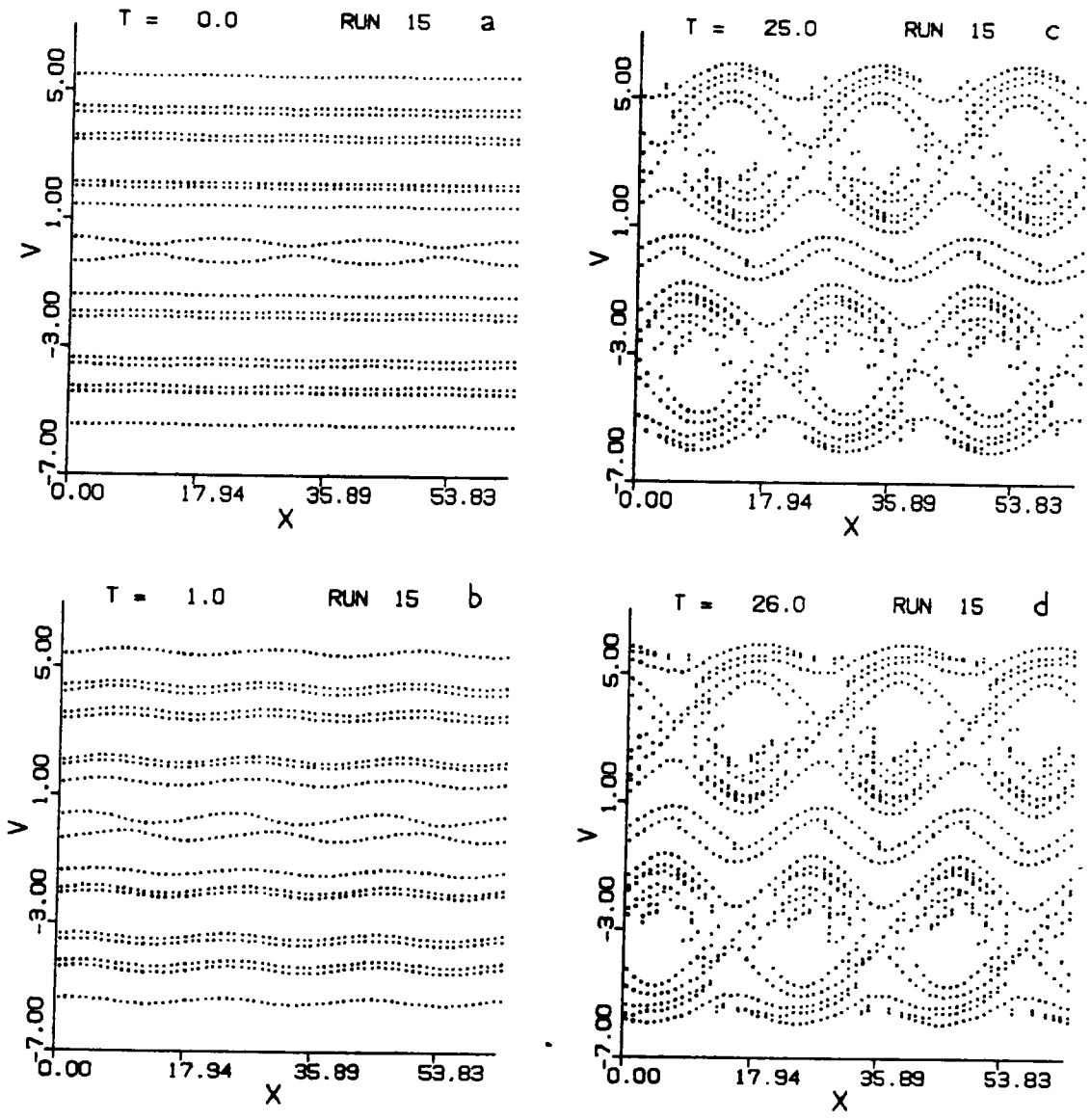


Fig. 5.30 (a)-(d) Level curves for the symmetric bump-on-tail case with $m = 3$ and $M = 512$.

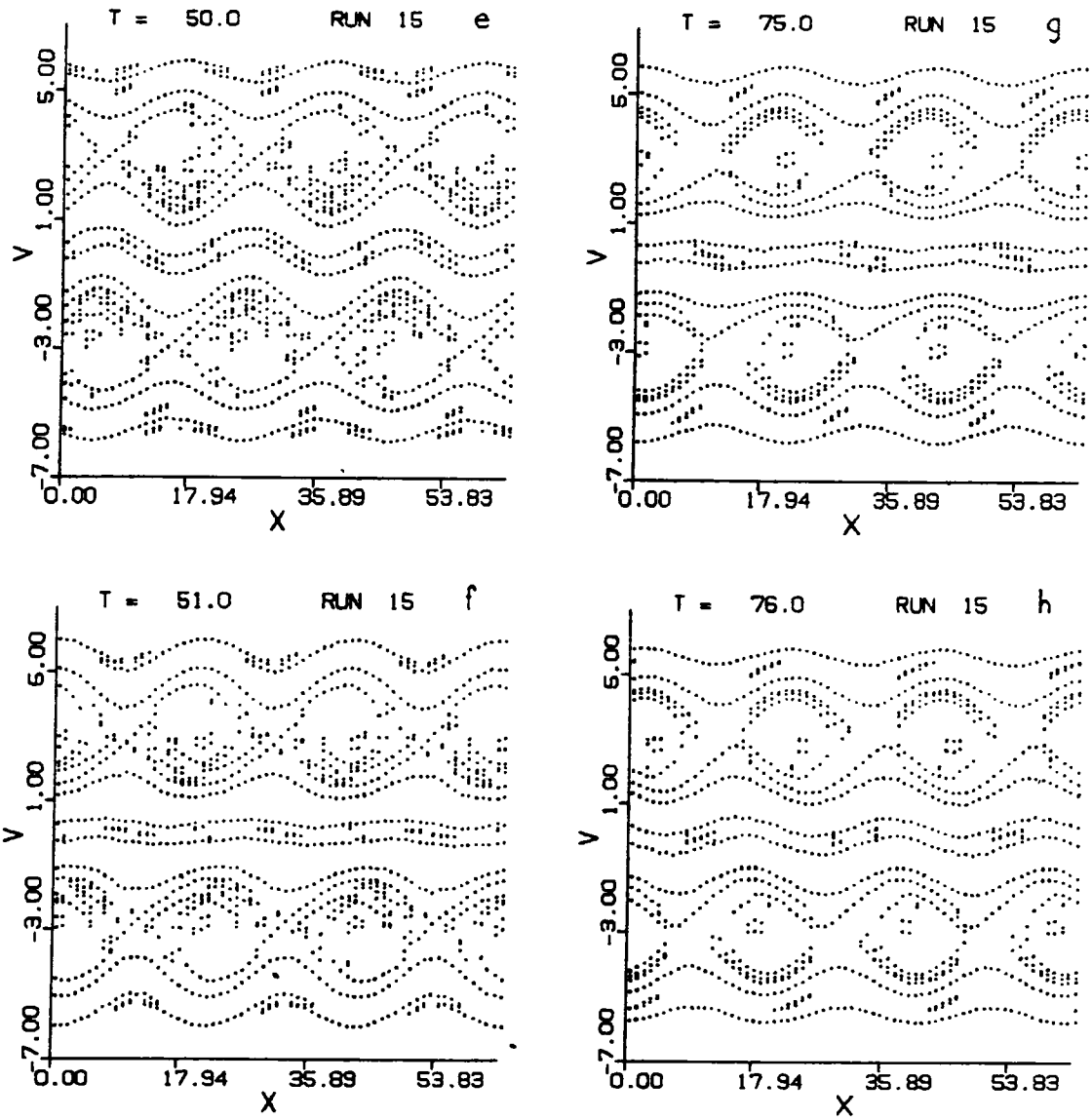


Fig. 5.30 (e)-(h) Level curves for the symmetric bump-on-tail case with $m = 3$ and $M = 512$.

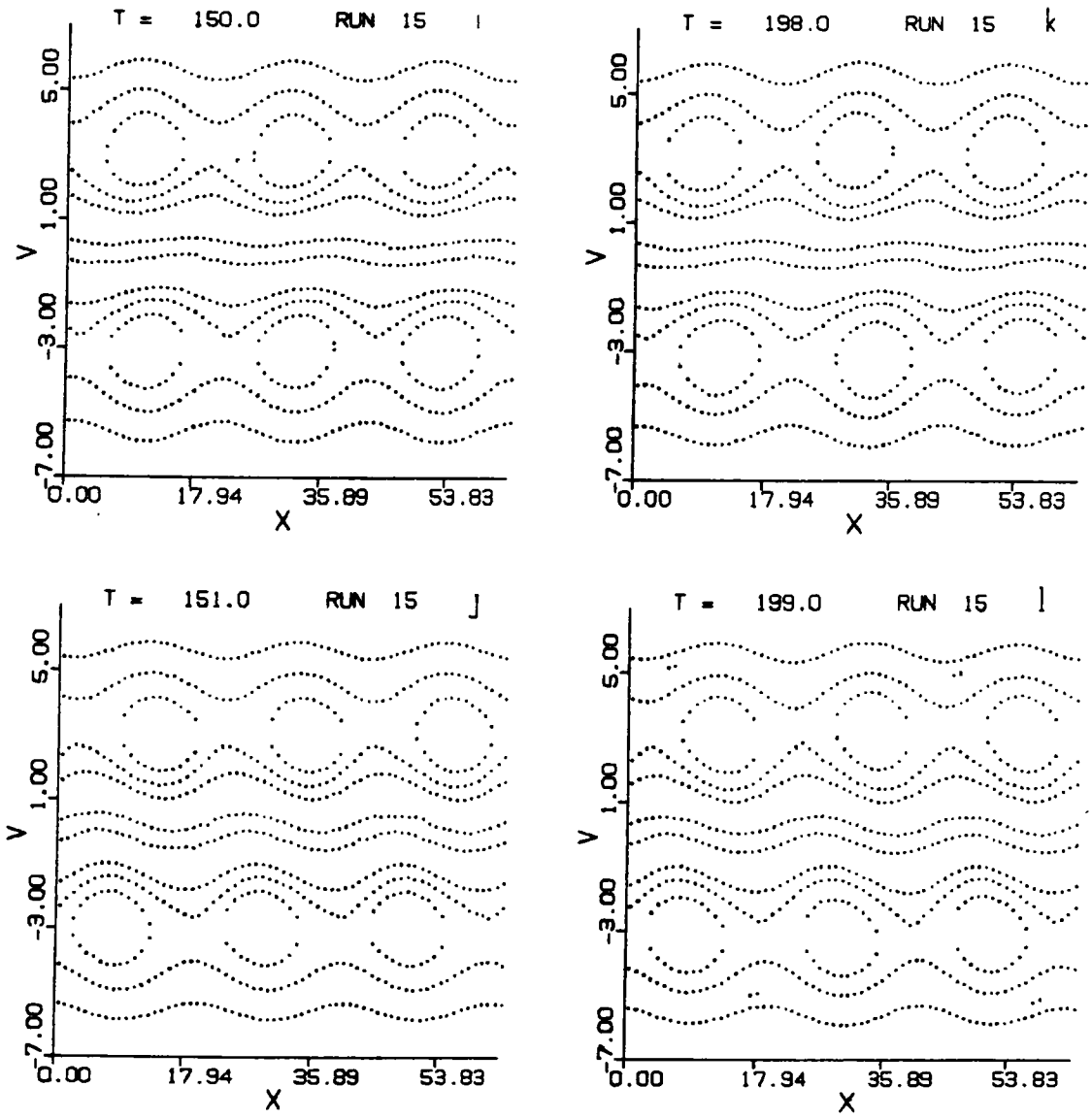


Fig. 5.30 (i)-(l) Level curves for the symmetric bump-on-tail case with $m = 3$ and $M = 512$.

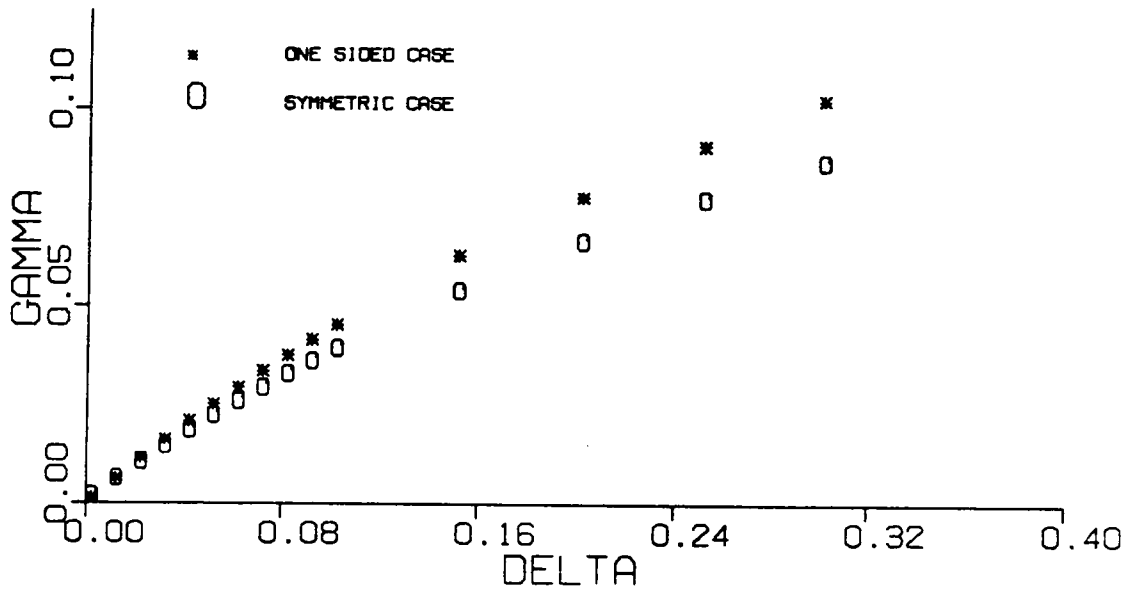


Fig. 5.31 Growth rate $\gamma(\Delta)$.

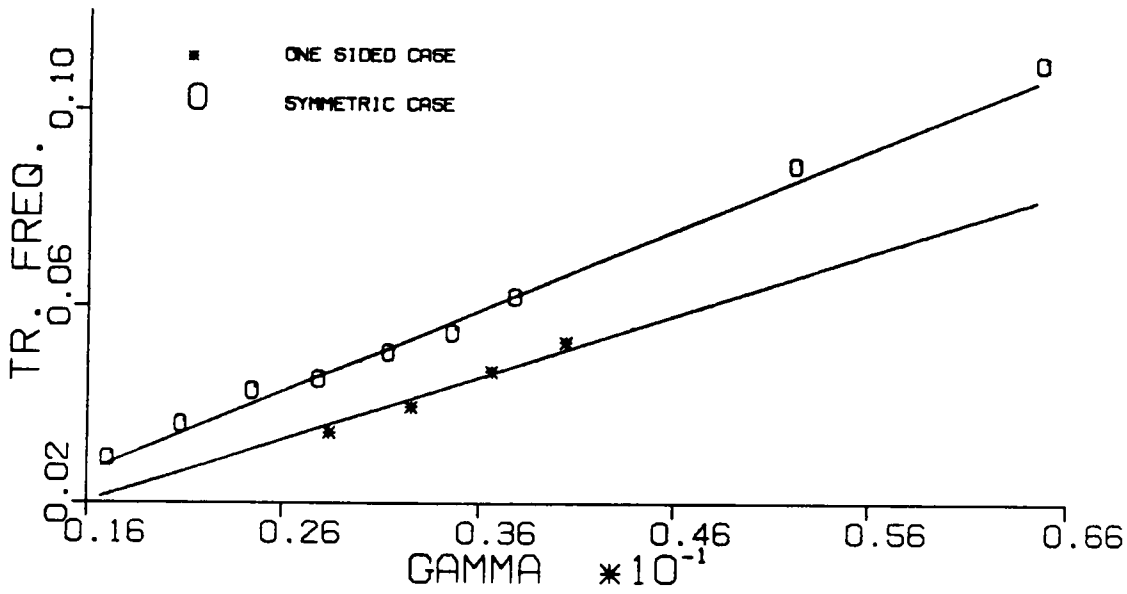


**Fig. 5.32** Trapping frequency $\omega_t(\gamma)$.

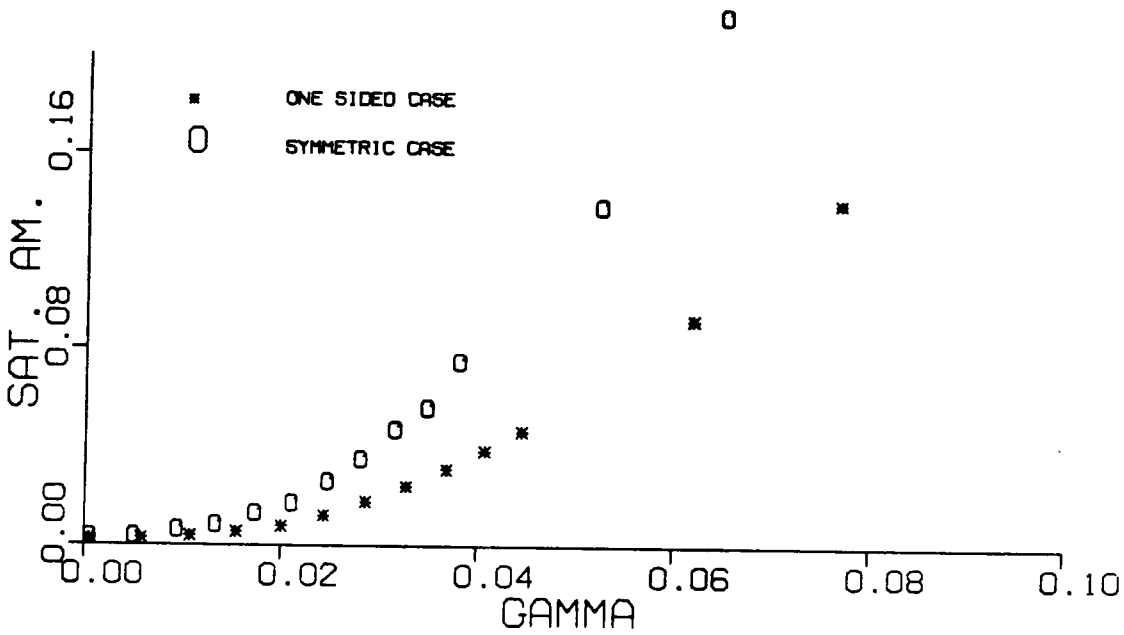


**Fig. 5.33** Saturation amplitude $\Gamma(\gamma)$.

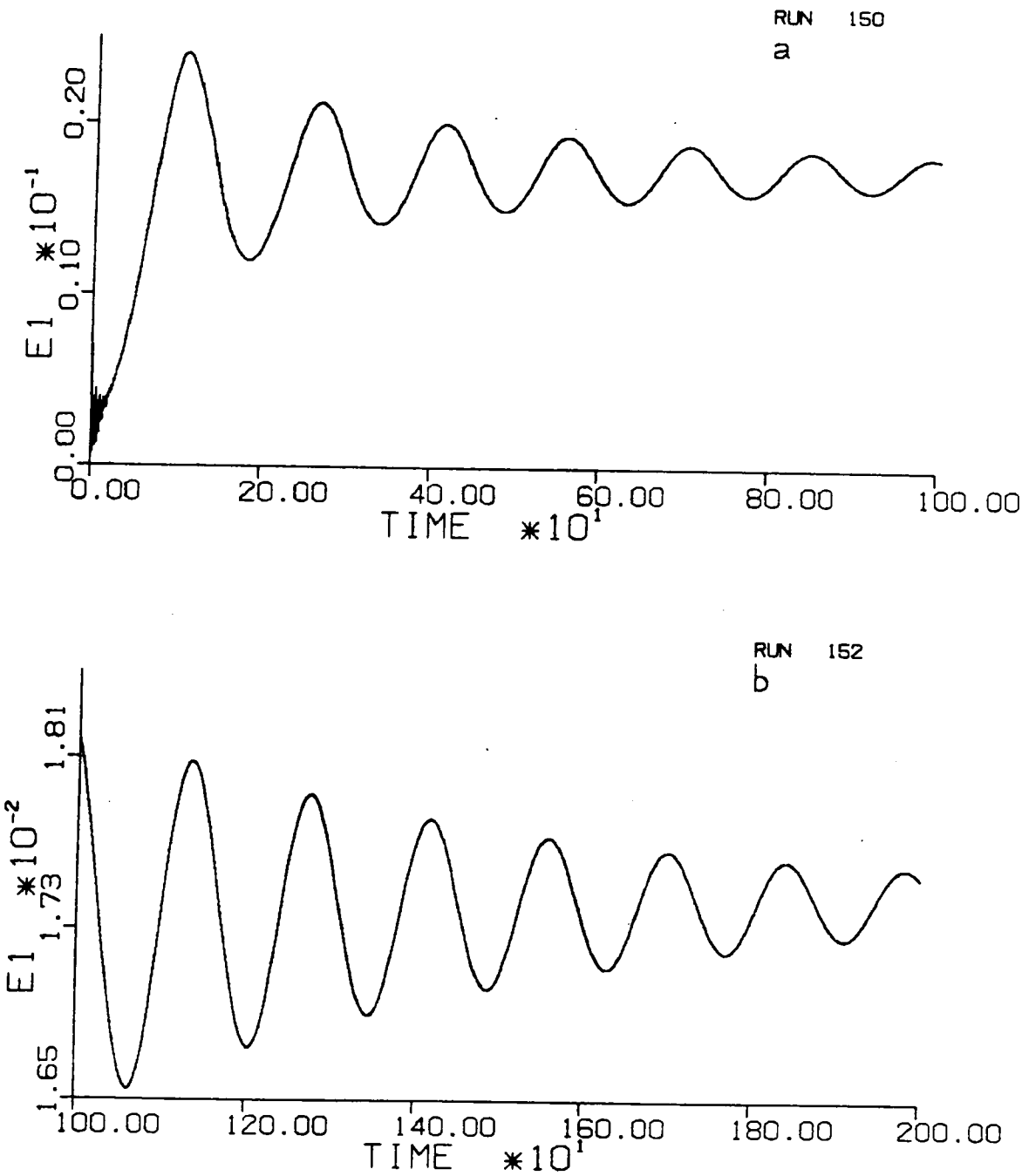


**Fig. 5.34** $|E_1|$ in linear scale for $0 \leq t \leq 1000$ (a) and for $1000 \leq t \leq 2000$ (b) for the one sided bump-on-tail case.

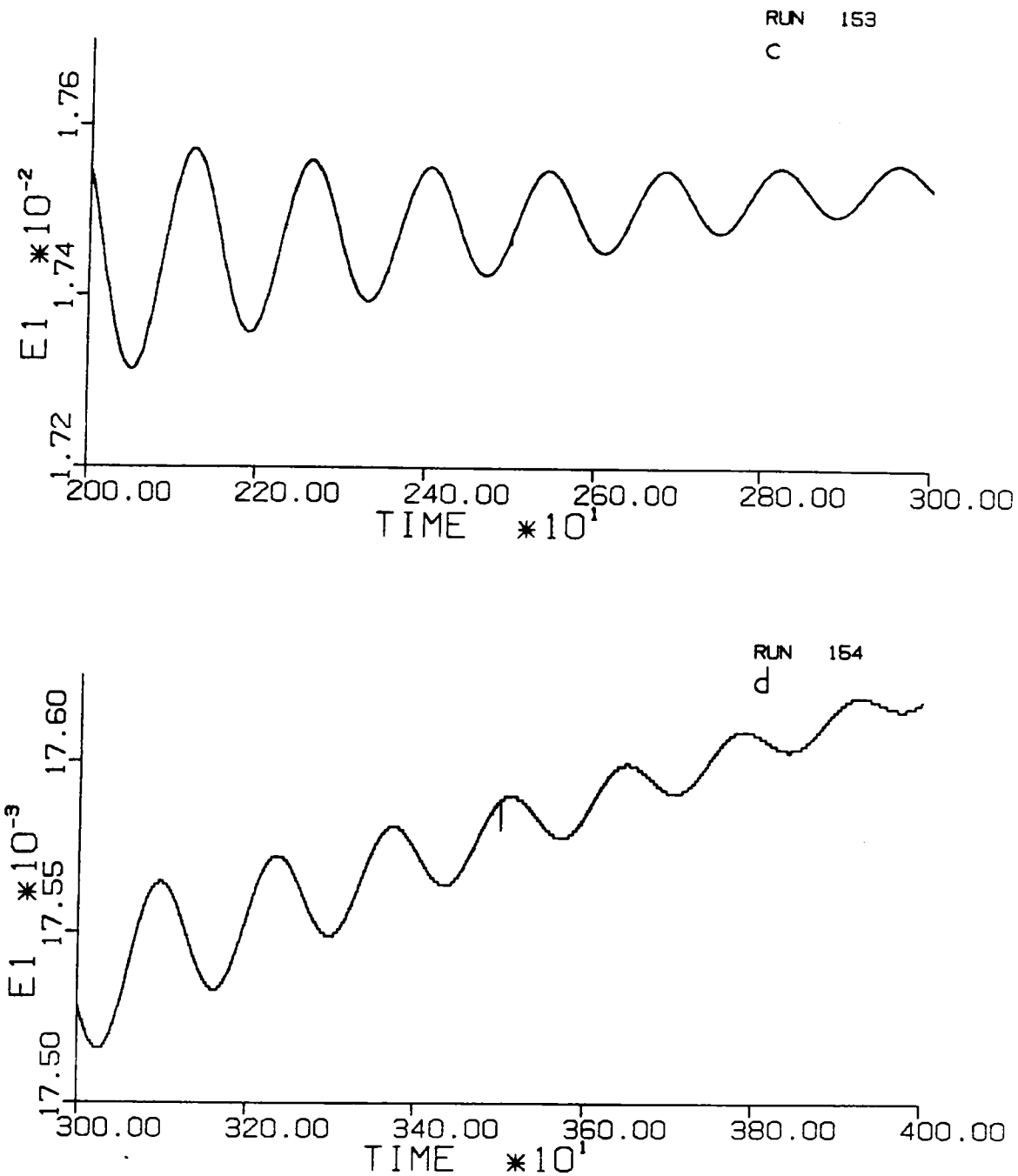


Fig. 5.34 $|E_1|$ in linear scale for $2000 \leq t \leq 3000$ (c) and for $3000 \leq t \leq 4000$ (d) for the one sided bump-on-tail case.

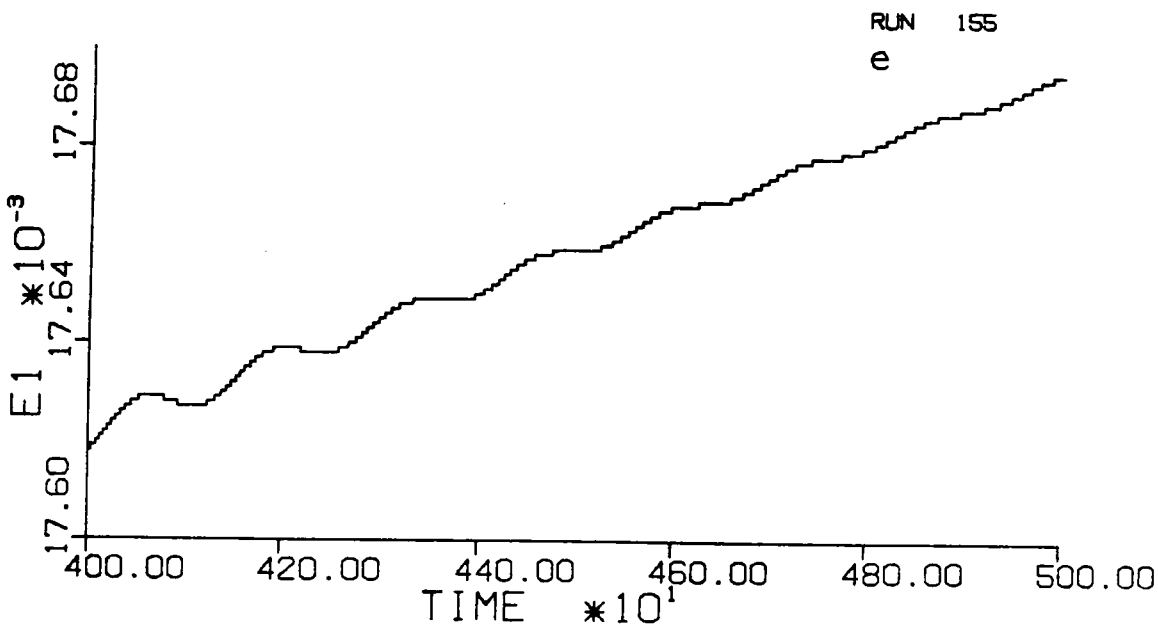


**Fig. 5.34** $|E_1|$ in linear scale for $4000 \leq t \leq 5000$ (e) for the one sided bump-on-tail case.

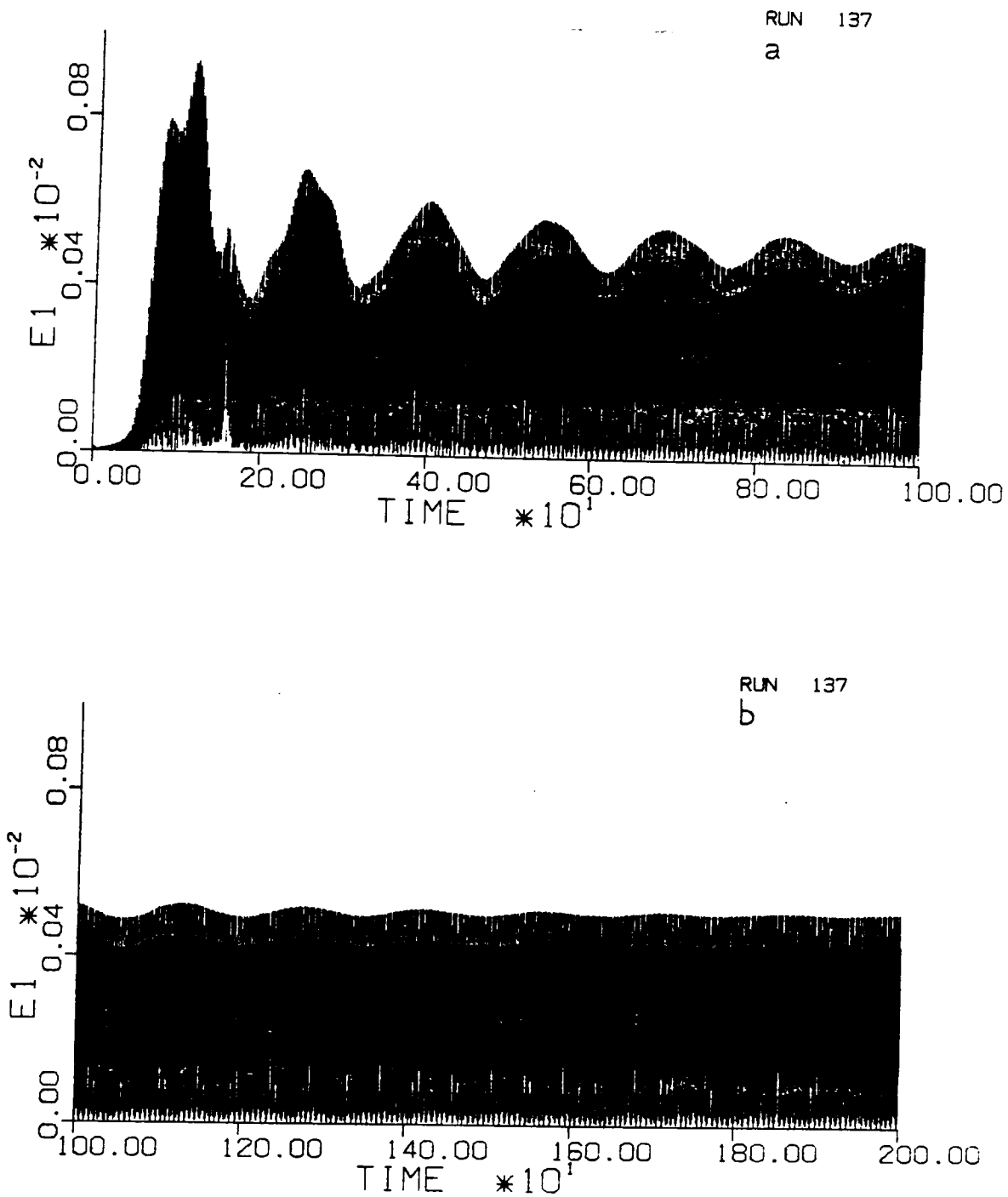


Fig. 5.35 $|E_1|$ in linear scale for $0 \leq t \leq 1000$ (a) and for $1000 \leq t \leq 2000$ (b) for the symmetric bump-on-tail case.

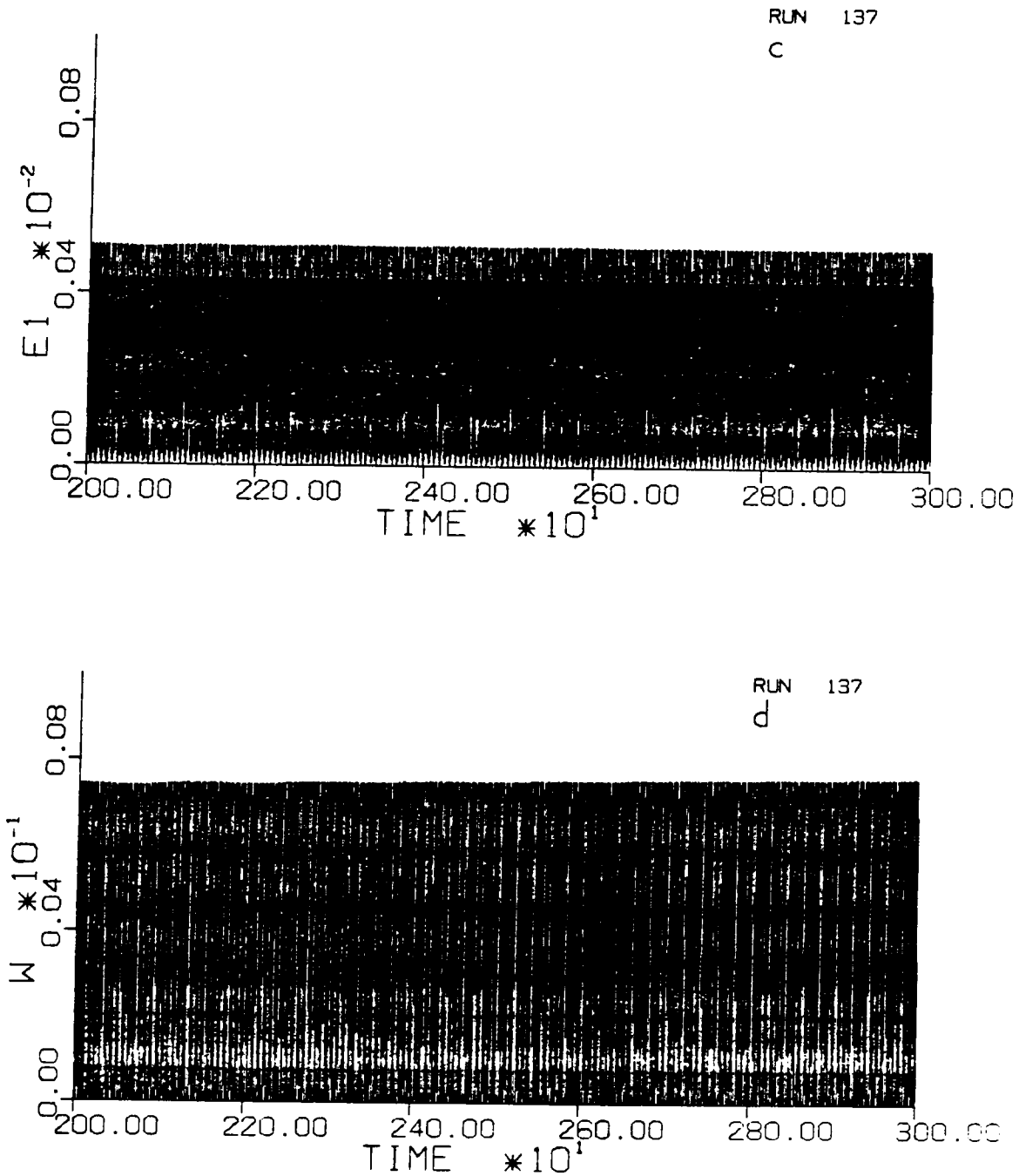


**Fig. 5.35** $|E_1|$ (c) and $W$ (d) in linear scale for $2000 \leq t \leq 3000$ for the symmetric bump-on-tail case.

Tables 5.1 Growth rate, trapping frequency and saturation amplitude for the (a) symmetric and (b) one sided bump-on-tail.

(A)

| Delta | k | gamma | omega | sat.am. | diff. |
|---|---|---|---|---|---|
| 0.00 | 0.4314 | 0.0 | ..... | 5.74E-3 | 0.0 |
| 0.01 | 0.4293 | 4.381E-3 | ..... | 5.98E-3 | 2.40E-3 |
| 0.02 | 0.4271 | 8.786E-3 | ..... | 8.92E-3 | 3.18E-3 |
| 0.03 | 0.4251 | 1.270E-2 | ..... | 1.09E-2 | 5.16E-3 |
| 0.04 | 0.4230 | 1.671E-2 | 2.75E-2 | 1.56E-2 | 9.86E-3 |
| 0.05 | 0.4210 | 2.045E-2 | 3.43E-2 | 1.98E-2 | 1.41E-2 |
| 0.06 | 0.4190 | 2.411E-2 | 4.13E-2 | 2.84E-2 | 2.27E-2 |
| 0.07 | 0.4171 | 2.752E-2 | 4.36E-2 | 3.76E-2 | 3.19E-2 |
| 0.08 | 0.4151 | 3.103E-2 | 4.91E-2 | 4.98E-2 | 4.41E-2 |
| 0.09 | 0.4132 | 3.431E-2 | 5.31E-2 | 5.84E-2 | 5.27E-2 |
| 0.10 | 0.4113 | 3.752E-2 | 6.04E-2 | 7.73E-2 | 7.16E-2 |
| 0.15 | 0.4023 | 5.194E-2 | 8.73E-2 | 1.41E-1 | 1.35E-1 |
| 0.20 | 0.3938 | 6.446E-2 | 1.08E-1 | 2.19E-1 | 2.13E-1 |

(B)

| Delta | k | gamma | omega | sat.am. | diff. |
|---|---|---|---|---|---|
| 0.00 | 0.4824 | 0.0 | ..... | 2.15E-3 | 0.0 |
| 0.01 | 0.4800 | 5.206e-3 | ..... | 2.83E-3 | 6.80E-4 |
| 0.02 | 0.4776 | 1.020E-2 | ..... | 3.89E-3 | 1.74E-3 |
| 0.03 | 0.4753 | 1.490E-2 | ..... | 5.45E-3 | 3.30E-3 |
| 0.04 | 0.4730 | 1.951E-2 | ..... | 7.91E-3 | 5.76E-3 |
| 0.05 | 0.4708 | 2.384E-2 | ..... | 1.21E-2 | 9.95E-3 |
| 0.06 | 0.4686 | 2.809E-2 | 3.32E-2 | 1.78E-2 | 1.57E-2 |
| 0.07 | 0.4664 | 3.227E-2 | 3.85E-2 | 2.40E-2 | 2.19E-2 |
| 0.08 | 0.4642 | 3.637E-2 | 4.57E-2 | 3.11E-2 | 2.90E-2 |
| 0.09 | 0.4621 | 4.022E-2 | 5.17E-2 | 3.85E-2 | 3.64E-2 |
| 0.10 | 0.4600 | 4.400E-2 | ..... | 4.65E-2 | 4.44E-2 |
| 0.15 | 0.4498 | 6.151E-2 | ..... | 9.21E-2 | 9.00E-2 |
| 0.20 | 0.4404 | 7.645E-2 | ..... | 1.40E-1 | 1.38E-1 |
| 0.30 | 0.4231 | 1.012E-1 | ..... | 2.26E-1 | 2.24E-1 |

## Chapter 6: Conclusions and outlook.

In this work, we have investigated numerically some aspects of the nonlinear behaviour of Vlasov solutions, with emphasis on the asymptotic states. Using the numerical code based on the well known splitting scheme algorithm that we have implemented on the Cray X-MP (and, later, on the Cray Y-MP) of the Pittsburgh Supercomputing Center, we have re-analysed some of the cases already investigated in the literature, reaching different conclusions even on the basis of the same numerical results. In particular, when perturbung a spatially symmetric homogeneous equilibrium distribution (either stable, like a maxwellian or unstable, like a bump-on-tail) with a reflection symmetric perturbation, we have come to the conclusion that the asymptotic state can be described as a superposition of two BGK solutions, but not as a BGK equilibrium by itself, since the electric field behaves like a standing wave and no reference frame can be found in which it can be cast in the form $E(x-Vt)$ for some real $V$. When perturbing a symmetric equilibrium distribution two travelling waves are excited, with opposite phase velocities; in this case, they also have equal amplitudes, so their superposition is a standing wave. In all the cases the electric field mode which was excited at $t = 0$ remained largely dominant throughout the whole simulation. In the maxwellian case, the behaviour observed for the electric field amplitude followed closely the predictions of O'Neil's model. Subsequently, we extended our investigations of the maxwellian and the symmetric bump-on-tail to include perturbations with different (non-symmetric) dependence on velocity. For the stable (maxwellian) case, the behaviour of the electric field at long times is that of a travelling wave with modulated amplitude, as expected since the two travelling waves excited at $\pm v_\phi$ have different amplitudes. In the unstable case, the two travelling waves excited at $t = 0$ both go unstable and saturate with the same amplitude and,

surprisingly, at the same time, giving rise to a standing wave in the electric field after saturation. Our long-time simulations with the symmetric bump-on-tail and the simulations with different velocity dependent perturbations are the first to appear.

We then analysed the one sided bump-on-tail equilibrium, carrying the simulation to longer times than was done before. A typical feature observed in this case is the beating between the unstable mode and the least damped mode, which happens to have phase velocity approximately opposite to that of the unstable mode. Small oscillations at this beating frequency are observed all the way in the nonlinear regime and there is no indication that they might be damped asymptotically. This behaviour is incompatible with a BGK equilibrium.

The only distribution for which the system seems to approach asymptotically a BGK equilibrium is the two-stream, as was already speculated in the literature, both analytically and numerically. Our results basically confirm this assertion, although a small curious violation of the symmetry properties of the solution is observed, a purely numerical effect that, we believe, does not affect the conclusions.

In all these cases, it seems that linear theory is well suited for describing not only the early evolution of the system, but also the asymptotic states, since the kind of space averaged distribution and electric field that are observed in the asymptotic state are compatible with a linear description and the quantities are seen to oscillate at a frequency whose value is given (within numerical errors) by the linear dispersion relation.

Separately, we have addressed the problem of the scaling of the saturation amplitude with the growth rate, on which serious discrepancies exist among different theoretical models. The question had already received numerical attention, but with

very inaccurate algorithms. However, our results agree with the indications given by these less accurate simulations. The problem is still partially open and much longer simulations are needed to solve all the discrepancies.

In all the cases that we have investigated, the square root-like scaling of the frequency of the amplitude oscillations with the strength of the perturbation in the linearly stable cases and with the saturation amplitude in the linearly unstable ones is confirmed.

Finally, in lieu of numerical verification of some recently made predictions about instability of standing waves and travelling waves for weakly unstable modes in presence of symmetric equilibrium distributions, predictions resulting from a model which includes collisional effects and uses bifurcation theory methods, we have modified the splitting scheme to include the Krook collisional model. On this point, we have only some preliminary results which agree with the results of linear theory in presence of collisions.

This work suggests a number of problems, either of a purely numerical or of a mathematical nature, which need further investigation.

Numerically, the inclusion in the splitting scheme of a suitable filtering procedure that eliminates the problems related to the filamentation and to recursion (possibly the one suggested by Klimas) seems to be the most urgent question. Furthermore, the smoothing of the fine structure in phase space which happens with the splitting scheme needs further investigation and deeper understanding. Longer simulations with the splitting scheme should be performed in order to address the open questions about the saturation of weakly unstable modes, question that has been addressed only with rather inaccurate algorithms. In particular, the ripples on the space averaged

distribution near $v = 0$, which are observed in the solutions obtained with other algorithms, do not appear at all with the splitting scheme, making longer simulations promising. Finally, more numerical work should be done in order to investigate the behaviour of the system in presence of collisions.

Analytically, much work is of course to be done, since a general theory for the full nonlinear system is still lacking. Perhaps, some phenomenological model that makes flexible use of some of the concepts of linear theory could be developed.

## References


[1] N. A. Krall. A. W. Trivelpiece, "Principles of Plasma Physics," McGraw-Hill Book Company, 1973.

[2] A. Vlasov, J. of Physics 9 (1945), p. 25.

[3] L. D. Landau, J. of Physics 10 (1946), p. 25.

[4] N. G. Van Kampen, Physica 21 (1955), p. 949.

[5] K. M. Case, Ann. Phys. 7 (1959), p. 349.

[6] M. D. Arthur, W. Greenberg, P. F. Zweifel, Phys. Fluids 20 (1977), p. 1926.

[7] J. P. Holloway, "Ph. D. Thesis," University of Virginia, 1989.

[8] C. Marchioro, M. Pulvirenti, Math. Meth. in the Appl. Sci. 8 (1986), p. 284.

[9] I. B. Bernstein, J. M. Green, M. D. Kruskal, Phys. Rev. 108 (1957), p. 546.

[10] T. O'Neil, Phys. Fluids 8 (1965), p. 2255.

[11] T. M. O'Neil, J. H. Winfrey, J. H. Malmberg, Phys. Fluids 14 (1971), p. 1204.

[12] C. Burnap, M. Miklavcic, B. W. Willis, P. F. Zweifel, Phys. Fluids 28 (1985), p. 110.

[13] A. Simon, M. N. Rosenbluth, Phys. Fluids 19 (1976), p. 1567.

[14] J. D. Crawford, Cont. Math. 28 (1984), p. 377.

[15] J. Denavit, W. L. Kruer, Phys. Fluids 14 (1971), p. 1782.

[16] G. Joyce, G. Knorr, H. K. Meier, J. Comput. Phys. 8 (1971), p. 53.

[17] G. Knorr, J. Comput. Phys. 13 (1973), p. 165.

[18] J. Denavit, J. Comput. Phys. 9 (1972), p. 74.

[19] C. G. Cheng, G. Knorr, J. Comput. Phys. 22 (1976), p. 330.

[20] M. M. Shoucri, R. J. Gagne', Phys. Fluids 21 (1978), p. 1168.

[21] M. M. Shoucri, Phys. Fluids 22 (1979), p. 2038.

[22] A. J. Klimas, J. Comput. Phys. 68 (1987), p. 202.

[23] J. Denavit, Phys. Fluids 28 (1985), p. 2773.

[24] A. Simon, S. Radin, R. W. Short, Phys. Fluids 31 (1988), p. 3649.

[25] A. J. Klimas, J. Cooper, Phys. Fluids 26 (1983), p. 478.

[26] J. Batt, "Ein Existenzbeweis fuer die Boltzmann-Vlasov-Gleichung in eindimensionalem Fall," Berichte der Kernforschungsanlage, Juelich, West Germany, 1963.

[27] J. Cooper, A. J. Klimas, J. Math. An. and Appl. **75** (1980), p. 306.

[28] A. J. Klimas, J. Math. Phys. **20** (1979), p. 2131.

[29] N. R. Lewis, K. R. Symon, Phys. Fluids **27** (1984), p. 192.

[30] B. Abraham-Shrauner, Phys. Fluids **27** (1984), p. 197.

[31] D. Roberts, J. Math. Phys. **26** (1985), p. 1529.

[32] B. Abraham-Shrauner, J. Math. Phys. **26** (1985), p. 1428.

[33] B. Abraham-Shrauner, J. Plasma Phys. **32** (1984), p. 197.

[34] D. Roberts, J. Plasma Phys. **33** (1985), p. 219.

[35] J. D. Crawford, P. Hislop, to appear.

[36] B. D. Fried, S. D. Conte, "The Plasma Dispersion Function," Academic Press, New York, 1961.

[37] A. J. Klimas, J. Comput. Phys. **50** (1983), p. 270.

[38] A. J. Klimas, R. Fitzenreiter, J. of Geophys. Res. **93** (1988), p. 9628.

[39] M. M. Shoucri, Phys. Fluids **21** (1978), p. 1359.

[40] M. M. Shoucri, Phys. Fluids **23** (1980), p. 2030.

[41] A. Ghizzo, P. Bertrand, M. Feix, G. Knorr, M. Shoucri, "Nonlinear Evolution of the Two-Stream Instability," Tokamak de Varennes, Varennes, Quebec, Canada, 1988.

[42] E. W. Larsen, C. Burnap, P. F. Zweifel, Transp. Theory and Stat. Phys. **12** (1983), p. 73.

[43] C. E. Rathmann, J. L. Vomvoridis, J. Denavit, J. Comput. Phys. **26** (1978), p. 408.

[44] J. D. Crawford, to appear.

## Appendix A: Inclusion of collisional effects in the splitting scheme.

As mentioned in Sect. 5.4, bifurcation theory methods have recently been used in the study of plasma instabilities. In a model that included a collisional term in the form of the Krook collision model, J.D.Crawford [...] predicted the existence of two regimes for weakly unstable modes in presence of symmetric unstable equilibrium distributions, regimes in which standing waves or travelling waves are seen to go unstable. Moreover, near the boundary of these two regions, interesting periodic behaviour should be observed, with possible occurrence of period doubling. We attempted to verify these predictions numerically, but due to difficulties in evaluating with the required accuracy the coefficients that appear in the equations on the stability boundary and because of lack of time, we have been unable to complete the work. However, as an intermediate result, we were able to include collisional effects in our code based on the splitting scheme algorithm. Here, we describe how collisional effects have been included in the splitting scheme algorithm and produce a few simulations performed with small collision frequency.

With the Krook collision model, Vlasov's equation becomes

$$\frac{\partial f}{\partial t} + v\frac{\partial f}{\partial x} - E\frac{\partial f}{\partial v} = -\nu_c(f - f_{eq}) \tag{A.1}$$

where $f_{eq}$ is the equilibrium distribution towards which collisions drive the system and $\nu_c$ is the collision frequency. We choose $f_{eq}$ to be locally maxwellian, so it has the form

$$f_{eq} = \rho(x,t)\frac{1}{2\pi}e^{-\frac{v^2}{2}} \tag{A.2}$$

In the presence of collisions, $f(x,v,t)$ is not any more constant along characteristics. since instead of having

$$\frac{df}{dt}|_{char} = 0$$

we now have

$$\frac{df}{dt}|_{char} = -\nu_c(f - f_{eq})$$

so the idea for producing numerical solutions of (A.1) is to account for the variation of $f$ along the Vlasov characteristics at each time step. We now have:

$$f(x(t), v(t), t) = f(x(t-\Delta t), v(t-\Delta t), t-\Delta t) - \nu_c \int_{t-\Delta t}^{t} dt' \left[ f(x(t'), v(t'), t') - \rho(x(t'), t') \frac{1}{\sqrt{2\pi}} e^{-\frac{v(t')^2}{2}} \right]$$

which, after using the trapezoidal rule, becomes

$$f(x(t), v(t), t) = f(x(t-\Delta t), v(t-\Delta t), t-\Delta t) - \nu_c \frac{\Delta t}{2} \left[ f(x(t), v(t), t) + f(x(t-\Delta t), v(t-\Delta t), t-\Delta t) - \frac{1}{\sqrt{2\pi}} (\rho(x(t), t) e^{-\frac{v^2}{2}} - \rho(x(t-\Delta t), t-\Delta t) e^{-\frac{v(t-\Delta t)^2}{2}}) \right]$$

and

$$f(x(t), v(t), t)\{1 + \frac{\nu_c \Delta t}{2}\} = f(x(t-\Delta t), v(t-\Delta t), t-\Delta t)\{1 - \frac{\nu_c \Delta t}{2}\} + \frac{\nu_c \Delta t}{2} \frac{1}{\sqrt{2\pi}} \left[ \rho(x(t), t) e^{-\frac{v(t)^2}{2}} + \rho(x(t-\Delta t), t-\Delta t) e^{-\frac{v(t-\Delta t)^2}{2}} \right] \quad (A.3)$$

where $f(x(t), v(t), t)$ is the value of the distribution function to be calculated at the mesh point $x(t) = x$, $v(t) = v$ and $f(x(t-\Delta t), v(t-\Delta t), t-\Delta t)$ is the value of the distribution along the Vlasov characteristic at the time $t - \Delta t$ and which is calculated by the code in the way described in Chapter 4. An assumption is needed at this point, since the second term on the right-hand-side of (A.3) contains $\rho(x(t), t)$ which implies the knowledge of $f(x, v, t)$. As time proceeds, $f(x, v, t)$ should become locally closer and closer to a maxwellian; therefore, we believe that only a small error is induced by assuming $\rho(x(t), t) \approx \rho(x(t-\Delta t), t-\Delta t)$. With this assumption (A.3) gives

$$f(x(t), v(t), t) = \frac{1 - \nu_c \Delta t/2}{1 + \nu_c \Delta t/2} f(x(t-\Delta t), v(t-\Delta t), t-\Delta t) + \frac{\nu_c \Delta t}{2} \rho(x(t-\Delta t), t-\Delta t) \frac{1}{\sqrt{2\pi}} \left[ e^{-\frac{v(t)^2}{2}} + e^{-\frac{v(t-\Delta t)^2}{2}} \right] \quad (A.4)$$

In the code, after the usual steps of the splitting scheme have been completed and $f(x(t-\Delta t), v(t-\Delta t), t-\Delta t)$ has been calculated by interpolation, $f(x(t), v(t), t)$ is calculated from (A.4) and the integration proceeds with the next time step. The inclusion of the collisional term slows down the code by a factor $\sim 5$.

According to the results of linear theory, when the Krook collision model is added to Vlasov's equation, a new linear dispersion is found, which gives for the frequency $\omega \approx \omega_r + i(\gamma - \nu_c)$, where $\omega_r + i\gamma$ is the solution without collisions. Looking in another way, the continuous spectrum of the operator $L_k$ introduced in Sect. 3.3 is shifted from the real line to the line $Re\lambda = -\nu_c$. Our numerical results agree with this analysis, thus confirming the validity of our algorithm. In fig. A.1 we show the amplitude of the fundamental mode of the electric field for the symmetric bump-on-tail case, as presented in Sect. 5.3.1, with $\nu_c = 0.05$. The growth rate without collisions was $\gamma \approx 0.14$ and now we have $\gamma \approx 0.08$, in good agreement. For the same case, figs. A.2a-f show the space averaged distribution function: note how the bump is washed away completely by collisions and the shape of the distribution at large times looks approximately maxwellian. In a different simulation, with maxwellian equilibrium distribution and $\nu_c = 0.1$, we see (figs. A3a-d) how collisions oppose the formation of the phase space vortices, which build up until $t \sim 30$ and then are destroyed by collisional effects as expected.

Although, because of the numerical difficulties mentioned above, we could not determine the regions along the stability boundary corresponding to the two different regimes predicted by Crawford, we produced a few simulations for the symmetric-bump-on-tail, with parameters very close to the stability boundary, in which we effectively observed the electric field amplitude oscillating with two frequencies during the early evolution of the system.In figs. A.4a-c the fundamental mode of the electric

field amplitude is shown for three different cases with the parameter values indicated in the captions. In all cases, the electric field is damped and never rises again, as one expects in presence of collisions. Note, in fig. A.4a, that the electric field has become so small that roundoff errors significantly influence the solution. These preliminary results are certainly favourable to Crawford predictions; however, more numerical work is needed to definitively confirm his model.

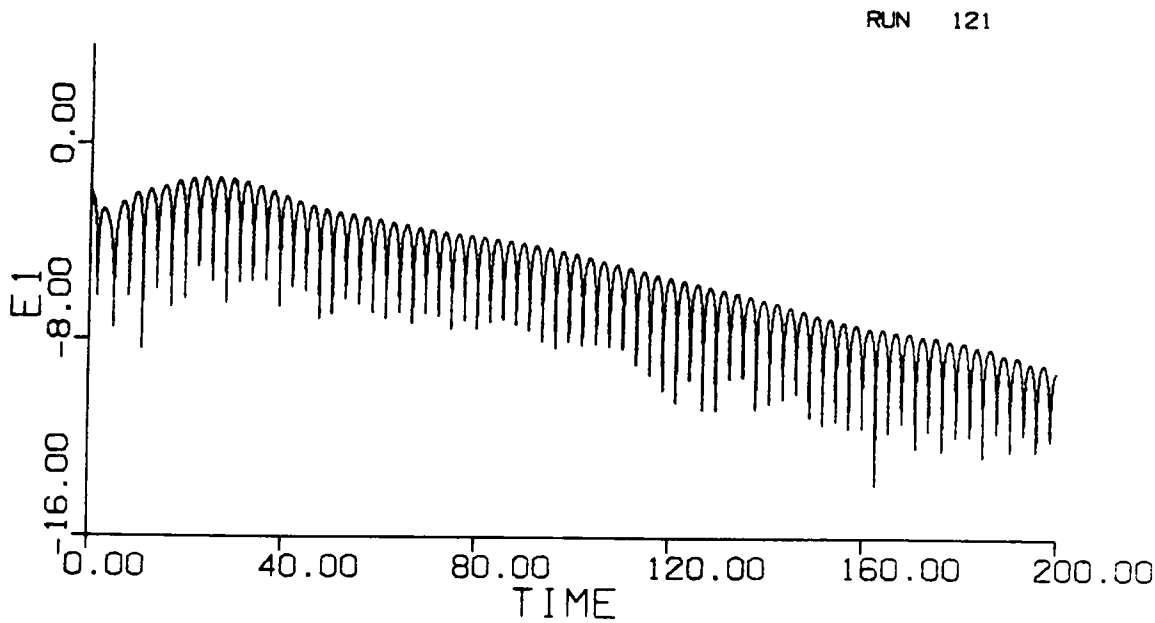


Fig. A.1 $|E_1|$ for the symmetric bump-on-tail case with collisions.

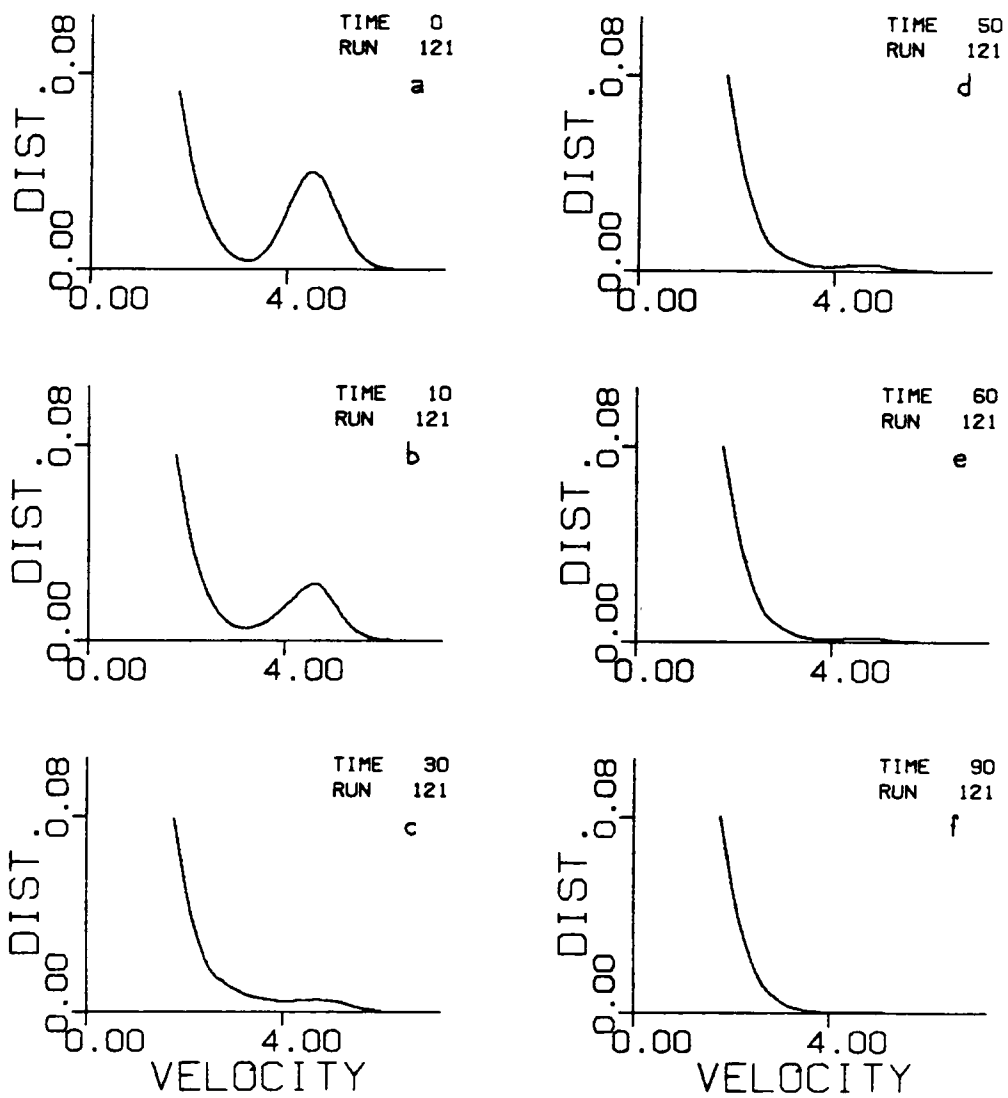


Fig. A.2 (a)-(f) Space averaged distribution for the symmetric bump-on-tail case with collisions.

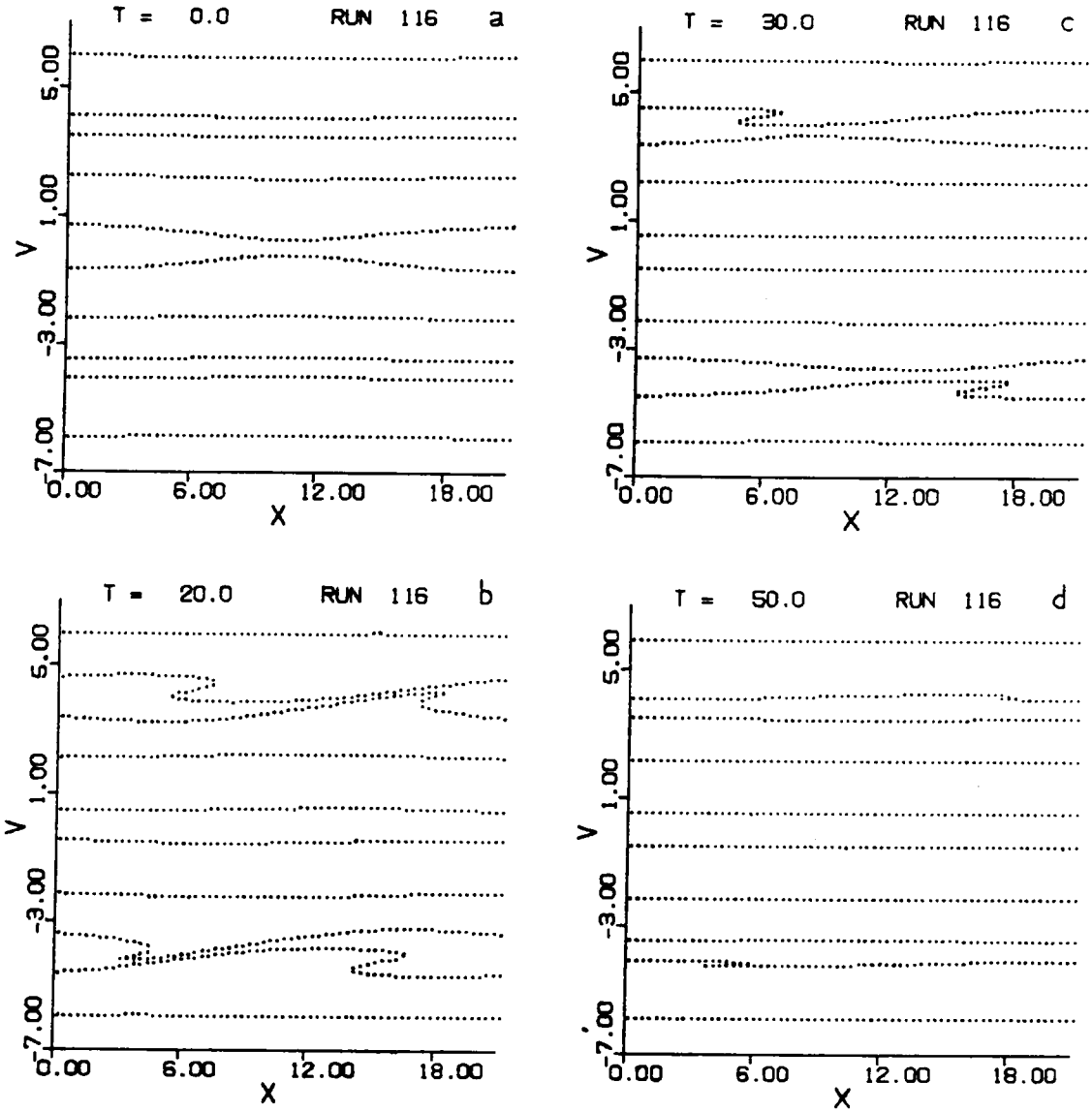


Fig. A.3 (a)-(d) Level curves for the maxwellian case with collisions.

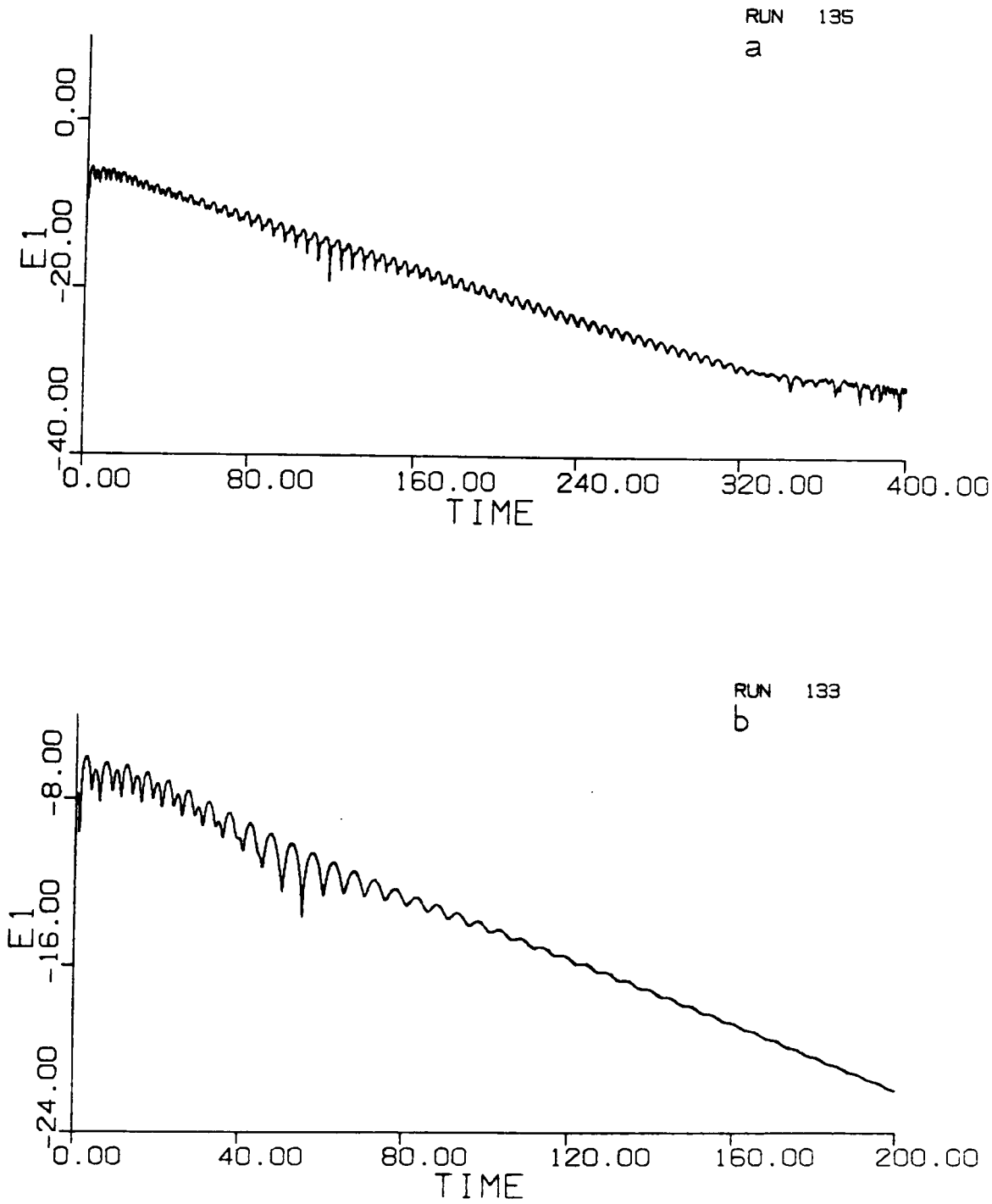


**Fig. A.4** $|E_1|$ for the symmetric bump-on-tail with collisions and $V_0 = 5.5$, $k = 0.31$ (a), $V_0 = 4.5$, $k = 0.38$ (b) and $v_t = 0.5$.

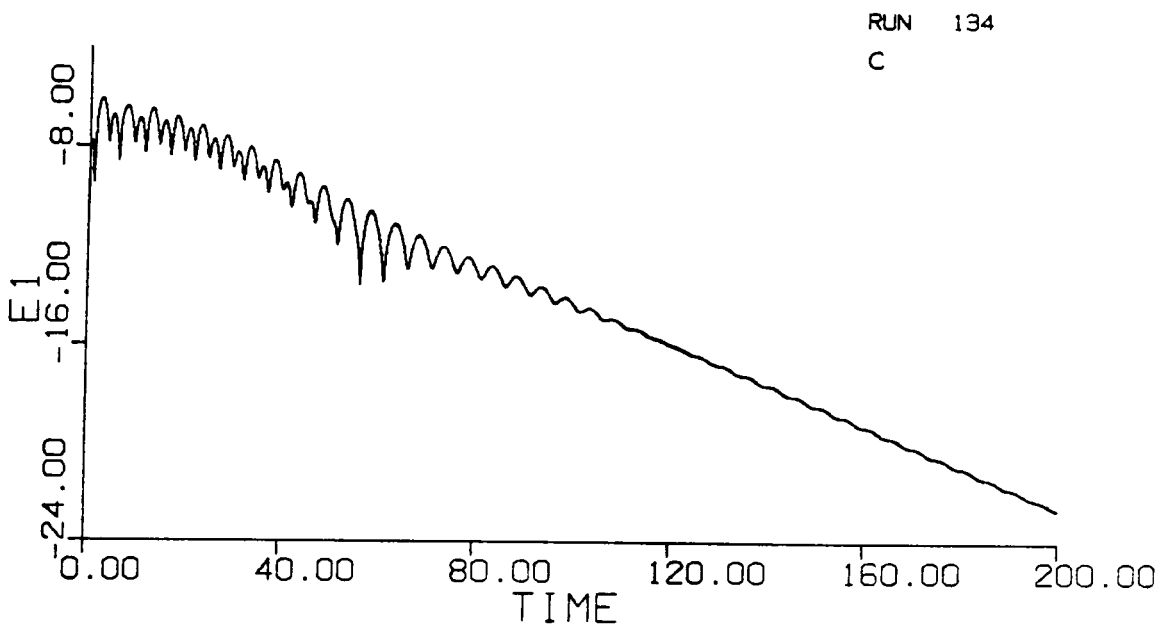


**Fig. A.4** $|E_1|$ for the symmetric bump-on-tail with collisions and $V_0 = 3.75$, $k = 0.40$ (c) and $v_t = 0.5$.

# APPENDIX B
# PROGRAM VP

```
c     ****************************************
c     * Initialize and define dimensions *
c     ****************************************
c
      dimension a(1200000)
c
      common / inte / nx,nxm1,nvm1,nvm,nvp,nvp1
      common / cnrun / nrun
c
c     ft01 : read initial distribution f(x,v)
c      open (unit=1,file='rr1',status='old')
c     ft02 : write final distribution <f(x,v)>
      open (unit=2,file='w2',status='new')
c     ft03 : read distribution <f(x,v)>
c     ft04 : symmetry test
      open (unit=4,file='w4',status='new')
c     ft05 : read data
      open (unit=5,file='rr',status='old')
c     ft06 : only for cpr file
c     ft07 : electric field amplitude
      open (unit=7,file='w7',status='new')
c     ft08 : averaged distribution
      open (unit=8,file='w8',status='new')
c     ft09 : energy and entropy
      open (unit=9,file='w9',status='new')
c     ft10 : write final distribution f(x,v)
      open (unit=10,file='w10',status='new')
c     ft11 : write f(x,v,t) at selected times
      open (unit=11,file='w11',status='new')
c     ft12 : write e(x,t) at the selected times
      open (unit=12,file='w12',status='new')
c
c     ieq = 1     maxwellian equilibrium distribution
c     ieq = 2     two stream (v**2 * maxwellian)
c     ieq = 20    two stream (sum of maxwellians)
c     ieq = 3     bump on tail (symmetric)
c     ieq = 30    bump on tail (one sided)
c     ieq = 4     continuation run with <f(x,v)>
c     ieq = 5     continuation run with f(x,v)
c     ieq = 6     cold background (symmetric)
c     ieq = 60    cold background (one sided)
c
c     icont = 0  not meant to be continued
c     icont = 1  <f(x,v)> written for continuation
c     icont = 2  f(x,v)   written for continuation
c
```

```
c     ipert = 0  f(x,v,0)=f0(v)*(1+eps*cos)
c     ipert = 1  f(x,v,0)=f0(v)*(1+eps*eps1(v)*cos)
c                (eps1(v) has to be put by hand in the code each time)
c     ipert = 2  f(x,v,0)=f0(v)*(1+eps*sin)
c
      imax = 1500000
      read (5,10) nrun
      read (5,10) nx, nv
   10 format (20x, 3i6)
      write (4,*) 'nrun = ', nrun
      write (7,*) 'nrun = ', nrun
      write (8,*) 'nrun = ', nrun
      write (9,*) 'nrun = ', nrun
      write (11,*) nrun, nx, nv
      write (12,*) nrun, nx
      nvsq = nv * nv
      nvm1 = nv - 1
      nvp1 = nv + 1
      nxp1 = nx + 1
      nxp1sq = nxp1 * nxp1
      nxnv = nxp1 * nv
      nxm1 = nx - 1
      nvm = nv / 2
      nvp = nvm + 1
      nw1 = 3 * nxm1 / 2 + 2
      nwx = 2 * nxp1
      nwv = 2 * nv
      nft = nxm1 / 2 + 1
c
         i1 = 1
         i2 = i1 + nxp1
         i3 = i2 + nv
         i4 = i3 + nv
         i5 = i4 + nxnv
         i6 = i5 + nxnv
         i7 = i6 + nxp1
         i8 = i7 + nxp1
         i9 = i8 + nxp1
        i10 = i9 + nxp1
       i11 = i10 + nxp1sq
       i12 = i11 + nvsq
       i13 = i12 + nxp1
       i14 = i13 + nv
       i15 = i14 + nxp1
       i16 = i15 + nv
       i17 = i16 + nxp1
       i18 = i17 + nv
       i19 = i18 + nv
       i20 = i19 + nv
       i21 = i20 + nv
```

```
        i22 = i21 + nv
        i23 = i22 + nv
        i24 = i23 + nv
        i25 = i24 + nv
        i26 = i25 + nv
        i27 = i26 + nxnv
        i28 = i27 + nv
        i29 = i28 + nxnv
        i30 = i29 + nwx
        i31 = i30 + nwv
        i32 = i31 + 2 * nft
        i33 = i32 + 2 * nw1
c
      if (i33.gt.imax) then
      write (6,*) 'i33 = ', i33
      write (6,*) 'imax = ', imax
c
      else
c
      call smain (a, a(i2), a(i3), a(i4), a(i5), a(i6), a(i7), a(i8),
     -            a(i9), a(i10), a(i11), a(i12), a(i13), a(i14),
     -            a(i15), a(i16), a(i17), a(i18), a(i19), a(i20),
     -            a(i21), a(i22), a(i23), a(i24), a(i25), a(i26),
     -            a(i27), a(i28), a(i29), a(i30), a(i31), a(i32),
     -            nxp1, nv, nwx, nwv, nft, nw1, nz, n11)
c
      endif
c
      stop
      end
c
c     ************************
c     * Driving subroutine*
c     ************************
c
      subroutine smain (x, v, vsq, f, fnew, e, ro, ro1, fi, bx, bv,
     -                  gx, gv, sx, sv, fx, fv, c1, c2, c3, c4,
     -                  c5, c6, c7, c8, fmold, fm, roold,
     -                  workx, workv, ft, work1,
     -                  nxp1, nv, nwx, nwv, nft, nw1, nz, n11)
c
      dimension x(nxp1), v(nv), f(nxp1,nv), fnew(nxp1,nv), e(nxp1),
     -          ro(nxp1), fx(nxp1), fv(nv), fi(nxp1),
     -          ro1(nxp1), bx(nxp1,nxp1), bv(nv,nv), gx(nxp1), gv(nv),
     -          sx(nxp1), sv(nv), c1(nv), c2(nv), c3(nv), c4(nv),
     -          c5(nv), c6(nv), c7(nv), c8(nv), fmold(nxp1,nv),
     -          fm(nv), roold(nxp1,nv),
     -          workx(nwx), workv(nwv)
      dimension tlevc(100)
```

```
      complex ft(nft), work1(nw1)
c
      common / cmesh / xi,xf,dx,dx3,dtmdx,dxdv,vmax,dv,dv3
      common / inte / nx,nxm1,nvm1,nvm,nvp,nvp1
      common / cwave / eps, rk, mode
      common / iflags / ieq, ipert, ielf, icont, icoll, imaxw
      common / cpert / vpert, vperth
      common / const / sq2pi, pi2, pi
      common / cfour / cft, cft1
      common / cjump / jumpm
      common / caver / istep
      common / times / ti, tf, dt
      common / cnrun / nrun
      common / cshift / vt, vtsq, v0, vdlt, zc, zp, zb
      common / campl / ampl0,ampl1, ampl2, ampl3, mode1, mode2, mode3
      common / coll / cnuc, coll1, coll2
      common / cmaxw / curr0
c
c     ************************
c     * Read initial data *
c     ************************
c
      read (5,100) ti, tf, dt
      read (5,100) xi, vmax
      read (5,200) mode, rk, eps
      read (5,300) ieq, ipert, icont, icoll, imaxw
      if (ieq.eq.3.or.ieq.eq.30) read (5,100) vt, v0, zp, zb
      if (ieq.eq.20) read (5,100) vt, v0, zp
      if (ieq.eq.6.or.ieq.eq.60) read (5,302) zc, zb, vt, v0, vdlt
      read (5,100) cnuc
      read (5,100) vpert, vperth
      read (5,200) istep, dtprt, dttest
      read (5,201) nt1, nt2, dtlevc
      ntlevc = nt1 * nt2
      read (5,301) (tlevc(i), i=1,ntlevc,nt2)
  100 format (20x, 4e12.0)
  200 format (20x, i6, 3e12.0)
  201 format (20x, 2i6, e12.0)
  300 format (20x, 5i6)
  301 format (20x, 10f6.1)
  302 format (20x, 5f8.4, e12.0)
c
      do 600 i = 1,nt1
      i1 = nt2 * (i-1)
      i1m1 = i1 - 1
      do 610 j = 2,nt2
      tlevc(i1+j) = tlevc(i1m1+j) + dtlevc
  610 continue
  600 continue
      tlevc(ntlevc+1) = tf + 1.0
```

```
      write (11,*) ntlevc
c
      ielf = 1
      ilevc = 1
      pi = 4.0 * atan(1.0)
      pi2 = 2.0 * pi
      sq2pi = sqrt(pi2)
      xf = pi2 * mode/ rk
      cft1 = mode / rk
      cft = 0.5 * cft1 / nxm1
c
      if (ieq.eq.3.or.ieq.eq.30.or.ieq.eq.20.or.ieq.eq.6.or.ieq.eq.60)
     -    vtsq = vt * vt
c
      mode1 = mode + 1
      mode2 = 2 * mode + 1
      mode3 = 3 * mode + 1
c     **********************
c     * Start time cycle *
c     **********************
c
      t = ti
      tprint = ti + dtprt
      ttest = ti + dttest
c
      call defb (bx, bv, workx, workv, nxp1, nv, nwx, nwv)
c
      call start (x, v, vsq, f, fx, fv, c1, c2, c3, c4,
     -            c5, c6, c7, c8, nxp1, nv)
      do 700 j = 1,nv
      fm(j) = fmaxw(v(j))
  700 continue
      call aver (f, v, t, 0, nxp1, nv)
      call dens (f, ro, nxp1, nv)
      if (imaxw.ne.0) call curr (f, v, curr0, nxp1, nv)
      call elf (e, ro, ro1, fi, ft, work1, t, nxp1, nw1, nft)
      if (tlevc(1).lt.dt) then
      call slevc (f, e, t, nxp1, nv)
      ilevc = ilevc + 1
      else
      continue
      endif
      call energy (vsq, f, e, w0, wt, we, 1, nxp1, nv)
      call entropy (f, entr0, nxp1, nv)
      dw = 0.0
      dentr = 0.0
      write (9,510) t, wt, we, w0, entr0, dw, dentr
      write (7,500) t, ampl0, ampl1, ampl2, ampl3, we
  500 format (1x, 6(1pe12.4, 1x))
```

```
      call symm (f, e, ro, t, nxp1, nv)
c
    1 continue
      t = t + dt
      if (t.le.tf) go to 3
      if (icont.eq.1) call aver (f, v, t, 1, nxp1, nv)
      if (icont.eq.0) return
      do 400 i = 1,nxp1
      do 410 j = 1,nv
      write (10,*) f(i,j)
  410 continue
  400 continue
      return
    3 continue
      if (icoll.eq.0) go to 5
      call dens1 (ro, roold, gx, bx, sx, c5, c6, c7, c8,
     -                  nxp1, nv)
    5 continue
c     ****************************
c     * First horizontal shift *
c     ****************************

      call shiftx (f, fnew, gx, bx, sx, c1, c2, c3, c4, nxp1, nv)
c
      do 10 i = 1,nxp1
      do 20 j = 1,nv
      f(i,j) = fnew(i,j)
   20 continue
   10 continue
c
      call dens (f, ro, nxp1, nv)
      call elf (e, ro, ro1, fi, ft, work1, t, nxp1, nw1, nft)
      call energy (vsq, f, e, w0, wt, we, 0, nxp1, nv)
      write (7,500) t, amp10, amp11, amp12, amp13, we
c
c     ********************
c     * Vertical shift *
c     ********************
c
      call shiftv (v, f, fnew, fmold, e, gv, bv, sv, nxp1, nv)
c
      do 30 i = 1,nxp1
      do 40 j = 1,nv
      f(i,j) = fnew(i,j)
   40 continue
   30 continue
c     ***************************
c     * Final vertical shift *
c     ***************************
c
```

```
      call shiftx (f, fnew, gx, bx, sx, c1, c2, c3, c4, nxp1, nv)
      call newf (f, fnew, fmold, fm, ro, roold, nxp1, nv)
c
      if (t.lt.tlevc(ilevc)) go to 4
      call slevc (f, e, t, nxp1, nv)
      ilevc = ilevc + 1
    4 if (t.lt.tprint) go to 2
      call aver (f, v, t, 0, nxp1, nv)
      tprint = tprint + dtprt
    2 if (t.lt.ttest) go to 1
      call dens (f, ro, nxp1, nv)
      call elf (e, ro, ro1, fi, ft, work1, t, nxp1, nw1, nft)
      call energy (vsq, f, e, w, wt, we, 1, nxp1, nv)
      call entropy (f, entr, nxp1, nv)
      dw = abs ((w-w0) / w0)
      dentr = abs ((entr-entr0) / entr0)
      write (9,510) t, wt, we, w, entr, dw, dentr
  510 format (1x, 7(1pe12.4, 1x))
      call symm (f, e, ro, t, nxp1, nv)
      ttest = ttest + dttest
c
      go to 1
      end
c
c     ****************************************
c     * Calculation of the electric field *
c     ****************************************
c
      subroutine elf (e, ro, ro1, fi, ft, work1, t, nxp1, nw1, nft)
c
      dimension e(nxp1), ro(nxp1), ro1(nxp1), fi(nxp1)
      complex ft(nft), work1(nw1)
c
      common / cmesh / xi,xf,dx,dx3,dtmdx,dxdv,vmax,dv,dv3
      common / inte / nx,nxm1,nvm1,nvm,nvp,nvp1
      common / cwave / eps, rk, mode
      common / iflags / ieq, ipert, ielf, icont, icoll, imaxw
      common / cfour / cft, cft1
      common / campl / ampl0,ampl1, ampl2, ampl3, mode1, mode2, mode3
      common / cmaxw / curr0
c
      e(1) = 0.0
      if (ielf.eq.0) then
c
      do 10 i = 2,nxm1
      im1 = i - 1
      e(i) = e(im1) + dx * (1.0 - 0.5*(ro(im1)+ro(i)))
   10 continue
      e(nx) = 0.0
```

```
      e(nxp1) = e(2)
c
      else
c
      do 20 i = 1,nxm1
      ro1(i) = 1.0 - ro(i)
   20 continue
      call rcfft2 (1, -1, nxm1, ro1, work1, ft)
      call rcfft2 (0, -1, nxm1, ro1, work1, ft)
      do 30 i = 2,nft
      ft(i) = (0.0,-1.0) * cft * ft(i) / (i-1)
   30 continue
      ft(1) = 0.0
      if (imaxw.ne.0) ft(1) = curr0 * sin(t)
      call crfft2 (1, 1, nxm1, ft, work1, e)
      call crfft2 (0, 1, nxm1, ft, work1, e)
      e(nx) = e(1)
      e(nxp1) = e(2)
      imax = isamax (nxp1, e, 1)
      amp10 = abs (e(imax))
      amp11 = 2.0 * abs (ft(mode1))
      amp12 = 2.0 * abs (ft(mode2))
      amp13 = 2.0 * abs (ft(mode3))
c
c      do 40 i = 2,nft
c      ft(i) = (0.0,1.0) * cft1 * ft(i) / (i-1)
c   40 continue
c      call crfft2 (1, 1, nxm1, ft, work1, fi)
c      call crfft2 (0, 1, nxm1, ft, work1, fi)
c      fi(nx) = fi(1)
c      fi(nxp1) = fi(2)
c
      endif
c
c      do 600 i = 1,nxp1
c      write (6,*) i, e(i), fi(i)
c  600 continue
      return
      end
c
c     ********************************
c     * Calculation of the density *
c     ********************************
c
      subroutine dens (f, ro, nxp1, nv)
c
      dimension f(nxp1,nv), ro(nxp1)
c
      common / cmesh / xi,xf,dx,dx3,dtmdx,dxdv,vmax,dv,dv3
```

```
      common / inte / nx,nxm1,nvm1,nvm,nvp,nvp1
c
      do 10 i = 1,nxm1
      sum1 = 0.0
      sum2 = 0.0
      do 20 j = 4,nvm1,3
      sum1 = sum1 + f(i,j)
   20 continue
      do 30 j = 2,nvm1,3
      sum2 = sum2 + f(i,j) + f(i,j+1)
   30 continue
      ro(i) = dv * (6.0*sum1 + 9.0*sum2) / 8.0
   10 continue
c
      ro(nx) = ro(1)
      ro(nxp1) = ro(2)
c
      return
      end
c
c     ******************************
c     * Initializing subroutine *
c     ******************************
c
      subroutine start (x, v, vsq, f, fx, fv, c1, c2, c3, c4,
     -                  c5, c6, c7, c8, nxp1, nv)
c
      dimension x(nxp1), v(nv), vsq(nv), f(nxp1, nv),
     -          fx(nxp1), fv(nv), c1(nv), c2(nv), c3(nv), c4(nv),
     -          c5(nv), c6(nv), c7(nv), c8(nv)
c
      common / cmesh / xi,xf,dx,dx3,dtmdx,dxdv,vmax,dv,dv3
      common / inte / nx,nxm1,nvm1,nvm,nvp,nvp1
      common / cwave / eps, rk, mode
      common / iflags / ieq, ipert, ielf, icont, icoll, imaxw
      common / const / sq2pi, pi2, pi
      common / times / ti, tf, dt
      common / cnrun / nrun
      common / cshift / vt, vtsq, v0, vdlt, zc, zp, zb
      common / coll / cnuc, coll1, coll2
c
      nvmm2 = nvm - 2
      x(1) = xi
      dx = (xf - xi) / nxm1
      dx3 = 3.0 / dx
      dtmdx = 0.5 * dt / dx
      v(1) = -vmax
      v(nv) = vmax
      dv = 2.0 * vmax / nvm1
      dvm = 0.5 * dv
```

```
      v(nvm) = -dvm
      v(nvp) = dvm
      dxdv = dx * dv
      dv3 = 3.0 / dv
      trec = pi2 / (rk*dv)
c
      if (icoll.ne.0) then
      coll0 = 0.5 * dt * cnuc
      coll0p1 = coll0 + 1.0
      coll1 = (1.0 - coll0) / coll0p1
      coll2 = coll0 / coll0p1
      else
      continue
      endif
c
      write (7,100) ti, tf, dt, xi, xf, nx, dx, vmax, nv, dv,
     -              mode, rk, eps, ieq, ipert, trec
      if (icoll.ne.0) write (7,101) cnuc
  100 format (//1x,'ti = ',1pe12.4,
     -          4x,'tf = ',1pe12.4, 4x,'dt = ',1pe12.4,
     -        //1x,'xi = ',1pe12.4, 4x,'xf = ',1pe12.4, 4x,'nx = ',i4,
     -          4x,'dx = ',1pe12.4,
     -        //1x,'vmax = ',1pe12.4, 4x, 'nv = ',i6, 4x,
     -             'dv = ',1pe12.4,
     -        //1x,'mode = ',i2, 4x,'k = ',1pe12.4, 4x,
     -             'eps = ',1pe12.4,
     -        //1x,'i equil. = ',i2, 4x, 'i pert. = ',i2,
     -        // 1x,'rec. time = ',1pe12.4//)
  101 format (1x,'coll. freq. = ', 1pe12.4//)
c
      do 10 i = 2,nxp1
      x(i) = x(i-1) + dx
   10 continue
      x(nx) = xf
c     v(1) = - vmax
c     v(nv) = vmax
c     do 20 j = 2, nvm1
c     v(j) = v(j-1) + dv
c  20 continue
c     v(nvp) = 0.0
      do 20 j = 1,nvmm2
      v(nvp+j) = v(nvm+j) + dv
      v(nvm-j) = v(nvp-j) - dv
   20 continue
      v(1) = - vmax
      v(nv) = vmax
      do 25 j = 1,nv
      vsq(j) = v(j) * v(j)
   25 continue
c
```

```
      do 30 i = 1,nxm1
      xx = x(i)
      if (ipert.ne.2) fx(i) = eps * cos(rk*xx)
      if (ipert.eq.2) fx(i) = eps * sin(rk*xx)
      if (ipert.ne.1) go to 30
      do 29 j = 2,nvm1
      f(i,j) = pert(v(j)) * fx(i)
   29 continue
   30 continue
c
      if (ieq.eq.1) then
      do 40 j = 2,nvm1
      fv(j) = exp(-0.5*vsq(j)) / sq2pi
   40 continue
      go to 1000
      else
      continue
      endif
c
      if (ieq.eq.2) then
      do 50 j = 2,nvm1
      fv(j) = vsq(j) * exp(-0.5*vsq(j)) / sq2pi
   50 continue
      go to 1000
      else
      continue
      endif
c
      if (ieq.eq.3) then
      do 60 j = 2,nvm1
      v1 = v(j) - v0
      v2 = v(j) + v0
      v1sq = v1 * v1
      v2sq = v2 * v2
      x1 = 0.5 * v1sq / vtsq
      x2 = 0.5 * v2sq / vtsq
      fp = zp * exp(-0.5*vsq(j)) / sq2pi
      fb = zb * (exp(-x1) + exp(-x2)) / sq2pi
      fv(j) = fp + fb
   60 continue
      go to 1000
      else
      continue
      endif
c
      if (ieq.eq.20) then
      do 400 j = 2,nvm1
      v1 = v(j) - v0
      v2 = v(j) + v0
      v1sq = v1 * v1
```

```
      v2sq = v2 * v2
      x1 = 0.5 * v1sq / vtsq
      x2 = 0.5 * v2sq / vtsq
      fv(j) = zp * (exp(-x1) + exp(-x2)) / sq2pi
  400 continue
      go to 1000
      else
      continue
      endif
c
      if (ieq.eq.30) then
      do 500 j = 1,nv
      v1 = v(j) - v0
      v1sq = v1 * v1
      x1 = 0.5 * v1sq / vtsq
      fp = zp * exp(-0.5*vsq(j)) / sq2pi
      fb = zb * exp(-x1) / sq2pi
      fv(j) = fp + fb
  500 continue
      go to 1000
      else
      continue
      endif
c
      if (ieq.eq.60) then
      do 600 j = 2,nvm1
      vd = v(j) / vdlt
      x1 = (v(j) - v0) / vt
      fc = zc * exp(- 0.5 * vd * vd) / vdlt
      fp = (1.0 - zb) * exp(- 0.5 * vsq(j))
      fb = zb * exp(- 0.5 * x1 * x1) / vt
      fv(j) = (fc + (1.0-zc)*(fp+fb)) / sq2pi
  600 continue
      go to 1000
      else
      continue
      endif
c
      if (ieq.eq.6) then
      do 700 j = 2,nvm1
  700 continue
      go to 1000
      else
      continue
      endif
c
      if (ieq.eq.4) then
      do 110 j = 1,nv
      read (3,*) vvv, fv(j)
  110 continue
```

```
      go to 1000
      else
      continue
      endif
c
 1000 if (ieq.ne.5) then
c
      do 120 i = 1,nxm1
      if (ipert.ne.1) then
      do 130 j = 2,nvm1
      f(i,j) = fv(j) * (1.0 + fx(i))
  130 continue
      else
      do 135 j = 2,nvm1
      f(i,j) = fv(j) * (1.0 + f(i,j))
  135 continue
      endif
      f(i,1) = 0.0
      f(i,nv) = 0.0
  120 continue
c
      else
c
      do 200 i = 1,nxp1
      do 210 j = 1,nv
      read (1,*) f(i,j)
  210 continue
  200 continue
c
c      do 300 i = 1,nxm1
c      do 310 j = 1,nv
c      f(i,j) = f(i,j) * (1.0 + fx(i))
c  310 continue
c  300 continue
c
      endif
c
      do 70 j = 1,nv
      f(nx,j) = f(1,j)
      f(nxp1,j) = f(2,j)
   70 continue
c
      do 80 j = 1,nvm
      dlt = - v(j) * dtmdx
      dlt1 = 1.0 - dlt
      dltsq = dlt * dlt
      dlt1sq = dlt1 * dlt1
      rdlt = 2.0 * dlt
      rdlt1 = 1.0 - rdlt
      rdltsq = rdlt * rdlt
```

```
      rdlt1sq = rdlt1 * rdlt1
      c1(j) = dlt * dlt1sq * dx
      c2(j) = dlt1 * dltsq * dx
      c3(j) = dlt1sq * (1.0 + 2.0*dlt)
      c4(j) = dltsq * (1.0 + 2.0*dlt1)
      c5(j) = rdlt * rdlt1sq * dx
      c6(j) = rdlt1 * rdltsq * dx
      c7(j) = rdlt1sq * (1.0 + 2.0*rdlt)
      c8(j) = rdltsq * (1.0 + 2.0*rdlt1)
   80 continue
c
      do 90 j = nvp,nv
      dlt = - v(j) * dtmdx
      dlt1 = 1.0 + dlt
      dlt1sq = dlt1 * dlt1
      dltsq = dlt * dlt
      rdlt = 2.0 * dlt
      rdlt1 = 1.0 + rdlt
      rdlt1sq = rdlt1 * rdlt1
      rdltsq = rdlt * rdlt
      c1(j) = dltsq * dlt1 * dx
      c2(j) = dlt1sq * dlt * dx
      c3(j) = dltsq * (1.0 + 2.0*dlt1)
      c4(j) = dlt1sq * (1.0 - 2.0*dlt)
      c5(j) = rdltsq * rdlt1 * dx
      c6(j) = rdlt1sq * rdlt * dx
      c7(j) = rdltsq * (1.0 + 2.0*rdlt1)
      c8(j) = rdlt1sq * (1.0 - 2.0*rdlt)
   90 continue
      return
      end
c
c     ****************************************
c     * Define initial spline coefficients *
c     ****************************************
c
      subroutine defb (bx, bv, workx, workv, nxp1, nv, nwx, nwv)
c
      dimension bx(nxp1,nxp1), bv(nv,nv), workx(nwx), workv(nwv)
c
      common / inte / nx,nxm1,nvm1,nvm,nvp,nvp1
c
      do 10 i = 1,nxp1
      do 20 j = 1,nxp1
      bx(i,j) = 0.0
   20 continue
   10 continue
      do 30 i = 1,nv
      do 40 j = 1,nv
      bv(i,j) = 0.0
```

```
   40 continue
   30 continue
c
      do 50 i = 2,nx
      ipl = i + 1
      iml = i - 1
      bx(i,ipl) = 1.0
      bx(i,iml) = 1.0
      bx(i,i) = 4.0
   50 continue
      bx(1,1) = 1.0
      bx(1,nx) = - 1.0
      bx(nxpl,2) = 1.0
      bx(nxpl,nxpl) = - 1.0
c
      do 60 i = 2,nvml
      ipl = i + 1
      iml = i - 1
      bv(i,ipl) = 1.0
      bv(i,iml) = 1.0
      bv(i,i) = 4.0
   60 continue
      bv(1,1) = 1.0
      bv(nv,nv) = 1.0
c
      call minv (bx, nxpl, nxpl, workx, detx, 1.0e-16, 0, 1)
      call minv (bv, nv, nv, workv, detv, 1.0e-16, 0, 1)
c
      return
      end
c
c     ************************************************
c     * One-dimensional spline interpolation in v *
c     ************************************************

      subroutine shiftv (v, f, fnew, fmold, e, gv, bv, sv, nxpl, nv)
c
      dimension f(nxpl,nv), fnew(nxpl,nv), e(nxpl), gv(nv),
     -          bv(nv,nv), sv(nv), fmold(nxpl,nv), v(nv)
c
      common / cmesh / xi,xf,dx,dx3,dtmdx,dxdv,vmax,dv,dv3
      common / inte / nx,nxml,nvml,nvm,nvp,nvpl
      common / times / ti, tf, dt
      common / cjump / jumpm
      common / iflags / ieq, ipert, ielf, icont, icoll, imaxw
      common / coll / cnuc, coll1, coll2
c
      jumpm = 0
c
```

```
      do 10 i = 2,nx
c
      do 15 j = 2,nvm1
      jp1 = j + 1
      jm1 = j - 1
      gv(j) = dv3 * (f(i,jp1)-f(i,jm1))
   15 continue
      gv(1) = 0.0
      gv(nv) = 0.0
      call mxv (bv, nv, gv, nv, sv)
c
      edt = e(i) * dt
c
      if (icoll.ne.0) then
      do 70 j = 1,nv
      vold = v(j) + edt
      fmold(i,j) = fmaxw (vold)
      if (abs(vold).gt.vmax) fmold(i,j)  = 0.0
   70 continue
      else
      continue
      endif
c
      edtdv = edt / dv
c
      if (edt.gt.0.0) then
c
      jump = edtdv
      jmax = nvm1 - jump
      jmaxp1 = jmax + 1
      dlt = edtdv - jump
      dltsq = dlt * dlt
      dlt1 = 1.0 - dlt
      dlt1sq = dlt1 * dlt1
      cc1 = dlt * dlt1sq * dv
      cc2 = dlt1 * dltsq * dv
      cc3 = dlt1sq * (1.0 + 2.0*dlt)
      cc4 = dltsq * (1.0 + 2.0*dlt1)
c
      do 20 j = 2,jmax
      jj = j + jump
      jjp1 = jj + 1
      fnew(i,j) = cc1*sv(jj) - cc2*sv(jjp1) +
     -            cc3*f(i,jj) + cc4*f(i,jjp1)
   20 continue
      do 30 j = jmaxp1,nv
      fnew(i,j) = 0.0
   30 continue
      fnew(i,1) = 0.0
c
```

```
      else
c
      jump = - edtdv
      jmin = 2 + jump
      jminm1 = jmin - 1
      dlt = edtdv + jump
      dlt1 = 1.0 + dlt
      dlt1sq = dlt1 * dlt1
      dltsq = dlt * dlt
      cc1 = dlt1 * dltsq * dv
      cc2 = dlt1sq * dlt * dv
      cc3 = dltsq * (1.0 + 2.0*dlt1)
      cc4 = dlt1sq * (1.0 - 2.0*dlt)
      do 40 j = jmin,nvm1
      jj = j - jump
      jjm1 = jj - 1
      fnew(i,j) = cc1*sv(jjm1) + cc2*sv(jj) +
     -            cc3*f(i,jjm1) + cc4*f(i,jj)
   40 continue
      do 50 j = 1,jminm1
      fnew(i,j) = 0.0
   50 continue
      fnew(i,nv) = 0.0
c
      endif
c
      if (jump.gt.jumpm) jumpm = jump
c
   10 continue
c
      do 60 j = 1,nv
      fnew(1,j) = fnew(nx,j)
      fnew(nxp1,j) = fnew(2,j)
      if (icoll.eq.0) go to 60
      fmold(1,j) = fmold(nx,j)
      fmold(nxp1,j) = fmold(2,j)
   60 continue
c
      return
      end
c
c     ************************************************
c     * One-dimensional spline interpolation in x *
c     ************************************************

      subroutine shiftx (f, fnew, gx, bx, sx, c1, c2, c3, c4, nxp1, nv)
c
      dimension f(nxp1,nv), fnew(nxp1,nv), gx(nxp1), bx(nxp1,nxp1),
     -          sx(nxp1), c1(nv), c2(nv), c3(nv), c4(nv)
c
```

```
      common / cmesh / xi,xf,dx,dx3,dtmdx,dxdv,vmax,dv,dv3
      common / inte / nx,nxm1,nvm1,nvm,nvp,nvp1
c
      do 10 j = 2,nvm
      do 20 i = 2,nx
      ip1 = i + 1
      im1 = i - 1
      gx(i) = dx3 * (f(ip1,j)-f(im1,j))
   20 continue
      gx(1) = 0.0
      gx(nxp1) = 0.0
      call mxv (bx, nxp1, gx, nxp1, sx)
      do 30 i = 2,nx
      ip1 = i + 1
      fnew(i,j) = c1(j)*sx(i) - c2(j)*sx(ip1) +
     -            c3(j)*f(i,j) + c4(j)*f(ip1,j)
   30 continue
      fnew(1,j) = fnew(nx,j)
      fnew(nxp1,j) = fnew(2,j)
   10 continue
c
      do 40 j = nvp,nvm1
      do 50 i = 2,nx
      ip1 = i + 1
      im1 = i - 1
      gx(i) = dx3 * (f(ip1,j)-f(im1,j))
   50 continue
      gx(1) = 0.0
      gx(nxp1) = 0.0
      call mxv (bx, nxp1, gx, nxp1, sx)
      do 60 i = 2,nx
      im1 = i - 1
      fnew(i,j) = c1(j)*sx(im1) + c2(j)*sx(i) +
     -            c3(j)*f(im1,j) + c4(j)*f(i,j)
   60 continue
      fnew(1,j) = fnew(nx,j)
      fnew(nxp1,j) = fnew(2,j)
   40 continue
c
      do 70 i = 1,nxp1
      fnew(i,1) = 0.0
      fnew(i,nv) = 0.0
   70 continue
c
      return
      end
c
c     ********************************************
c     * Calculation of electric field energy *
c     ********************************************
```

```
      subroutine energy (vsq, f, e, w, wt, we, ii, nxp1, nv)
c
      dimension vsq(nv), f(nxp1,nv), e(nxp1)
c
      common / cmesh / xi,xf,dx,dx3,dtmdx,dxdv,vmax,dv,dv3
      common / inte / nx,nxm1,nvm1,nvm,nvp,nvp1
c
c
      we = 0.0
      do 30 i = 2,nxm1
      we = we + e(i)*e(i)
   30 continue
      we = dx * we
c
      if (ii.eq.0) return
c
      wt = 0.0
      do 10 i = 1,nxm1
      sum = 0.0
      do 20 j = 2,nvm1
      sum = sum + vsq(j)*f(i,j)
   20 continue
      wt = wt + sum
   10 continue
      wt = dxdv * wt
c
      w = wt + we
c
      return
      end
c
c     ***********************************
c     * Calculation of total entropy *
c     ***********************************
c
      subroutine entropy (f, entr, nxp1, nv)
c
      dimension f(nxp1,nv)
c
      common / cmesh / xi,xf,dx,dx3,dtmdx,dxdv,vmax,dv,dv3
      common / inte / nx,nxm1,nvm1,nvm,nvp,nvp1
c
      entr = 0.0
      do 10 i = 1,nxm1
      sum = 0.0
      do 20 j = 2,nvm1
      if (f(i,j).ne.0.0) sum = sum - f(i,j)*alog(abs(f(i,j)))
   20 continue
      entr = entr + sum
```

```
   10 continue
      entr = dxdv * entr
c
      return
      end
c
c     ********************************************************
c     * Calculation of the space averaged distribution *
c     ********************************************************
c
      subroutine aver (f, v, t, iaver, nxp1, nv)
      dimension f(nxp1, nv), v(nv)
c
      common / inte / nx,nxm1,nvm1,nvm,nvp,nvp1
      common / caver / istep
c
      if (iaver.eq.1) go to 50
      write (8,100) t
  100 format (///1x,'averaged distribution at t = ',1pe12.4//)
c
      do 10 j = nvp,nv,istep
      j1 = nvp1 - j
      sum1 = 0.0
      sum = 0.0
      do 20 i = 1,nxm1
      sum = sum + f(i,j)
      sum1 = sum1 + f(i,j1)
   20 continue
      fav = sum / nxm1
      fav1 = sum1 / nxm1
      write (8,110) v(j), fav, fav1
  110 format (1x, 3(1pe12.4, 1x))
   10 continue
      return
c
   50 continue
c
      do 30 j = 1,nv
      sum = 0.0
      do 40 i = 1,nxm1
      sum = sum + f(i,j)
   40 continue
      fav = sum / nxm1
      write (2,*) v(j), fav
   30 continue
      return
c
      end
c
c     ********************
```

```
c     * Symmetry check *
c     ********************

      subroutine symm (f, e, ro, t, nxp1, nv)
c
      dimension f(nxp1, nv), e(nxp1), ro(nxp1)
c
      common / inte / nx,nxm1,nvm1,nvm,nvp,nvp1
c
      write (4,100) t
  100 format (///1x, 'symmetry check at t = ',1pe12.4//
     -        1x, 'electric field'//)
c
      do 10 i = 1,nx
      i1 = nxp1 - i
      asymm = 0.0
      if (e(i).ne.0.0) asymm = abs ((e(i) + e(i1)) / e(i))
      write (4,110) i, e(i), e(i1), asymm
  110 format (1x, i6, 3(1x, 1pe12.4))
   10 continue
c
      write (4,120)
  120 format (//1x,'density'//)
      do 15 i = 1,nx
      i1 = nxp1 - i
      asymm = 0.0
      asymm = abs ((ro(i) - ro(i1)) / ro(i))
      write (4,110) i, ro(i), ro(i1), asymm
   15 continue
c
      asmax = 0.0
      imax = 0
      jmax = 0
      do 20 i = 1,nx
      i1 = nxp1 - i
      do 30 j = 2,nvm
      j1 = nvp1 - j
      asymm = abs ((f(i,j)-f(i1,j1)) / f(i,j))
      if (asymm.lt.asmax) go to 30
      asmax = asymm
      imax = i
      jmax = j
   30 continue
   20 continue
c
      write (4,130) asmax, imax, jmax
  130 format (/1x, 'max. asymmetry of the distr. = ',1pe12.4,4x,
     -        'at i = ',i6, 4x,'j = ',i6)
c
      return
```

```
      end
c
c     ******************************************************
c     * Definition of velocity dependent perturbations *
c     ******************************************************
c
      function pert (v)
      common / const / sq2pi, pi2, pi
      common / iflags / ieq, ipert, ielf, icont, icoll, imaxw
      common / cshift / vt, vtsq, v0, vdlt, zc, zp, zb
      common / cpert / vpert, vperth
      x = (v - vpert)
      pert = 1.0 / (x*x + vperth*vperth)
      end
c
c     ******************************************************
c     * Output routine for the distribution function *
c     ******************************************************
c
      subroutine slevc (f, e, t, nxpl, nv)
c
      dimension f(nxpl,nv), e(nxpl)
      common / inte / nx,nxml,nvml,nvm,nvp,nvpl
c
      write (11,*) t
      write (12,*) t
c
      do 40 i = 1,nx
      write (12,*) e(i)
   40 continue
      do 50 i = 1,nx
      write (11,*) (f(i,j),j=1,nv)
   50 continue
c
      return
      end
c
c     ******************************************************
c     * Calculation of the density with collisions *
c     ******************************************************
c
      subroutine densl (ro, roold, gx, bx, sx, c5, c6, c7, c8,
     -                  nxpl, nv)
c
      dimension ro(nxpl), roold(nxpl,nv), gx(nxpl), bx(nxpl,nxpl),
     -          sx(nxpl), c5(nv), c6(nv), c7(nv), c8(nv)
      common / cmesh / xi,xf,dx,dx3,dtmdx,dxdv,vmax,dv,dv3
      common / inte / nx,nxml,nvml,nvm,nvp,nvpl
c
      do 10 j = 2,nvm
```

```
      do 20 i = 2,nx
      ip1 = i + 1
      im1 = i - 1
      gx(i) = dx3 * (ro(ip1)-ro(im1))
   20 continue
      gx(1) = 0.0
      gx(nxp1) = 0.0
      call mxv (bx, nxp1, gx, nxp1, sx)
      do 30 i = 2,nx
      ip1 = i + 1
      roold(i,j) = c5(j)*sx(i) - c6(j)*sx(ip1) +
     -             c7(j)*ro(i) + c8(j)*ro(ip1)
   30 continue
      roold(1,j) = roold(nx,j)
      roold(nxp1,j) = roold(2,j)
   10 continue
c
      do 40 j = nvp,nvm1
      do 50 i = 2,nx
      ip1 = i + 1
      im1 = i - 1
      gx(i) = dx3 * (ro(ip1)-ro(im1))
   50 continue
      gx(1) = 0.0
      gx(nxp1) = 0.0
      call mxv (bx, nxp1, gx, nxp1, sx)
      do 60 i = 2,nx
      im1 = i - 1
      roold(i,j) = c5(j)*sx(im1) + c6(j)*sx(i) +
     -             c7(j)*ro(im1) + c8(j)*ro(i)
   60 continue
      roold(1,j) = roold(nx,j)
      roold(nxp1,j) = roold(2,j)
   40 continue
c
      do 70 i = 1,nxp1
      roold(i,1) = 0.0
      roold(i,nv) = 0.0
   70 continue
c
      return
      end
c
c     ****************************************
c     * New distribution with collisions *
c     ****************************************
c
      subroutine newf (f, fnew, fmold, fm, ro, roold, nxp1, nv)
c
      dimension f(nxp1,nv), fnew(nxp1,nv), fmold(nxp1,nv), fm(nv),
```

```
     -          ro(nxp1), roold(nxp1,nv)
c
      common / coll / cnuc, coll1, coll2
      common / iflags / ieq, ipert, ielf, icont, icoll, imaxw
      common / inte / nx,nxm1,nvm1,nvm,nvp,nvp1
c
      if (icoll.eq.0) then
      do 10 i = 1,nxp1
      do 20 j = 1,nv
      f(i,j) = fnew(i,j)
   20 continue
   10 continue
c
      else
c
      call dens (fnew, ro, nxp1, nv)
      do 30 i = 2,nxm1
      do 40 j = 2,nvm1
      f(i,j) = coll1 * fnew(i,j) +
     -         coll2 * (roold(i,j)*fmold(i,j) + ro(i)*fm(j))
   40 continue
   30 continue
c
      endif
      return
      end
```

The two page vita has been removed from the scanned document. Page 1 of 2

The two page vita has been removed from the scanned document. Page 2 of 2